2011

The Role of the Stereociliary Glycocalyx in Hair Bundle Cohesion

Adria Claire Le Boeuf

THE ROLE OF THE STEREOCILIARY GLYCOCALYX IN HAIR BUNDLE COHESION

A Thesis Presented to the Faculty of

The Rockefeller University

in Partial Fulfillment of the Requirements for

the degree of Doctor of Philosophy

by

Adria Claire Le Boeuf

June 2011

THE ROLE OF THE STEREOCILIARY GLYCOCALYX IN HAIR BUNDLE COHESION

Adria Claire Le Boeuf, Ph.D.

The Rockefeller University 2011

The sensory hair cells of the inner ear are exquisitely sensitive machines that translate the broad dynamic range of sound intensities in our auditory landscape into the electrical language of neurons. The mechanosensitive organelle of the hair cell is the hair bundle, a cluster of linked, finger-like, membrane-ensheathed projections, stereocilia, emerging from the cell's apical surface. As a structure, the hair bundle is highly conserved, changing little yet performing many functions throughout the vertebrate evolutionary tree. The mechanosensitivity of the hair bundle is achieved by the tension-gating of mechanosensitive channels joined to proteinaceous tip links that connect the distal tips of neighboring stereocilia along the axis of mechanosensitivity. When the hair bundle is deflected and the distal tips of stereocilia shear in relation to one another, tension is applied to the tip links causing the mechanotransduction channels to open. This allows cations to flow in and depolarize the cell membrane triggering synaptic release at the base of the cell, and consequently sending the information to the brain.

The cell membranes in the hair bundle face a difficult task when the

bundle oscillates in response to sound. For efficient auditory mechanotransduction, it is essential that all stereocilia move nearly in unison, shearing at their distal tips yet maintaining contact without membrane fusion, yet the mechanism producing this cohesion is unknown nor have physical forces associated with it ever been measured. The mechanism I have tested in my doctoral work is that of counterion-mediated tethering of negatively charged sugars on opposing stereociliary membranes. Using capillary electrophoresis, I demonstrated that the stereociliary glycocalyx acts as a negatively charged polymer brush, necessary for the soundness of the glyco-tethering hypothesis. I found by force-fiber photomicrometry that when the distal tips of stereocilia were brought together they formed elastic attachments in a manner dependent on the presence of *N*-linked sugars and the surrounding ionic environment. Ca^{2+}- and Mg^{2+}-mediated attachments varied in their strength and susceptibility to overcharging, though Mg^{2+} played a larger role in the observed adhesion. Both partial deglycosylation and removal of divalent ions from surrounding solutions dramatically reduced adhesiveness. During the process of adhesion between the distal tips of stereocilia, chaotic stick-slip friction was observed and appeared qualitatively similar to stick-slip associated with earthquakes. Together, these results indicate that stereocilia are likely to form glycan- and divalent ion-mediated attachments to one another that may provide the necessary cohesion for auditory hair bundles. This indicates the importance of the glycocalyx for hearing, and more generally, the biomechanics of cellular adhesion.

ACKNOWLEDGMENTS

I thank those who've encouraged me along this path, those who didn't judge this book by its cover, and those who recognized this spark of creativity and intellectual adventure and encouraged me to pursue science.

In chronological order: I thank my parents for their 'boring' discussions about elephant seal mating behavior over dinner as I was growing up and for their astute observations on the behavior of my 'sub-adult male' colleagues in grade school. Before turning 18, I already had a rich appreciation for evolutionary biology and our behavioral adaptations. I especially thank my mother for her desire to instill in me scientific excitement and rigor at a young age e.g. *Porcellio scaber*'s light avoidance response at age 9. I thank Mr. Moir, my 6th grade teacher, who first made science cool and creative problem solving fun. His excitement was a catalyst. I am especially thankful to my mother for helping me get through junior high and high school with my sense of scientific curiosity intact, in spite of my teachers.

I give huge thanks to Leda Cosmides and John Tooby of the Center for Evolutionary Psychology at the University of California at Santa Barbara (UCSB). These brilliant, warm people did such great work and at the same time were so humane and inclusive in their scientific process, even to the college freshman I was then. Leda was my first scientific role model, and she gave me faith that my scientific strengths were worth pursuing. I also thank Aaron Sell, John and Leda's student at the time, for guidance and for a glimpse of how thoroughly science can

color one's world-view.

I thank Stu Feinstein, Les Wilson and Sasha Levy from the Neuroscience Research Institute at UCSB. I thank Stu, for having me in his lab for a number of years, allowing me to do real research as an undergraduate and as a tech, putting up with me, and being a kind, caring, boss. I thank Sasha for discovering with me what a fun and exciting ride science can be, for his infectious intellectual drive, and for allowing me to be a partner rather than an underling.

I'm grateful to the Rockefeller University Graduate Program for the opportunity to do my PhD here. I give special thanks to Sid, Emily, Cris, Marta, Kristen and Michelle for all their care, support and attention through the years.

I thank Cori Bargmann, both as a committee member and as the advisor I spent many months with when I first came to Rockefeller. Her breadth of scientific inquisitiveness and her calm strength continue to inspire to me.

I thank the Physics and Biology department at Rockefeller for its kind welcome to a physics-curious biologist such as myself. Special thanks to Thomas Risler, Daniel Andor, Omar Ahmed, Michael Krieger, Anton Zilman, Maria Geffen and the other various members of the brilliant but now defunct Learning Club. Thanks to Nick Khuri and Eddie Cohen for their support. I give particular thanks to Daniel Andor for his patience and many hours of physics tutelage when I first began my quest into the domain of physics.

I thank my advisor Jim Hudspeth, for his enveloping scientific passion, quirkiness, and awe-inspiring professorial skills. No one can give a talk so

convincingly, so compellingly, as Jim can. He is a phenomenal editor. He has such an encyclopedic breadth of knowledge it made me suspect at times that he might not actually be human. Who else could come up with the idea of fly wings' hairs as an alternative to nanofabrication? I also thank Jim for giving me faith that a successful professor can be involved in lab work throughout his or her career, and productively at that. I hope some trace of his skill has rubbed off on me a bit in my four years working with him.

I thank the glorious and diverse people of the Hudspeth lab. I've made so many strong friendships in this lab that at times it caused me concern that I didn't get out enough. In the scientific sphere, I give great thanks to Brian Fabella, Alexander Darbinjan, Manolo Castellano-Munoz, Daniel Andor, Jonathan Fisher, Taeryn Kim, Suchit Patel, Samuel Lagier, Deborah Yeoh-Wang and Dáibhid Ó Maoiléidigh for their help, advice and great discussions. I've especially appreciated Jonathan Fisher for both his scientific and personal support and wisdom. Extra thanks also go to Alex Darbinjan and Brian Fabella for helping me build and conquer the force-fiber micromechanics set-up and all its beautiful artifacts.

I am grateful to my funding sources, the Women & Science Foundation, and the National Institute for Deafness and Communication Disorders for financially supporting my doctoral work.

I am grateful to the members of my faculty advisory committee—Sandy Simon, David Gadsby and Cori Bargmann—for providing me with insightful

comments and questions, and for their guidance and support when necessary. I particularly want to thank Dan Hammer for traveling from Philadelphia to serve as my external examiner on the committee.

Lastly, I want to thank those who've given me support outside of lab, where I often needed it most. I again thank my family, especially my brothers, Remy and Pascal, for their care and alternate perspective during this time in New York. I thank my friends, especially Marie, Aleks and Taeryn. Most of all, I thank Sam. I cannot fathom how many times he has helped me calm down and put the world in perspective. He has been a pillar of calm, strength and understanding. Thank you all.

TABLE OF CONTENTS

LIST OF FIGURES

LIST OF TABLES

1 INTRODUCTION

Noise-induced hearing loss accounts for the majority of functionally significant hearing loss in humans, affecting approximately 26 million people in the United States alone (NIDCD). A number of proximate mechanisms can cause noise-induced hearing loss, notably, metabolic exhaustion of hair cells, the sensory cells of the inner ear, and damage to their hair bundles, the mechanosensory organelles (Gelfand, 2009). Although hair cells do succumb throughout our lives to excess stimulation, they normally tolerate decades of use and abuse.

1.1 THE BASICS OF HEARING

The hair cell, the mechanoreceptor of the inner ear, shows evidence of a remarkable battle between evolution and physical limitations. Each hair cell is an exquisitely sensitive machine whose task is to represent the mechanical stimuli of sound vibrations as neural signals (Hudspeth, 2008). The mechanosensitive organelle of the hair cell is the hair bundle, a cluster of linked, finger-like projections, the stereocilia, emerging from the cell's apical surface (Figure 1.1). Each stereocilium is composed of a dense actin core surrounded by membrane highly decorated with glycoproteins, glycosphingolipids and proteoglycans. Amidst this glycocalyx, proteinaceous tip links connect the stereocilia along the axis of hair-bundle sensitivity; it is at the point of connection between the tip link and the stereocilium where the transduction channel and the seat of mechanosensitivity lie.

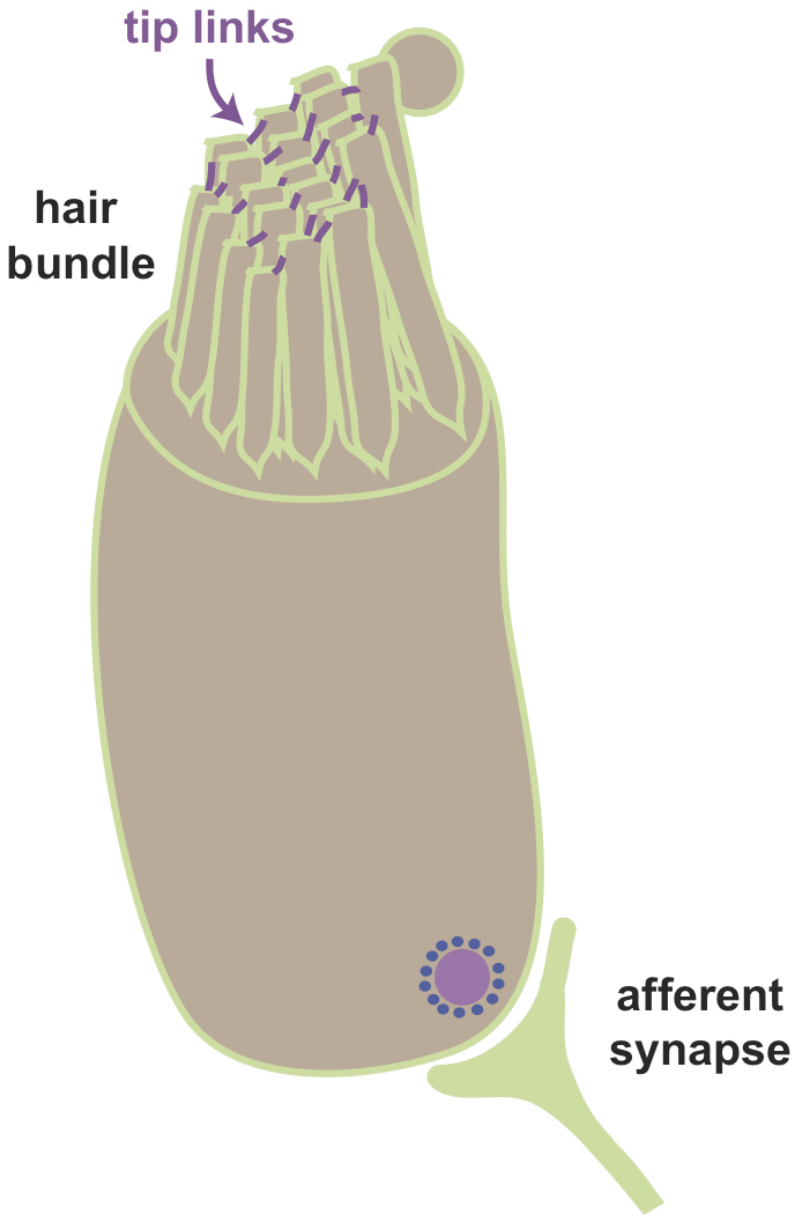

Figure 1.1: The hair cell. The hair bundle, a collection of interlinked stereocilia crowns the hair cell at its apical surface. When the bundle is deflected, tension is applied to tip links, which open mechanosensitive channels, depolarizing the cell. Depolarization results in synaptic release at the ribbon synapse at the base of the cell.

When one hears a sound, the vibrations at all component frequencies are passed from the tympanum, to the ossicles of the middle ear, and then on to the fluids inside the cochlea. Within the cochlea, the sensory hair cells are organized tonotopically along the basilar membrane in the organ of Corti (Figure 1.2), which spirals from the base to the apex of the snail-shaped cochlea, with high-frequency-sensitive hair cells found at the base, and low-frequency-sensitive hair cells at the apex. The motion of the fluids in the chambers above and below the basilar membrane causes a traveling wave to propagate along the basilar membrane and peak at the position of hair cells sensitive to the stimulus frequency. This sound-induced fluid movement applies mechanical force to the hair bundles, which sway back and forth along their axis of mechanosensitivity, matching the frequency of the sound with their oscillation (Jacobs and Hudspeth, 1990). When an individual hair bundle is deflected, the distal-most tips of the stereocilia shear against one another (Jacobs and Hudspeth, 1990; Karavitaki and Corey, 2010), applying tension to tip links connecting the tops of adjacent stereocilia. This tension pulls open the mechanotransduction channels, allowing cations to flow in and depolarize the cell, which in turn effects neurotransmitter release at the base of the cell.

As a high-frequency hair bundle oscillates in response to high-pitched sounds, its component stereocilia must slide against one another at remarkable speeds, cycling in our cochleae at up to 20,000 cycles per second (20 kHz), and

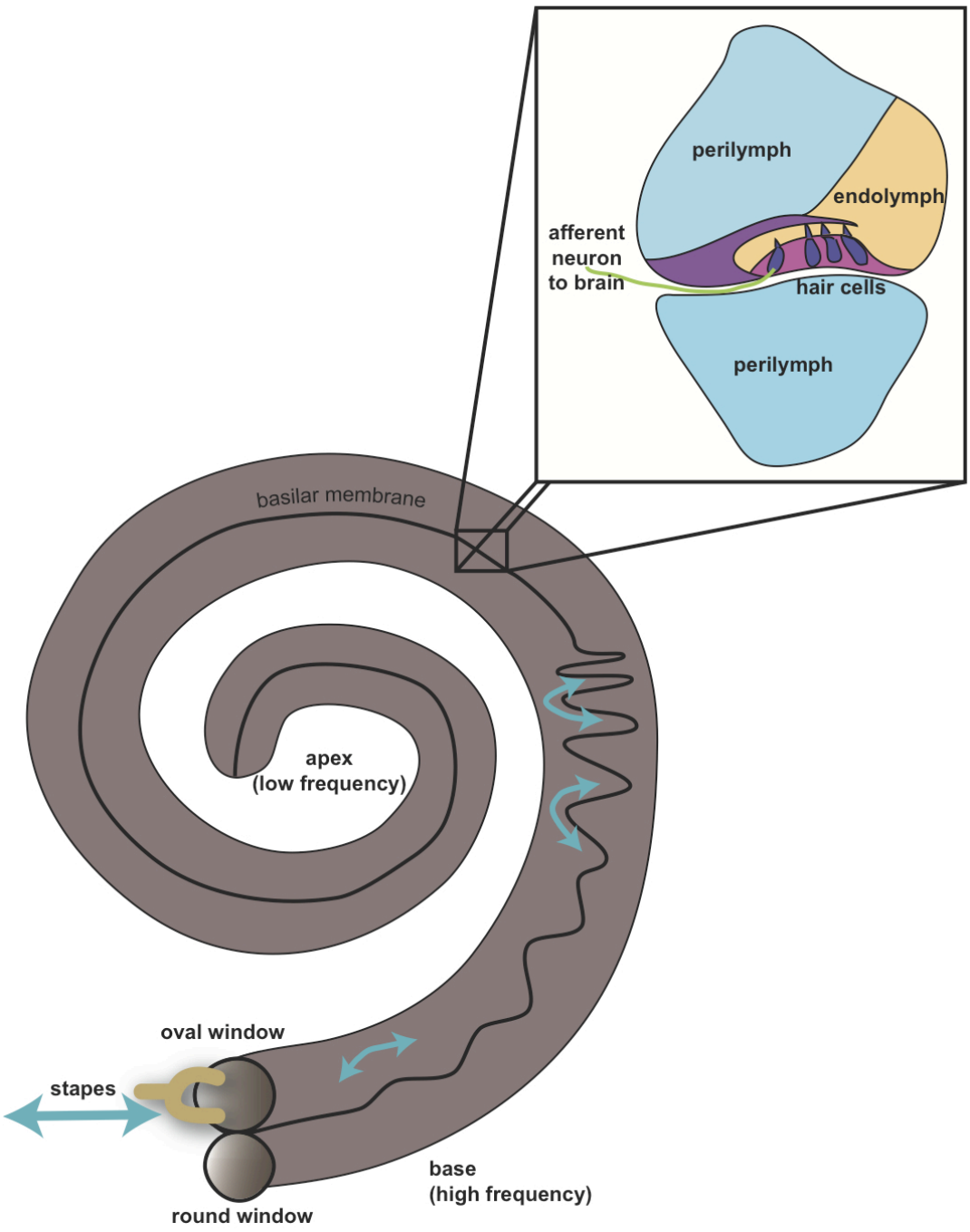

Figure 1.2: The mammalian cochlea and organ of Corti. Sound pressure waves cause the stapes to push in and out against the oval window. This causes an active traveling wave to propagate along the basilar membrane, peaking at the stimulation frequency. This movement of the fluids in the cochlea deflects the hair bundles, causing the hair cells to release neurotransmitter and thus signal to the brain through the afferent neurons. Blue arrows indicate back-and-forth fluid movement.

in some mammalian cochleae at greater than 100,000 cycles per second (100 kHz) (Ketten, 1997). Among people who suffer from age-related hearing loss, high-frequency-tuned hair cells are typically the first to deteriorate, indicating that use-induced degradation is dependent on the frequency of hair cell stimulation (Gelfand, 2009).

The hair cells of the inner ear also accomplish the difficult task of transducing sounds over a dynamic range of approximately six orders of magnitude in amplitude, from sub-nanometer deflections of the hair bundles owing to Brownian motion up through tens-of-nanometer deflections induced by the loud urban environment of New York City. To achieve this responsiveness, hair cells exhibit four signature phenomena that characterize the so-called active process. First, the cell compresses an enormous range of stimulus intensities into a relatively narrow range of responses in what is termed the compressive non-linearity (Choe et al., 1998; Martin and Hudspeth, 2001). Second, to allow us to sense quiet sounds or small deflections of the hair bundle, the hair cell amplifies its mechanical inputs (Le Goff et al., 2005; Martin and Hudspeth, 1999; Martin et al., 2000). Third, in order to transmit frequency-specific information to the brain, each hair cell is tuned to a specific frequency (Choe et al., 1998; Martin et al., 2001). Finally, the hair cell sometimes becomes unstable and oscillates spontaneously, producing faint sounds called spontaneous otoacoustic emissions, indicative mathematically that the hair cell operates on the edge of a Hopf bifurcation (Bozovic and Hudspeth, 2003; Martin et al., 2003; Martin et al.,

2001).

The active process of the inner ear expends energy to enhance the sensitivity and frequency selectivity of hearing. To enable us to hear high-frequency sounds, up to 20 kHz, the hair cells must physically not only oscillate but amplify at these frequencies, fending off dissipative viscous drag at low Reynolds number, Brownian motion and friction from within the bundle. The necessary mechanical work thought to underlie the power of the hair bundle is done by adaptation, the process whereby the hair bundle shifts its range of sensitivity in the positive or negative direction, depending on the magnitude and direction of stimulation (Eatock, 2000; Eatock et al., 1987; Howard and Hudspeth, 1987; Martin and Hudspeth, 1999). Adaptation is brought about by myosin-1c motors found at the insertional plaques at the distal tips of the stereocilia (Batters et al., 2004; Gillespie and Cyr, 2004; Gillespie et al., 1993; Hasson et al., 1997; Holt et al., 2002). When the hair bundle is deflected in the negative direction and held there, the myosin-1c molecules appear to ascend the actin cores of the stereocilia, raising the insertional plaques of the tip links and shifting responsiveness in the negative direction. When the hair bundle is deflected and maintained in the positive direction, the myosin-1c molecules and thus the insertional plaques slide down the stereocilia at a pace proportional to the tension in the tip links, shifting responsiveness in the positive direction (Figure 1.3A). When a hair bundle is subjected to a force step (Figure 2 of Howard and Hudspeth, 1987), one observes a small twitch in displacement on a timescale of

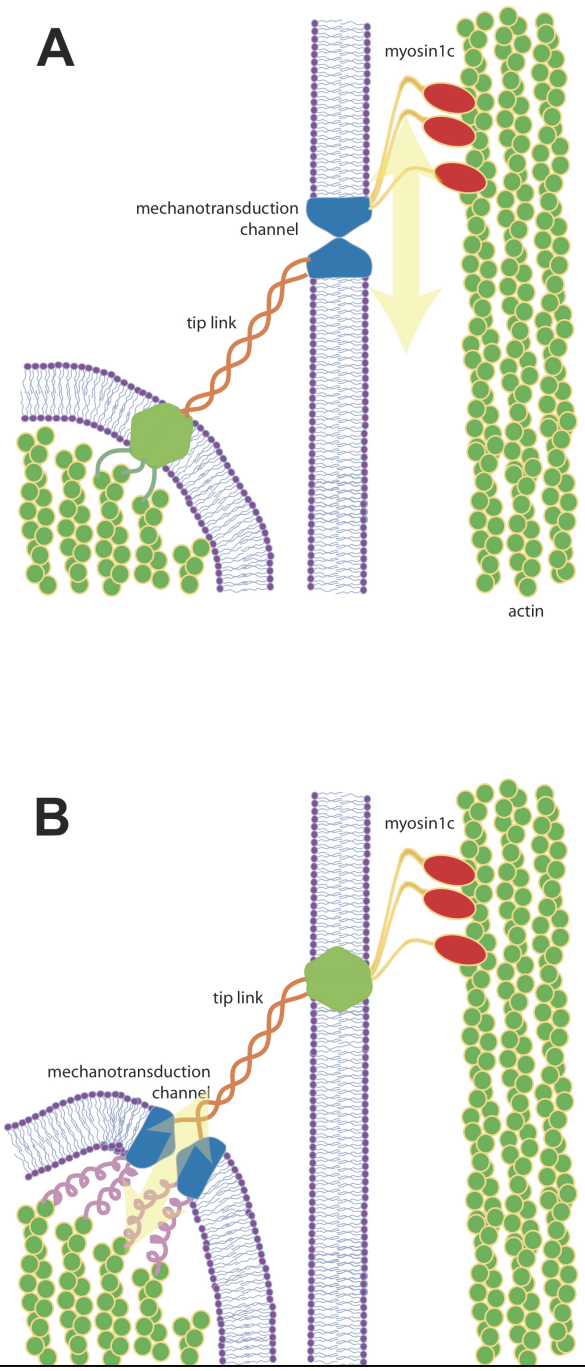

Figure 1.3: Adaptation Mechanisms. A, The classical model of adaptation holds that the mechanotransduction channel, Ca^{2+}-sensitive myosin1c molecules, and upper insertional plaque move up and down together to adapt the hair bundle to strong stimuli. B, Another potential mechanism for adaptation, given the new positioning of the mechanotransduction channel (Beurg et al., 2009), might instead involve membrane- or protein-stretching around the channel at the lower tip-link insertion point. Both models involve alternation of tip link tension.

milliseconds, associated with a large, inward transient of transduction current. This response is followed by slow adaptation and mechanical relaxation on a timescale of a few tens of milliseconds that corresponds well with the climbing and slipping rates of the myosin molecules (Benser et al., 1996; Howard and Hudspeth, 1987; Wu et al., 1999).

Until recently, the mechanotransduction channel was though to be positioned at the point of connection between the tip link and the taller stereocilium, associated with the upper insertional plaque. Elegant physical models based on this geometry related the influx of Ca^{2+} through the transduction channel to the sliding of the insertional plaque and channel open probability (Choe et al., 1998; Nadrowski et al., 2004). Recently, the work of Beurg et al., 2009 indicated that the channel is more likely at the lower end of the tip link, at the point of connection with the lower stereocilium. This topic is still in debate, but if the channel is indeed localized at the lower end of the tip link, the mechanism by which tip link tension is modified during adaptation is likely to differ from the previous physical modeling (Corey, 2009, Figure 1.3B).

1.2 MECHANOSENSATION

Mechanosensation, the conversion of mechanical stimuli into neural signals, underlies much of our sensory experience: touch, hearing, balance, and pain. For an organism to successfully interact with the physical world it must be able to perceive the ubiquitous mechanical stimuli that make up its everyday

environment. Thus, unsurprisingly, mechanotransduction is a universal property of all living organisms, with mechanosensitive proteins present in eubacteria, archaea and eukarya (Blount and Moe, 1999; Garcia-Anoveros and Corey, 1997; Kloda and Martinac, 2001; Koch, 1994; Koprowski and Kubalski, 2001). The earliest mechanosensors were likely used by bacteria and unicellular organisms to cope with osmotic stress in a changing environment. Evolution has since adapted mechanosensation to a variety of other problems: sensation of sound, gravity, touch, pain, proprioception, blood pressure, vascular maintenance, tension in tendons and muscles, cellular locomotion, tissue development, morphogenesis, gravitaxis, turgor control, and likely many other as yet undiscovered applications (Gebauer et al., 1999; Gillespie and Walker, 2001; Ingber, 1997; Ko and McCulloch, 2001; Lee and Huang, 2000; Lynch et al., 1998; Pickard and Ding, 1993; Tavi et al., 2001; Welsh et al., 2002).

Despite this wide variety of applications of mechanosensation, there are common elements in the mechanics of the mechanotransduction machinery. In sensory systems, the sensors themselves must be fast and sensitive. In contrast, mechanosensation in development occurs on a slower timescale, which often results in complex signal transduction cascades. The simplest mechanoreceptor known is the channel MscL in *Escherichia coli*, which opens in response to membrane tension from osmotic stress in the absence of any tethering molecules (Sukharev et al., 1994). Many mechanosensitive channels in multicellular organisms are thought to employ the architecture of a tethered-ion channel, where

extracellular mechanical forces are directed by proteinaceous tethers to an ion channel that is also tethered internally to the cytoskeleton (Gillespie and Walker, 2001; Hu et al., 2010). When force is applied, the channel opens rapidly, amplifying the signal by allowing the entry of many ions across a steep concentration gradient. Mechanical forces can also be detected by changes in membrane lipid composition or arrangement in a manner that does not require tethering (Christensen and Corey, 2007). Slower forces can be sensed through the cell surface receptors such as integrins that are connected to the cytoskeleton through accessory proteins that effect changes in gene expression (Evans and Calderwood, 2007; Parsons et al., 2010).

Some common mechanosensory channels in metazoans have emerged in recent years, the DEG/ENaC, TREK and TRP families of ion channels (Figure 1.4, reviews: (Gillespie and Walker, 2001; Xiao and Xu, 2010). The putative mechanosensitive cation channel in *Drosophila melanogaster* hair bristles is NompC, a TRP channel. Both TRP channels and the DEG/ENaC channels are involved in *C. elegans* perception of light touch. The mechanosensitive channel in vertebrate hair cells is still unknown. Mechanosensitivity has been reported in many sub-families of TRP channels (Kamkin and Kiseleva, 2007; Kang et al., 2010; Kwan et al., 2009). However, many TRP channels appear to be polymodal, activated by a variety of stimuli including temperature, pH and lipid-like compounds (Christensen and Corey, 2007). The DEG/ENaC family also perform diverse functions (Kellenberger and Schild, 2002). Degenerins mec-4 and mec-10

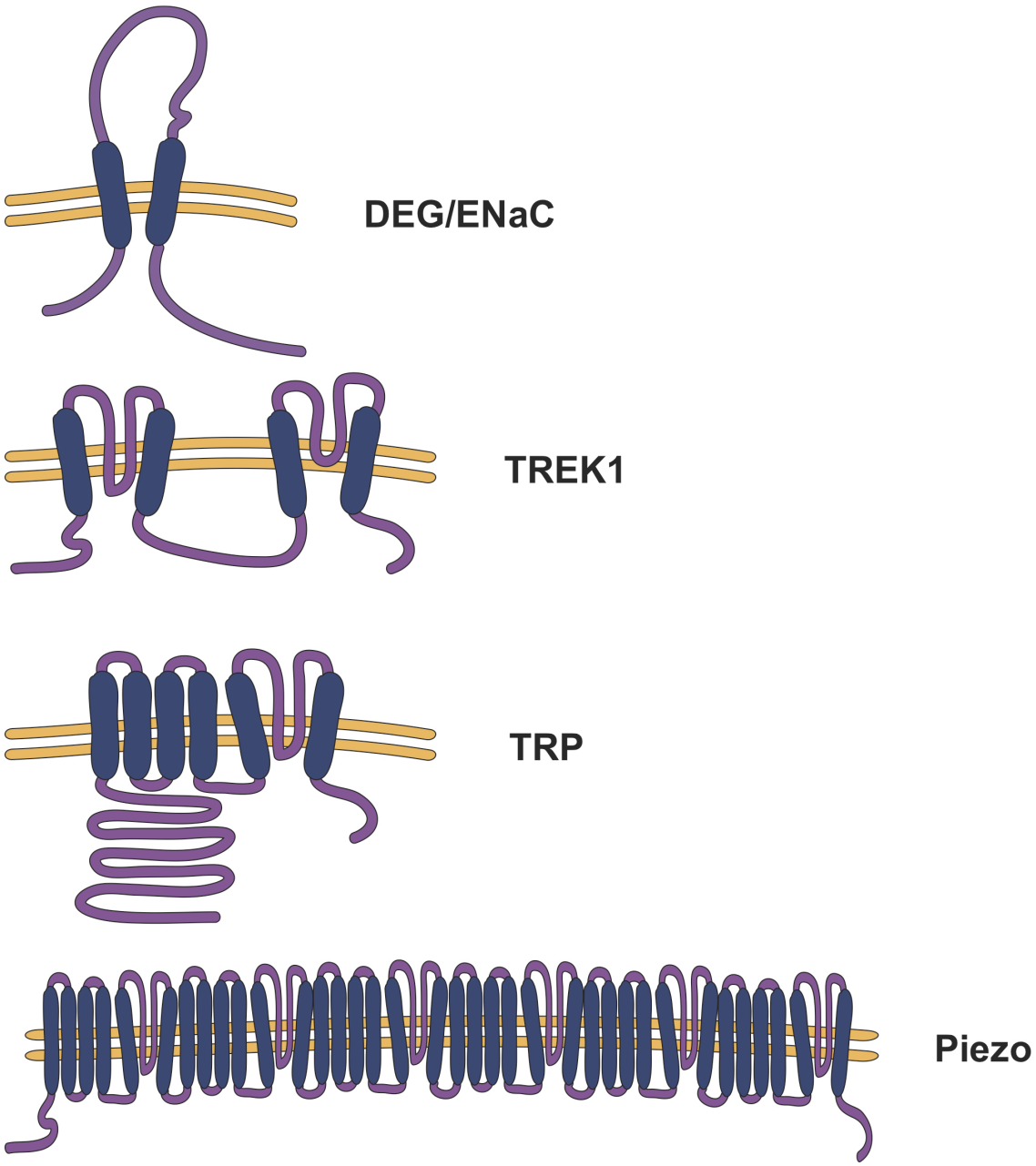

Figure 1.4: Mechanosensitive channel types.

mediate the light touch response in *C. elegans* and other degenerins may play a role in other animals' mechanosensation; ENaCs, epithelial Na^+ channels, are typically involved in Na^+ transport on the lung and kidney, and salty taste perception by the tongue; ASICs are proton-sensitive channels that may be involved in acidosis induced pain. A K^+ channel found in mammals, TREK1, also appears to be mechanosensitive (Maingret et al., 2002). Two new mechanosensitive proteins Piezo1 and Piezo2 have just been found to constitute an entirely new family of channels (Coste et al., 2010; Xiao and Xu, 2010).

As opposed to other sensory modalities like vision, smell, and taste, the biophysical mechanism by which touch, hearing, and balance are sensed by their receptors still remains mysterious. The most compelling recent proposal for the auditory mechanotransduction channel (Corey et al., 2004), TRPA1, fell flat when the mouse knock-out of the gene did not result in hearing loss (Bautista et al., 2005; Kwan et al., 2006). It is not yet clear whether either of the Piezo proteins or an undiscovered family member might be expressed in hair cells. Together, the discovery of Clarin-1, a tetraspanin-like actin-organizing protein part of the Usher Syndrome complex (Tian et al., 2009), and the knock-out of integrin a8b1 that disrupts stereociliary development (Littlewood Evans and Muller, 2000), suggest that perhaps in addition to the fast mechanotransduction channel, the hair bundle may also have a slower integrin-based mechanosensation complex utilized during development. The fast mechanotransduction channel of the hair bundle, however, continues to remain elusive.

1.3 HAIR BUNDLE COHESION

As a hair bundle oscillates, it is unclear how stereocilia manage to move against one another without splaying and without excessive friction. Stereocilia membranes are likely to avoid fusion and maintain their integrity through the help of the glycoproteins, glycosphingolipids and proteoglycans of the glycocalyx, thought to be negatively charged (Dolgobrodov et al., 2000; Pries et al., 2000; Varki, 2007). However, it is not clear what stops thermal noise from further separating stereocilia and thus indiscriminately opening mechanotransduction channels across the bundle. Both mechanical models and experiments (Jacobs and Hudspeth, 1990; Karavitaki and Corey, 2010) indicate that successive stereocilia in each file undergo shearing motions at their points of contact. However, the cause of experimentally observed friction in the movement of the hair bundle may instead come from hydrodynamic drag (Baumgart, 2010). In spite of erratic forces due to Brownian motion and potential friction from hydrodynamics or dissipative movements within the bundle, the hair bundle remains highly cohesive. Under thermal excitation, the hair bundle with all its component stereocilia moves cohesively without splay even at frequencies in excess of 10 kHz (Kozlov et al., 2007).

Mechanoelectrical transduction in the hair bundle functions most efficiently when upon stimulation all channels open in unison. As each channel opens and lets in depolarizing cations, the depolarizing signals of all channels combine. When all mechanotransduction channels open in unison, the signal to the base of

the cell is temporally clear and the resultant synaptic release provides an unambiguous signal to the auditory nerve (Karavitaki and Corey, 2010; Kozlov et al., 2007). If the mechanotransduction channels gate in series, with tension pulling open channels at the tallest stereocilia before tension is even applied to the channels of the shorter stereocilia, the temporal signatures of each channels' opening would be smeared together (Nam et al., 2006; Silber et al., 2004). The result would be an ambiguous message of low temporal accuracy to the synaptic release machinery at the base of the cell. To enable unified gating, the hair bundle must move cohesively without undue separation of the stereocilia but with a constant rate of sliding between the distal tips of adjacent stereocilia. Not only is hair bundle cohesion valuable for efficient mechanotransduction, it also is likely protective for the hair bundle. Excessive noise can induce hearing loss through splay, breakage, and even fusion of stereocilia, which in turn lead to hair-cell death (Gelfand, 2009).

What mechanisms might efficiently distribute the energy of a stimulus across the hair bundle without unduly constraining stereociliary movements? Stereociliary cohesion is likely to be produced by a combination of four mechanisms (Figure 1.5). The most obvious mechanism for cohesion would be the filamentous connections between stereocilia—basal links, shaft connectors, top connectors, and tip links (Bashtanov et al., 2004; Nayak et al., 2007; Pickles et al., 1989, Figure 1.6). As previously mentioned, tip links connect the distal tips of stereocilia along the axis of mechanosensitivity, where they transfer changes in

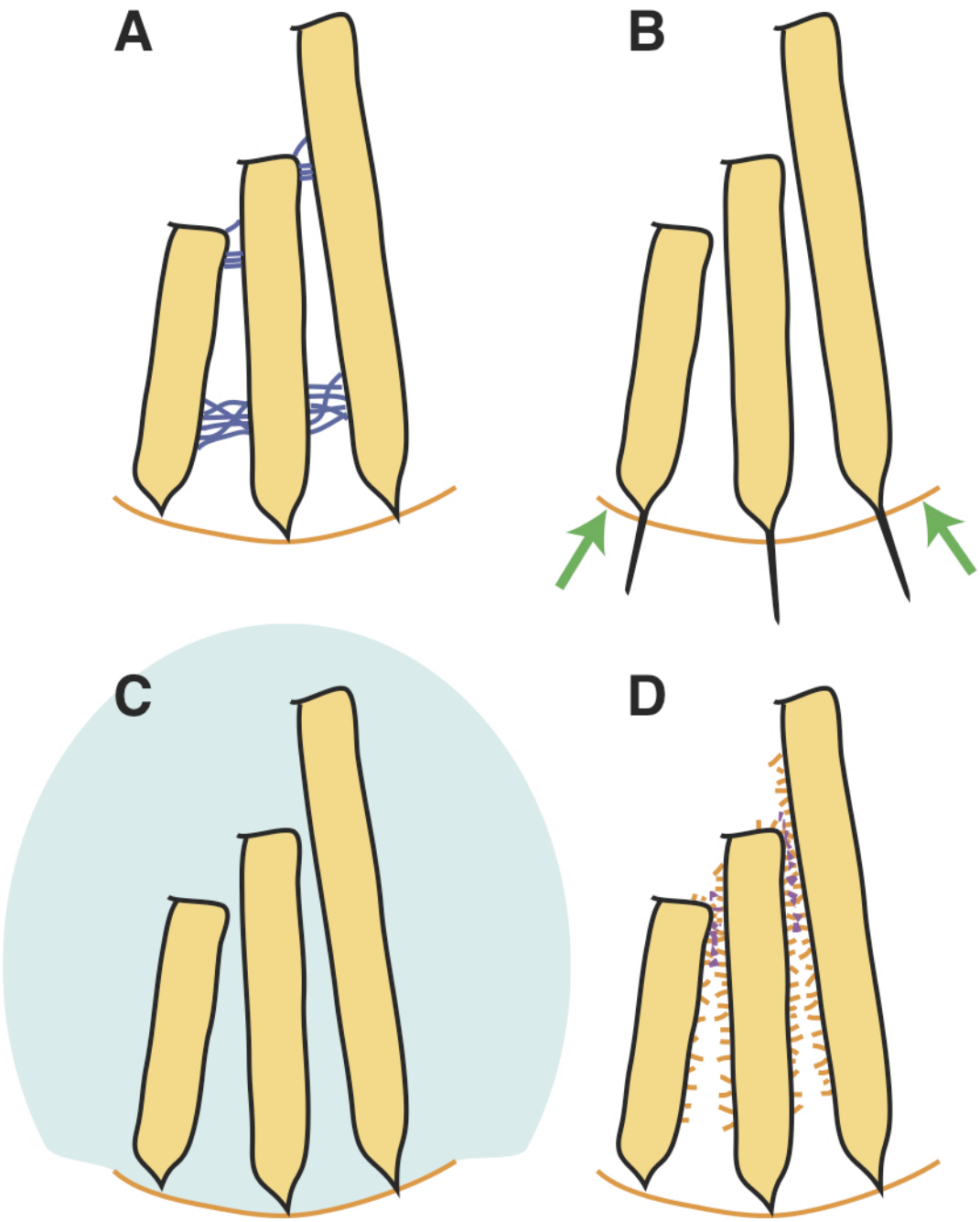

Figure 1.5: Four potential mechanisms for hair bundle cohesion: A, Proteinaceous linkages between stereocilia, B, force exerted on stereociliary rootlets by the curvature of the cuticular plate, C, hydrodynamic viscosity, and D, electrostatic tethering of stereociliary glycocalyces.

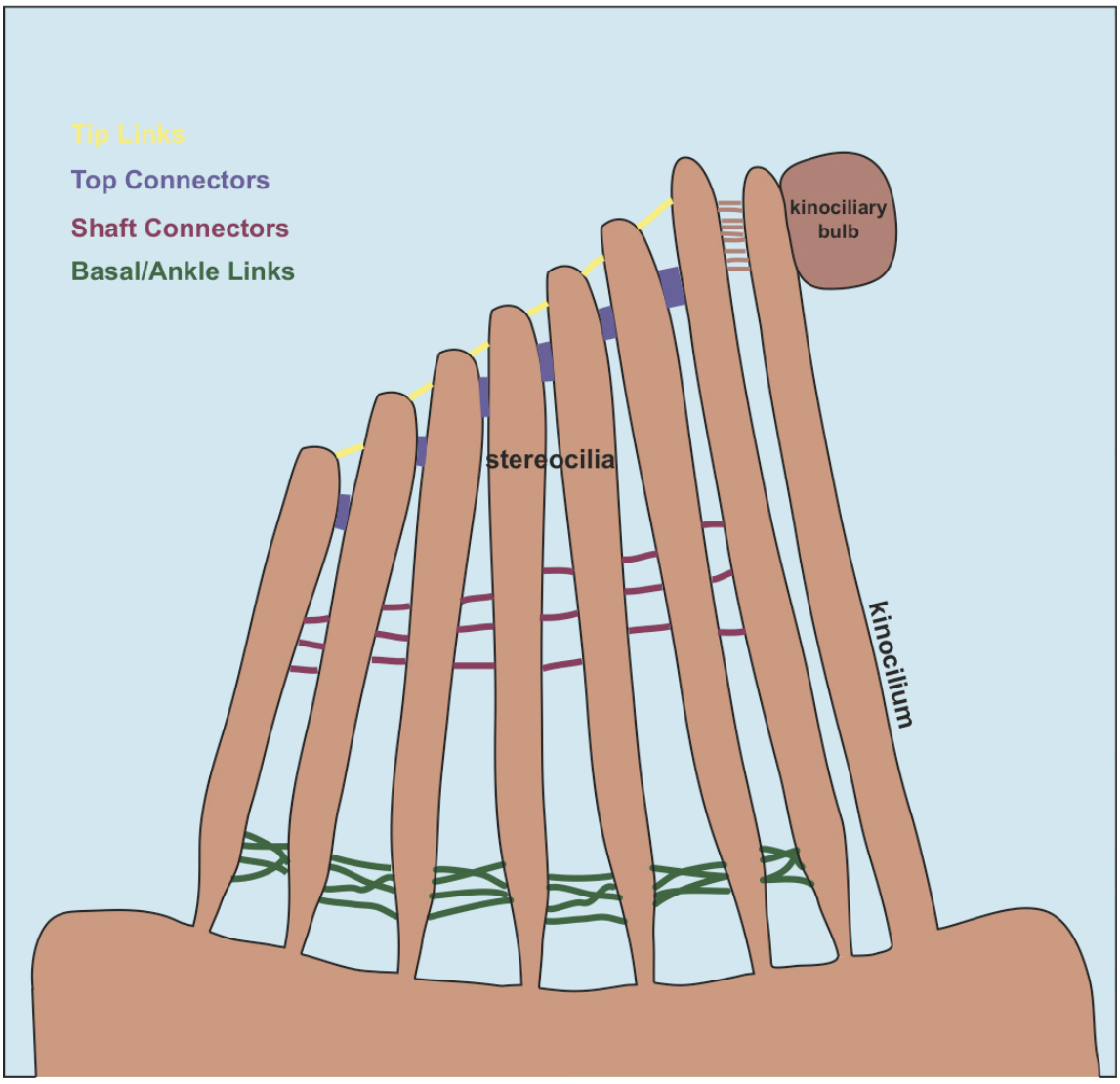

Figure 1.6: Linkages within the hair bundle. Tip links (yellow), top connectors (lavender), shaft connectors (magenta), basal or ankle links (green) connect stereocilia together. In addition some links connect the kinocilium to the tallest stereocilia (brown).

tension induced by bundle deflection to the mechanotransduction channels (Pickles et al., 1984). Each tip link is made up of four molecules, a helically intertwined dimer of cadherin-23, and another helically intertwined dimer of protocadherin-15, both of which are highly glycosylated (Kazmierczak et al., 2007; Rzadzinska et al., 2005; Senften et al., 2006; Siemens et al., 2004). With but one tip link connecting each pair of adjacent height-ranked stereocilia, these connections are fragile and can be disrupted by loud sounds, rough treatment, and the removal of Ca^{2+} ions from the surrounding solution (Assad et al., 1991; Pickles et al., 1987). Each of the other linkage types is both more stable and present in greater numbers than the tip links. Basal or ankle links interconnect stereocilia along all three axes of their hexagonal array just above the stereociliary taper at the base of the hair bundle. These long and filamentous links can be removed both by treatment with the protease subtilisin and by removal of Ca^{2+} with the chelator BAPTA (Bashtanov et al., 2004; Nayak et al., 2007). The very large G-protein coupled receptor 1 (Vlgr1) and usherin have been associated with these basal links in both chick and mouse (Adato et al., 2005; Pickles et al., 1987). Shaft connectors connect stereocilia to one another along their length; these links are sensitive to subtilisin but not BAPTA and have been associated with protein tyrosine phosphatase receptor Q, Ptprq (Goodyear et al., 2003; Goodyear and Richardson, 2003). Top connectors connect the distal tips of stereocilia just below tip links, and these are sensitive neither to protease treatment nor to Ca^{2+} chelation (Goodyear and Richardson, 1992; Nagel et al.,

1991). Recently, the secreted extracellular protein Stereocilin was associated with top connectors in mice (Verpy et al., 2008).

When the majority of these connections are removed with a combination of subtilisin and BAPTA treatments, the bundle remains cohesive (Karavitaki and Corey, 2010; Kozlov et al., 2007). Further, in theory, if stimuli had to propagate across a hair bundle though these links connecting the stereocilia in series, the angular amplitude of stereociliary movement would decrease from the tallest to the shortest stereocilium (Nam et al., 2006; Silber et al., 2004), and additionally, the mechanotransduction channels would gate in series rather than in parallel, reducing the signal to noise ratio of the hair cell's mechanical-to-electrical transduction.

Stereocilia might also be forced together by stress in their elastic basal insertions into the cuticular plate. The cuticular plate is a dense network of cytoskeletal components that lies inside the hair cell body just below the hair bundle. The stereociliary 'rootlets' insert into this close-packed mesh. In healthy hair cells, the cuticular plate appears concave; if stereociliary rootlets emerge from the cuticular plate at a 90° angle, this concavity could push the distal tips of stereocilia together. However, while stereociliary rootlets do appear somewhat pre-stressed, this mechanism is unable to supply sufficient force to rein in large stererociliary fluctuations (Karavitaki and Corey, 2010).

A third mechanism that could produce hair bundle cohesion is hydrodynamic drag (Baumgart, 2010). At the low Reynold's number regime in

which the hair bundle functions, viscous forces dominate and likely disallow stereocilia from separating from one another at a range of frequencies. The fluid between stereocilia is confined to such a small space that its viscosity likely keeps stereocilia from separating due to the energetic cost. Hydrodynamic effects undoubtedly play a role in hair bundle cohesion, though they are unlikely to be sufficient for maintenance of cohesion, especially when stereocilia encounter low frequency perturbations (Baumgart, 2010). When movements are slow, water molecules can rearrange without much energetic cost.

A last mechanism that might account for hair bundle cohesion is counterion-tethering of neighboring negatively-charged stereociliary glycocalyces (Figure 1.5D). Although, surfaces of like charge ordinarily repel one another, at certain distances and in the presence of appropriate counterions, they can attract. This provocatively named phenomenon, “like-charged attraction,” has been observed in a variety of systems including plates, rods, DNA, and virus particles (Butler et al., 2003; Grønbech-Jensen et al., 1997; Ha and Liu, 1997; Kornyshev and Leikin, 1999; Lyubartsev et al., 1998). Multivalent counterions play a central role tethering apposing charged surfaces.

From electron micrographs of hair bundles stained with polycationic dyes (Csukas et al., 1987; Neugebauer and Thurm, 1986; Santi and Anderson, 1986), the stereociliary glycocalyx appears to be negatively charged, providing like-charged surfaces that could be tethered by the Ca^{2+} and/or Mg^{2+} present in physiological endolymph. This mechanism could be particularly adept at providing

inter-stereociliary cohesion: adhesive forces between individual negatively charged molecules would be weak, but abundant, allowing collectively strong but adaptable connections to be formed (Chang and Hammer, 2000; Chang et al., 2000; Goetz et al., 1994).

Hair bundle cohesion is likely to occur through a combination of these mechanisms. For my thesis work, I have explored this last mechanism of hair bundle cohesion, divalent-mediated electrostatic tethering of stereociliary glycocalyces.

1.4 CELL-CELL ADHESION

To understand adhesion between stereocilia, let us first explore other types of cell adhesion in biology. Control of differential adhesion between cells is essential for all multicellular life and much of unicellular life as well. Cellular adhesion mediates a wide range of physiological processes from cell migration of immune or cancer cells, to cell recognition for organization of tissues, to viral infection, to fertilization (Alberts et al. 2002; Evans and Calderwood, 2007). Adhesion is typically thought to occur though a lock-and-key type mechanism where specifically expressed cell adhesion receptors form precise adhesions with relevant surfaces. The main mediators of cell adhesion are integrins, immunoglobulins domain proteins, lectins and cadherins (Alberts et al., 2002). Another lesser-known and lesser-studied adhesion occurs through weaker carbohydrate-carbohydrate interactions (Boggs et al., 2008; Bucior and Burger,

2004; Fernandez-Busquets et al., 2009; Sackmann and Bruinsma, 2002).

1.4.1 INTEGRINS

Integrins, the best understood of cell adhesion receptors, mediate a diverse range of biological functions and exhibit a variety of attachment strengths and time-scales (Evans and Calderwood, 2007; Parsons et al., 2010). Integrins can form cell-cell adhesions when binding to members of the immunoglobulin superfamily, or they can form cell-substrate adhesions by adhering to the carbohydrate-rich extracellular matrix, typically made up of collagen, fibronectin and/or laminin. Formed by the non-covalent linkage of membrane spanning α and β subunits, integrins connect intracellular and extracellular domains by transmitting information in both directions through their conformation and binding ability (Evans and Calderwood, 2007; Hynes, 2002; Parsons et al., 2010). Integrin-based adhesions are sensitive to extracellular Ca^{2+} and Mg^{2+} through binding sites for these divalents in their extracellular domains. The intracellular domain of the β-subunit mediates the connection of integrins to the actin-based cytoskeleton through intracellular anchor proteins such as talin, α-actinin, and filamin.

1.4.2 CADHERINS

Cadherins, named for 'Ca^{2+}-dependent adhesion,' are molecules from a large superfamily that bind to one another on opposing cell membranes in a manner sensitive to extracellular Ca^{2+} (Alberts et al. 2002; Kemler, 1993). There are tissue-specific subfamilies of cadherins: E-cadherins in epithelial tissue and

N-cadherins in neuronal tissue, though other non-classical cadherins are also expressed in these tissues as well. Cadherin molecules have a small intracellular domain, a transmembrane domain and a variable number of repeating extracellular cadherin domains. Similarly to integrins, cadherins also connect to the cytoskeleton intracellularly through anchors proteins, in this case, catenins. These outside-in and inside-out connections allow signaling between intracellular and extracellular domains. Cadherins play a special role in hearing, with a dimer of cadherin-23 and dimer of protocadherins-15 forming the tension-transducing element of the hair bundle, the tip link (Kazmierczak et al., 2007; Siemens et al., 2004).

1.4.3 LECTINS AND SELECTINS

Lectins are highly variable but extremely specific glycan-binding proteins found in both animals (selectins) and plants (lectins) (Alberts et al. 2002; Gabius, 2009; Gabius et al., 2002). Lectins are often transmembrane proteins expressed on a cell's surface that bind specific sugar moieties in the surrounding plasma or on other cell surfaces. Selectins play an important role in getting white blood cells in and out of injured tissue through a process called leukocyte rolling. In the event of inflammation, endothelial cells express P-selectins sensitive to the glycans present on leukocytes in order to recruit them. Once leukocytes attach weakly, they are pushed by fluid flow, making and breaking weak carbohydrate-selectin attachments until their target is reached. Lymphoctyes can also express L-selectins that recognize certain glycans expressed by endothelial cells allowing

them to adhere inside blood vessels. Selectins play important roles in the liver, sensing the presence of various carbohydrates in serum (Ashwell, 1982). Lectins and selectins are also widely used by humans, with applications ranging from determination of ABO blood types to bio-terrorism (Endo et al., 1987). Lastly, lectin binding can be selectively blocked by pre-adsorption of certain carbohydrates.

1.4.4 IMMUNOGLOBULIN SUPERFAMILY

Immunoglobulin superfamily (IgSF) cell adhesion molecules, unlike integrins, cadherins, and lectins, form adhesions though to be more insensitive to Ca^{2+} and Mg^{2+}. IgSF cell adhesion molecules are defined as having one or more Ig-like domains characteristic of antibody molecules (Alberts et al. 2002; Williams and Barclay, 1988). While integrins and lectins are heterophilic and cadherins are homophilic, IgSF adhesion molecules can either bind each other, as in the case of NCAMs, or they can bind other molecules, as in the case of SIGLECs, lectin-like Ig proteins that bind sugar moieties.

1.4.5 CARBOHYDRATE-CARBOHYDRATE ADHESION

Another realm of biologically relevant cell adhesion is mediated by weak polyvalent interactions (Boggs et al., 2008; Bucior and Burger, 2004; Pincet et al., 2001). Complex carbohydrates, glycoproteins, glycolipids and proteoglycans, adorn all cell surfaces and constitute the most prominent class of cell surface molecule (Gabius, 2009). There is growing evidence that these molecules themselves can bind to each other to form functional cell–cell interactions (Boggs

et al., 2008; Boubelik et al., 1998; Bucior et al., 2004; Pincet et al., 2001; Santacroce and Basu, 2004; Todeschini and Hakomori, 2008). At present, only a few examples of low-affinity carbohydrate–carbohydrate interactions are known (Boubelik et al., 1998; Bucior et al., 2004; Eggens et al., 1989; Geyer et al., 2000; Hakomori, 2002; Haseley et al., 2001; Kojima et al., 1994; Santacroce and Basu, 2004). A beautiful example from the natural world is that of sponge cells: when cells from different species are dissociated and put together in a Ca^{2+}-rich environment, they self-associate with their own species using large, branched, species-specific proteoglycans (Haseley et al., 2001). One type of adhesion termed a glycosynapse is a glycosphingolipid self-interaction shown to occur through multivalent interaction of Lewis X carbohydrates (Boggs et al., 2008; Hakomori, 2002).

In sum, a variety of mechanisms enable cell-cell adhesion; most biological cell-cell adhesion utilizes strong, stable, cell-cell attachments. The type of cell adhesion between the distal tips of stereocilia is likely to have different qualities. The apposing stereociliary membranes must be tethered but their point of connection must be able to change: either with an *elastic connection*, with an extremely *stiff connection able to slide* through the plasma membrane when force is applied, or with *weak but numerous connections* that can be easily broken and reformed.

1.5 THE GLYCOCALYX

The stereociliary membranes of the hair bundle are coated with a layer of sugars (Santi and Anderson, 1987; Tsuprun and Santi, 2002). In fact, all cells found in nature display an outer layer of glycans and glycoconjugates that together form the glycocalyx, from the greek words meaning 'sugar' and 'shell' (Pries et al., 2000; Varki, 2007). The glycocalyx is made up of three main types of molecules, membrane-bound glycoproteins, secreted proteoglycans, and glycolipids (Figure 1.7). In general, many proteins are glycosylated, especially extracellular and secreted proteins (Alberts et al. 2002; Gabius, 2009; Varki, 2007). The glycans that decorate proteins typically reside on the protein's outer folds. Thus, both at the level of the protein and at the level of the cell, glycans are in the powerful position at the interacting surface, able to modulate and mediate a variety of processes. Given the enormous importance of protein-protein interactions in molecular biology and cell-cell interactions in development and physiology, it is a wonder that glycobiology is not more in the research limelight.

The main reason that the study of glycans has not yet flourished in comparison to that of amino or nucleic acids is because glycans exhibit great combinatorial diversity combined with poorly understood function, making decoding the immense biological diversity of glycans and glycoconjugates that much more difficult. A few simple points of variation: glycan chains can be either linear or branched, glycosidic linkages can be either α- or β-linkages, glycans can be acetylated or sulfated, and there are approximately 20 monosaccharide

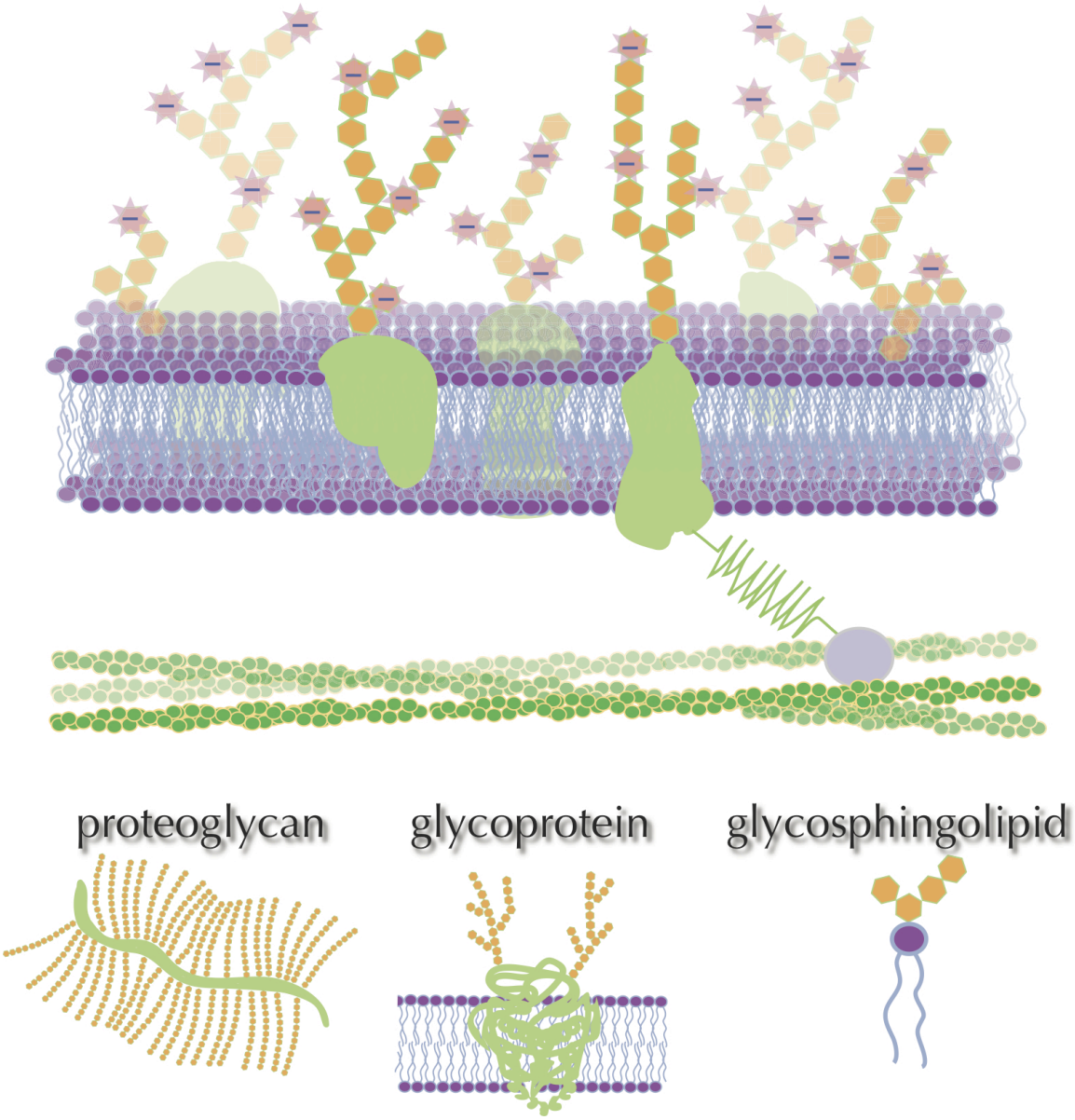

Figure 1.7: The glycocalyx. The glycocalyx is a collection of sugars groups from different underlying components on the cell's outer surface. The main components of the glycocalyx are proteoglycans, glycoproteins and glycolipids. Generic sugar rings are depicted in orange, protein green, membrane phospholipids purple.

building blocks to choose from (Varki, 1999). Consequently the potential range of codeable variation in glycobiology is enormous. Unfortunately, given all of these points of variation and the possibility of many conformations for each carbohydrate ring, complex structural predictions and molecular dynamics are currently out of the question.

While little is known specifically about the sugars of the stereociliary glycocalyx, typical glycocalyx components, glycoproteins, glycolipids, and proteoglycans, are generally known to vary in their sugar composition (Gabius, 2009). Transmembrane and membrane-associated proteins are typically glycosylated with *N*-linked sugars, pre-built structure often made up of approximately 14 sugar rings, typically, mannose, N-acetylglucosamine, N-acetylgalactosamine, fucose and sialic acid residues. Secreted proteoglycans are more typically glycosylated with O-linked sugars, which are built up ring by ring on the protein. The most common O-linked sugar is N-acetylgalactosamine, making up 'mucin-type' glycans. This reducing terminal N-acetylgalactosamine residue is sometimes also decorated with galactose, N-acetylglucosamine, and sialic acid residues. Proteoglycans generally have a much higher carbohydrate-to-protein ratio than do glycoproteins. Glycosphingolipids also contribute to the glycocalyx, particularly in neural tissue. Gangliosides are complex glycosphingolipids with a ceramide backbone typically connected to 3-6 esterified sugars, one of which, a sialic acid.

While glycobiology is less studied at the moment, it has provided valuable

tools in decades past, enabling some course description of the hair bundle's glycocalyx. When labeled with polycationic dyes such as Alcian blue and Ruthenium red, hair bundles appear coated with a negatively charged glycocalyx (Santi and Anderson, 1986, 1987; Tsuprun and Santi, 2002), though measures of glycocalyx thickness varied. In fact, routine electron microscopy is unlikely to yield an accurate measure of glycocalyx length because charged structures like the glycocalyx often collapse under the strong chemical treatments used in sample preparation. A number of groups have labeled auditory structures with glycan-binding lectins, again yielding variable results (Baird et al., 1993; Gil-Loyzaga and Brownell, 1988; Katori et al., 1996b; Sugiyama et al., 1991; Warchol, 2001). Labeling of mammalian hair bundles with wheat germ agglutinin lectin (Gil-Loyzaga and Brownell, 1988; Katori et al., 1996b) suggests the presence of keratan sulfate proteoglycans (KSPGs). KSPGs are found in a number of highly lubricated structures, for example, the cornea of the eye. They are also found in the tectorial membrane of the mammalian cochlea. The high-molecular-weight and highly glycosylated tectorial membrane component tectorin, may itself be a KSPG (Killick and Richardson, 1997). Using antibody labeling, the presence of keratan sulfate on mammalian stereocilia was confirmed, particularly at the distal tips of stereocilia (Katori et al., 1996a). Sialyl Lewis X (sLe^x), a tetrasaccharide carbohydrate often implicated in cell-cell adhesion and immune recognition, was also found to localize specifically near the distal tips of sensory inner hair cell stereocilia (Hozawa et al., 1993).

What are the functional properties of this glycocalyx? In physical terms, the glycocalyx can be thought of as a charged polymer brush, composed of many surface-bound branched chains made up of smaller subunits, some of which are negatively charged. Charged polymer brushes are one of the most well lubricated molecular-scale systems studied to date (Klein et al., 1993; Raviv et al., 2003; Tadmor et al., 2003), combining the lubricating electrostatic properties of like-charged surfaces and the lubricating entropic properties of polymer brushes. These properties are useful to the hair bundle because hydrophobic lipid membranes in close apposition often fuse if not held apart, especially if they undergo fast shearing motions at their points of close apposition. When high shear velocity is paired with friction, the energy lost to heat per cycle $P_{friction}$ is proportional to the square of the stimulation frequency ω:

$$\left\langle P_{friction} \right\rangle = \frac{\omega^2 \xi x_0^{\,2}}{2}$$

where ξ is the coefficient of friction and x_0 is the amplitude of movement. If much energy is lost to heat, membranes will warm and become more prone to fusion. In the most extreme circumstances—loud, high-frequency stimulation of a mammalian hair cell—the shear velocity reaches 3 mm·s^{-1}, a movement fast enough to strike a match! No other organelle in multicellular organisms is known to display motions of such velocity. One way to reduce the amount of energy lost to heat is to reduce ξ by increasing lubrication. The like-charged polymer brushes of apposing stereociliary glycocalyces may provide this lubrication to the oscillating hair bundle.

As I've tested here, apposing glycocalyces may provide anchor points to tether neighboring stereocilia and provide cohesion to the hair bundle. Divalent-mediated tethering between polymer-brush-coated surfaces has not been theoretically analyzed but it is known to occur in biology. For example, in sponges, Ca^{2+} ions tether large proteoglycan molecules emerging from the surfaces of opposing cells (Bucior et al., 2004; Dammer et al., 1995; Pincet et al., 2001). Another example of strong connections between carbohydrates is the glycosphingolipid-based glycosynapse between metastatic cancer cells (Hakomori, 2002). Carbohydrate-carbohydrate adhesion often occurs through multivalent-ion-dependent tethering (Boubelik et al., 1998; Fernandez-Busquets et al., 2009; Kojima et al., 1994).

1.6 SUMMARY

The life-long functioning of our auditory sensory cells requires that the rigid, rodlike stereocilia in a mechanosensory hair bundle maintain cohesion as they shear against one another during the bundle's oscillation in response to sound. When hair-bundle cohesion is mildly compromised, mechanotransduction is less efficient. More extreme, damage-induced loss of cohesion causes hair-cell death and permanent hearing loss. The mechanism of this cohesion is unknown, in part because no measurements have been made heretofore of the adhesive forces between stereocilia. In this work, I have proposed and tested the hypothesis that divalent-mediated tethering of glycans in the glycocalyces of apposed

stereociliary membranes provides part of the adhesive force that maintains hair-bundle cohesion.

2 MATERIALS AND METHODS

2.1 TISSUE DISSECTION

Adult anoles (*Anolis carolinensis*, Carolina Biological Supply Co.) and tokay geckos (*Gecko gekko*, LLL Reptile) were injected intraperitoneally with a lethal dose, approximately 30 $mg \cdot kg^{-1}$ of sodium pentobarbital (Nembutal, Abbott Laboratories). After decapitation, the lower jaw was removed to expose the ventral floor of the skull and the cochleae were dissected (Figure 2.1). The sacculi of American bullfrogs (*Rana catesbeiana*) were obtained as described (Kozlov et al., 2007).

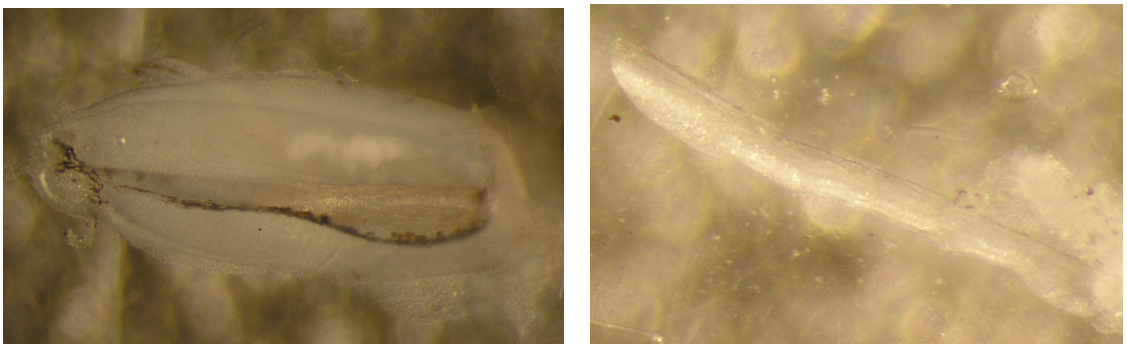

Figure 2.1: The cartilaginous cochlear limbus surrounds the basilar papilla of the gecko (left); the isolated basilar papilla, approximately 1.5 mm in length, is composed mostly of hair cells (right).

2.2 ELECTROPHORESIS

The isolated basilar papilla of a gecko or anole or the sacculus of a bullfrog was placed on a glass slide with approximately 20 μl of the solution to be tested. The tissue was covered with a coverslip that was then slid back and forth over the

papilla to dissociate stereocilia. Alternatively, the tissue was manipulated against the slide with forceps as indicated in the section on stereociliary isolation. The stereocilia-containing fluid was pipetted into a square glass capillary tube with a hydrophobic surface (Sigmacote, Sigma). Measuring electrodes (Teflon-coated silver wire, Medwire) were inserted into the two ends of the capillary, which was then placed into a pre-cooled plastic chamber. Each end of the capillary was covered and secured with 1% low-melting point agarose of the same ionic strength and osmolarity as the solution to be tested; the center of the capillary remained optically accessible. After the compartments holding each end of the capillary were filled with the solution to be tested, driving electrodes, silver-silver chloride electrode pellets (A–M Systems), were inserted into the fluid. While a power supply applied a voltage of 60 V between these electrodes, stereocilia were imaged with an upright microscope with a 40X objective lens and differential-interference-contrast optics. The voltage V and distance d between the two measuring electrodes were determined. Video recording of the migrating stereocilia allowed individual stereociliary velocities v to be recorded. The electrophoretic mobility μ was then calculated as:

$$\mu = \frac{vd}{V}.$$

During each experiment, after approximately five minutes of observation with a voltage of one polarity, the polarity was reversed and migrating stereocilia were observed for another five minutes.

2.3 LECTIN LABELING

The isolated auditory organs of tokay geckos or anoles were incubated for one hour in artificial endolymph with 20 $\mu g \cdot mL^{-1}$ of a FITC-conjugated lectin (EY Labs). The tissue was washed with artificial perilymph, fixed with 4% formaldehyde for 30 minutes, and mounted in Vectashield for confocal imaging. For phalloidin-labeled papillae, fixation was performed in 4% formaldehyde with 0.1% Triton-X-100, and papillae were subsequently incubated for 45 min with 40 $\mu g \cdot mL^{-1}$ of fluorophore-conjugated phalloidin before mounting and visualization. The entire procedure was conducted at room temperature.

For the cholera toxin B subunit images, anole papillae were incubated with 1 mM biotinylated-cholera-toxin B subunit in artificial anole perilymph for 10-15 minutes, then with streptavidin-conjugated quantum dots for 10 minutes. Images were acquired with a 2-photon microscope built and operated by Dr. Samuel Lagier.

2.4 DEGLYCOSYLATION

Anole basilar papillae were incubated for 1 hour at 30°C in 1 mL of artificial endolymph containing 100 μL of 10x G7 buffer solution (New England BioLabs) and 20,000 units of PNGaseF (New England BioLabs). Papillae were then washed and dissociated in the appropriate solution.

2.5 ISOLATION OF STEREOCILIA FOR MANIPULATION

The auditory organ was moved to the coverslip bottom of an experimental chamber that had been rendered hydrophobic (Sigmacote, Sigma), and covered with approximately 500 μL of the solution to be tested. The basilar papilla was separated from the surrounding limbic structures with forceps and a 26-gauge needle. The tissue was then pressed against the bottom of the chamber with the hair bundles down and gently rubbed until it was completely dissociated. The stereocilia were allowed to settle for approximately five minutes. The stereocilia were stable for over 4 hr except for those bathed in low-ionic-strength medium, which began to bleb after 2 hr.

2.6 FORCE-FIBER FABRICATION

Flexible stimulus fibers were fabricated from borosilicate glass rods 1.2 mm in diameter (World Precision Instruments). Each fiber was first reduced with an electrode puller, then pulled still finer in a direction perpendicular to its shank (Howard and Hudspeth, 1988). To facilitate measurement of the fiber tip's position, the fiber's optical contrast was increased by a 100-nm coating of gold-palladium (Hummer 6.2, Anatech). Fibers were trimmed with fine forceps until their stiffnesses were 100-300 $\mu N \cdot m^{-1}$ and their damping constants were 70-300 $nN \cdot s \cdot m^{-1}$, as determined by analysis of the power spectrum of Brownian motion in water (Benser et al., 1996; Howard and Hudspeth, 1988).

2.7 EXPERIMENTAL PROCEDURE

Preparations were observed with a mechanically stabilized upright microscope (Olympus BX51WI) equipped with differential-interference-contrast optics and a 40X water-immersion objective lens (LUMPlanFI/IR, NA 0.80). Stereocilia were illuminated by a low-noise 200 W mercury arc lamp (X-cite exacte). To minimize mechanical noise, the microscope was mounted on an internally damped, air-suspended table (Cleantop II, TMC) within an acoustically and seismically isolated room. For photodiode measurements, the diffusing filter, polarizer, and analyzer were removed to increase the illumination.

In each experiment, a force fiber was mounted horizontally at its base in a holder attached to a piezoelectrical actuator that was in turn secured to a micromanipulator. Stereocilia were manipulated and the associated movements were measured with a photodiode system. The stiffness of each fiber was measured (Benser et al., 1996) before every experiment: when the fiber had a stereocilium attached and was within 20 μm of the experimental chamber's bottom. A piezoelectric actuator (Physik Instrumente) was used to displace the fiber's base to deliver mechanical stimuli to the tip and thus to the attached stereocilium. The actuator was driven by a matched power supply (E-663, Physik Instrumente). The micromanipulator (ROE-200, MPC-200, MP-285, Sutter Instruments) produced vertical movements in steps of 62.5 nm. The image of the fiber's tip was magnified 1,000x and projected onto a dual photodiode connected

to a circuit that calculated the normalized difference between the amounts of light falling on the two halves. Force-fiber displacement was calibrated before measurements from each pair of stereocilia by using a calibration piezoelectrical actuator (P-840.60 with power supply E-663, Physik Instrumente) to offset the fiber's image over the photodiodes by known distances. Before each individual recording, the fiber's image was moved by a known distance and the photodiodes' voltage output was recorded for calibration.

For each pair of stereocilia, recording began with the fiber's tip and attached stereocilium 1-3 μm above the level at which the two stereocilia would contact. The stereocilium-endowed fiber descended in 125 nm steps, moving back and forth in 1 Hz triangle waves at each vertical position until contact was achieved, at which point 18-30 further triangle waves were recorded. The procedure was repeated with increasing normal force at intervals of -125 nm to an final offset of -500 nm. Contact was defined as noticeable change in stiffness or dissipation. Each stereocilium was used only once. The data for each condition were obtained from five to nine stereociliary pairs, with the exception of EDTA, which involved only three.

2.8 ANALYSIS

Stimuli were presented and data acquired with LABVIEW (version 8.6, National Instruments). Measurements of the commanded displacements and fiber movements were sampled at 100 μs intervals. Data were analyzed in Matlab R2010a.

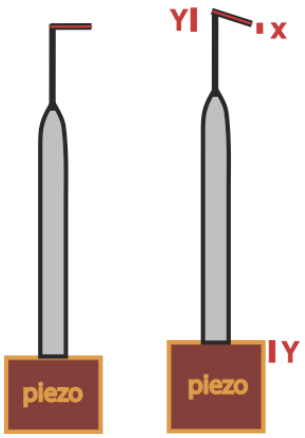

Figure 2.2: Force-fiber stimulation and flexion. A piezoelectrical actuator is used to displace the force-fiber base by a distance Y. If the tip of the force-fiber encounters no opposing force, the tip will also move by the distance Y. Alternately, if there is an opposing force the tip will only move by a distance X. The force applied to the fiber's tip can be found from the fiber's stiffness and the difference between Y and X.

The force *F* exerted by the fiber was given by $F = K(Y - X)$, in which K is the fiber's stiffness, *Y* the displacement at fiber's base, and *X* the displacement at the fiber's tip. The energy *W* dissipated by hydrodynamic drag on the fiber and attached stereocilium was estimated from the relation $W = 16\xi\hat{X}^2/T$, in which ξ is the drag coefficient, $\hat{X}$ the peak-to-peak displacement of the fiber's tip, and *T* the period. This value was subtracted from the total dissipation measured during each cycle.

The adhesion between stereocilia was computed by determining the slope of a straight-line fit to the displacement-force relation with a first-order least-squares algorithm (polyfit, Matlab). Dissipation was calculated from the area within the hysteresis loop of the displacement-force data (polyarea, Matlab).

Power laws were fit and *p*-values determined using a published algorithm and associated MATLAB programs (http://tuvalu.santafe.edu/~aaronc/powerlaws/(Clauset et al., 2009). Fitting was done using maximum likelihood and the Kolmogorov-Smirnov test was used to

compute a *p*-value for the estimated power-law fit. Log-normal and stretched-exponential fits were also compared to the data, but neither fit was superior to the power law.

2.9 DETECTION OF STICK-SLIP EVENTS

To find steps corresponding to stick-slip events, we compared the means of the data in two adjacent time windows. The algorithm required that the data be sampled at equal intervals and that they be normally distributed within a sufficiently small time window, a stipulation that could be confirmed *a posteriori*. The data were not assumed to be drawn from distributions with the same variance, for the external force applied to the stereocilia might alter the distribution of fluctuations.

The time series corresponding to each triangle-wave cycle was separated into its three constant-velocity sections, the corners were discarded, and the sign of the middle section was inverted such that the mean position decreased with time. Two non-overlapping, contiguous, 30 ms windows were moved across each section of the displacement record in steps of one point, and the means of the two windows were compared. We wished to test the null hypothesis that $m_1 - s_{\min} = m_2$ against the alternative that $m_1 - s_{\min} > m_2$, in which m_1 is the mean of the data in the first window, m_2 is the mean of the data in the second window, and $s_{\min}$ is a lower bound on the slip size. Including a larger number N of data points in a window produced better estimates for the mean of the data in that

window but degraded the temporal resolution. Applying the two-sample, one-tailed Welch's *t*-test to compare the data windows yielded a *p*-value representing the probability of obtaining the test result if the null hypothesis were correct. This test does not assume the same variance for each time window; instead, the change in force at a slip implied that the variances would differ.

By advancing in steps of one point and comparing the two windows, we generated a series of *p*-values corresponding to each test along the time series. If the local minima in this series were $\{p_j^{min}\}$, steps occurred at the times corresponding to $p_j^{min} < p_{th}$, in which p_{th} was a threshold significance level of 10^{-40}. These *p*-value extrema were found using the MATLAB extrema function. The difference between the mean values in the two windows at a given slip event provided the slip size and the force corresponding to the mean value in the first window constituted the rupture force.

2.10 IONIC CONDITIONS

Artificial endolymph contained 170 mM KCl, 2 mM NaCl, 3 mM D-glucose, 1 mM creatine, 1 mM sodium pyruvate, and 5 mM HEPES with a pH of 7.3 and an osmolality of 360 mOsmol·kg^{-1}. The Mg^{2+} and Ca^{2+} in the solution were only trace amounts contaminating the monovalent salts, likely less than 10 μM (Freeman et al., 1994; Freeman et al., 1993). For the EGTA, EDTA, or gentamicin condition, 1 mM of the substance was included in the artificial endolymph. The low-ionic-strength solution contained 5 mM KCl, 350 mM D-mannitol, 1 mM

EGTA, and 5 mM HEPES. The pH was not adjusted from 5.5 so that the low ionic strength would not be compromised. Low-Ca^{2+} and low-Mg^{2+} solutions contained artificial endolymph plus 250 μM of the relevant ion. The high-Ca^{2+} and high-Mg^{2+} solutions contained an additional 4 mM of $CaCl_2$ or $MgCl_2$. Solutions used in electrophoresis experiments contained 5-150 mM NaCl, 250 μM $CaCl_2$, 5 mM HEPES, and D-mannitol to maintain a constant osmolality of 240 mOsmol·kg^{-1}.

2.11 Size Exclusion

Anole basilar papillae were isolated and incubated in endolymph with 1 mM di-8-ANEPPS (Sigma) for 10 min. After a wash in endolymph, papillae were placed into endolymph supplemented with 500 μM·mL^{-1} of 70,000 MW fluoroscein dextran and imaged by confocal microscopy.

2.12 Immunohistochemistry

Anole papillae were isolated and fixed for 2 hr in PBS, 0.1% Triton-X-100, with 4% formaldehyde at room temperature. After blocking for 1 hr in 20% goat serum, 1% BSA, and 0.1% Triton-X-100, papillae were incubated with primary antibodies against stereocilin and acetylated-tubulin overnight at 4°C. The stereocilin antibody was graciously provided by E. Verpy and C. Petit (Verpy et al., 2008). After washing three times in PBS, the papillae were incubated with secondary antibodies for 2 hr. During the last 30 min of this incubation the solution

was supplemented with 40 $\mu g \cdot mL^{-1}$ of fluorophore-conjugated phalloidin. The papillae were then washed, mounted in Vectashield, and imaged by confocal microscopy.

3 THE STEREOCILIARY GLYCOCALYX

3.1 INTRODUCTION

In order to demonstrate the role of divalent-mediated tethering of glycocalyces in hair bundle cohesion we must first demonstrate that the glycocalyx varies along the length of stereocilia and that the stereociliary glycocalyx is indeed negatively charged. As previously mentioned, a number of groups have labeled auditory structures with lectins to assess the presence of various sugars (Baird et al., 1993; Furness and Hackney, 1985; Gil-Loyzaga and Brownell, 1988; Goodyear and Richardson, 1994; Sugiyama et al., 1991; Warchol, 2001), but few have studied variation along individual stereocilia.

A number of groups have remarked on the importance of the negatively charged glycocalyx in the maintenance of structural integrity in the hair bundle (Dolgobrodov et al., 2000; Neugebauer and Thurm, 1986). Due to its extensive labeling with polycationic dyes, the hair bundle's glycocalyx is thought to be negatively charged (Santi and Anderson, 1986, 1987; Tsuprun and Santi, 2002). Additionally, the application of multivalent cations often results in stereociliary fusion (Furness and Hackney, 1986; Neugebauer and Thurm, 1987; Takumida et al., 1989a; Takumida et al., 1989b). In spite of these indications, quantitative data on stereociliary charge has not yet been put forth.

3.2 THE STEREOCILIARY GLYCOCALYX IS A NEGATIVELY-CHARGED POLYMER BRUSH

To address the functional role of the stereociliary glycocalyx in the cohesion and alleviation of friction in the hair bundle, we first characterized the electrostatic properties of the glycocalyx. The surface sugars of the glycocalyx can be characterized by electrophoresis, wherein particles in an electric field migrate at varying speeds depending on the thickness, density and quantity of charge on the particle's surface. A small, smooth, charged object migrating in an electric field in solutions of varying ionic strength follows the classic Smoluchowski relation:

$$\mu = \frac{U}{E} = \frac{\zeta}{\eta\kappa}$$

in which μ is the electrophoretic mobility, U the velocity, E the electric field, ζ the electrokinetic potential or charge density, η the viscosity of the solution, and κ^{-1} the Debye length (Figure 3.1). The Debye length is the distance from a given charge at which its electric field is shielded by counterions, given by:

$$\kappa^{-1} = \sqrt{\frac{\varepsilon_r \varepsilon_0 k_B T}{2 N_A e^2 I}}$$

where I is the ionic strength of the solution, ε_0 the permittivity of free space, ε_r the dielectric constant, k_B Boltzmann's constant, T temperature, N_A Avogadro's number and e the elementary charge. The Debye length decreases with increasing ionic strength. An object coated in a charged polymer brush, such as

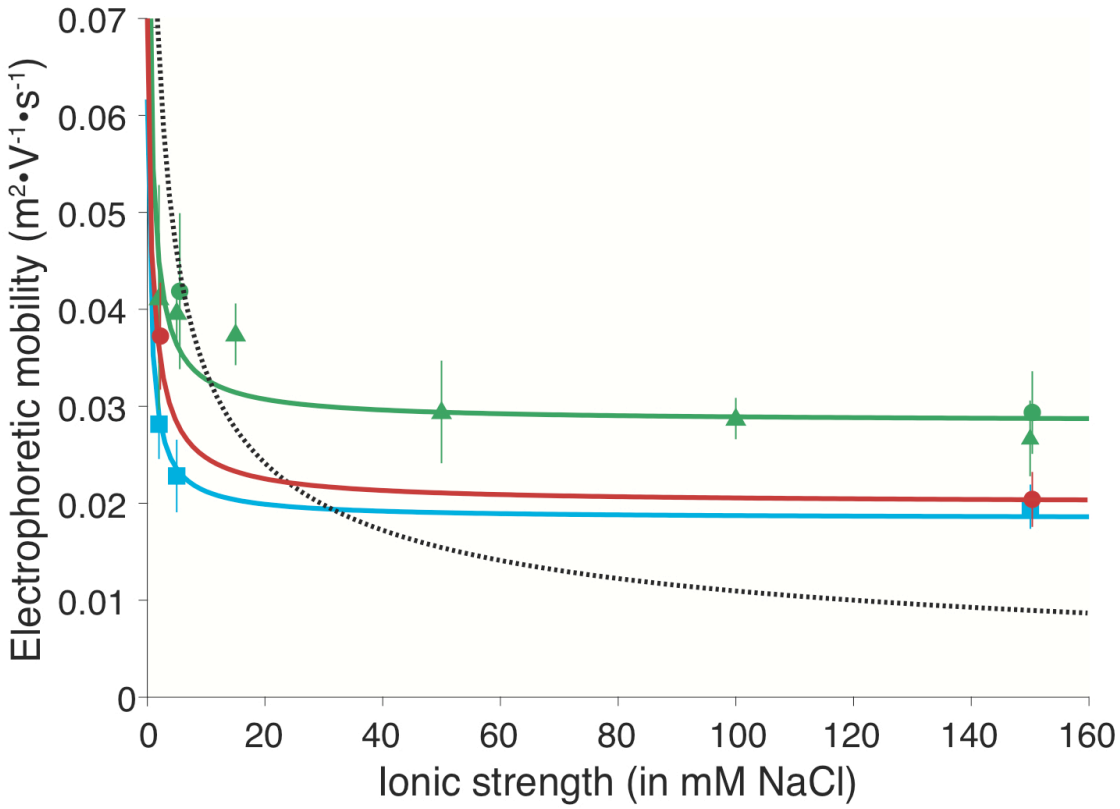

Figure 3.1: Electrophoretic mobilities calculated from capillary electrophoresis of individual stereocilia from different species at varying ionic strengths. The dashed black line is the prediction based on the classical model for a smooth charged particle. The three solid lines represent fits to the model for particles coated in a charged polymer brush (Levine et al., 1983). The uppermost line (green) shows fits to the data from geckos (triangles) and anoles (circles); the same charge density was used for the fit to the classical model. The middle line (red) shows the effect of deglycosylation on anole stereocilia (circles). The bottom line (blue) present results from the frog (squares). Data are presented as means $\pm$ SEMs of approximately 50 measurements of individual stereocilia in each of one to five experiments.

the glycocalyces of erythrocytes and stereocilia, fits an alternative relation that incorporates the Debye-Hückel, Navier-Stokes, and Poisson-Boltzmann equations (Levine et al., 1983; Wunderlich, 1982):

$$\mu = \left(\frac{-\sigma}{2\beta\eta\kappa^2}\right)\left\{\begin{array}{l}\left(1-e^{-2\beta\kappa}\right)\left(1+\dfrac{\kappa\tanh\beta\gamma}{\gamma}\right)+\left(\dfrac{2\kappa^2}{\gamma^2}\right)\left(1-\dfrac{1}{\cosh\beta\gamma}\right) \\ \quad +\left(\dfrac{\kappa^2}{\kappa^2-\gamma^2}\right)\left[1+e^{-2\beta\kappa}-\dfrac{\kappa\left(1-e^{-2\beta\kappa}\right)\tanh\beta\gamma}{\gamma}-\dfrac{2e^{-\beta\kappa}}{\cosh\beta\gamma}\right]\end{array}\right\}.$$

Here β is the thickness of the glycocalyx, γ is a frictional interaction constant defined by

$$\gamma = \sqrt{6\pi aN}\,,$$

in which *a* is the mean radius of the filaments in the charged polymer brush and *N* is the average number of polymer segments per unit volume. An important qualitative difference between the smooth and polymer-brush models is that the electrophoretic mobility of a smooth particle approaches zero with increasing ionic strength, whereas a glycocalyx-coated particle has a non-zero electrophoretic mobility at all ionic strengths. This asymptote in mobility is due to the charged residues internal to the glycocalyx, which cannot be fully shielded by counterions owing to steric hindrance.

To quantify the charge on the stereociliary glycocalyx, we performed capillary electrophoresis in solutions of varying ionic strength on stereocilia isolated from hair cells of the basilar papilla of the tokay gecko (*Gekko gecko*). These stereocilia were used for two reasons. First, owing to their large size, they are easily identifiable by differential-interference-contrast microscopy. Second,

tokay geckos can hear frequencies at least as great as 6 kHz, higher than most other reptiles and amphibians (Brittan-Powell et al., 2010; Manley, 1972), so their hair bundles are representative of those sensitive to moderately high frequencies (Manley, 2000). We also made mobility measurements on stereocilia from the basilar papilla of the anole (*Anolis carolinensis*) and the sacculus of the bullfrog (*Rana catesbeiana*), which sense frequencies ranging from 1-7 kHz (Brittan-Powell et al., 2010) and 10 Hz-1 kHz (Corey and Hudspeth, 1983a), respectively.

All stereocilia tested complied better with expectations for a particle coated with a charged polymer brush (Levine et al., 1983) than with those for a smooth charged particle (Figure 3.1). Both anole and gecko stereocilia exhibited a higher charge density than frog stereocilia. To confirm that we indeed assayed the effects of the stereociliary glycocalyx, we measured the electrophoretic mobility of stereocilia whose glycocalyces had been partially removed by exposure to the endoglycosidase PNGaseF. The electrophoretic mobility of glycosidase-treated anole stereocilia was decreased to the approximate level of frog stereocilia (Figure 3.1).

During electrophoresis experiments, stereocilia consistently oriented with their long axes parallel to the electric field. Upon reversal of the field, individual stereocilia often reoriented by 180° while changing direction, indicating that one end was more charged than the other. Experiments with anole stereocilia, in which the blunt distal tips are clearly distinguishable from the tapered bases,

revealed that the tip is the more negatively charged end (Figure 3.2). It is notable that the forward-directed end of the stereocilium is not the end favored hydrodynamically, indicating that stereocilia do not reorient for hydrodynamic reasons.

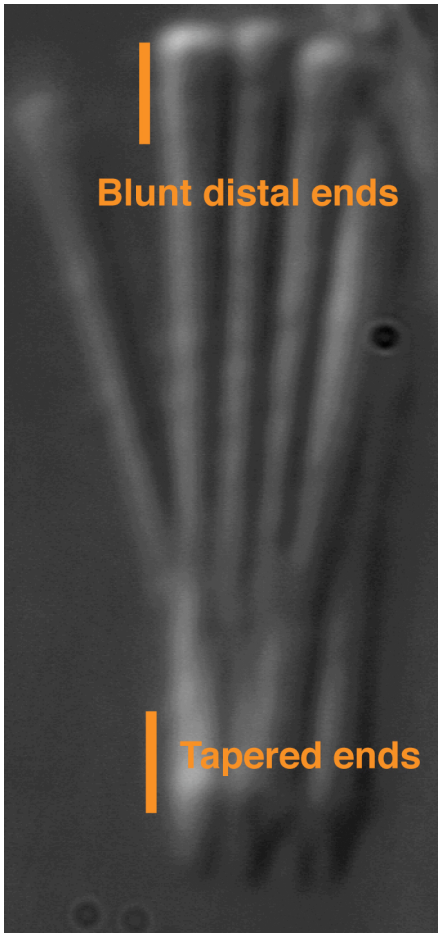

Figure 3.2: An isolated anole hair bundle. Blunt distal tips and tapered ends of anole stereocilia. As opposed the more well-known stereocilia of the frog sacculus, anole stereocilia become wider toward their distal ends. Anole hair bundles are free-standing stimulated only by fluid movement, while frog saccular hair bundles are tethered to an overlying tectorial structure.

3.3 VARIATION IN GLYCANS ALONG STEREOCILIA

3.3.1 LECTIN LABELING

To further explore variation along the length of the stereociliary glycocalyx, we labeled hair cells of the Tokay gecko's basilar papilla with a variety of FITC-conjugated lectins and imaged by confocal microscopy. Each lectin that bound stereocilia showed variable binding along the length of stereocilia. Labeling with many different lectins reevaled different collections of sugars in the different regions of the hair bundle, stereociliary tapers, shafts, and distal tips, and kinociliary shafts and bulbs (Figure 3.3, Table 1). In addition to variation within the bundle, we also looked at variation along the basilar papilla. We subjectively quantified lectin binding by fluorescence intensity, where brighter fluorescence indicates either higher concentrations of a relevant sugar moiety in that region of the hair bundle, or greater access to that moiety for the lectin. Lectin sugar specificities were obtained from the lectin source.

Using these fluorescence-based estimates, we roughly determined the glycan representation within the stereociliary glycocalyx of the gecko basilar papilla (Figure 3.4). The glycocalyx appears to mainly consist of negatively charged glycans with a high representation of mannose, GlcNAc, and different types of sialic acid. Stereociliary tapers and kinociliary bulbs were often strongly labeled by the same lectins. A few lectins, *Erythrina cristagalli* lectin and *Maackia amurensis* agglutinin, showed variation in their stereociliary distribution along the

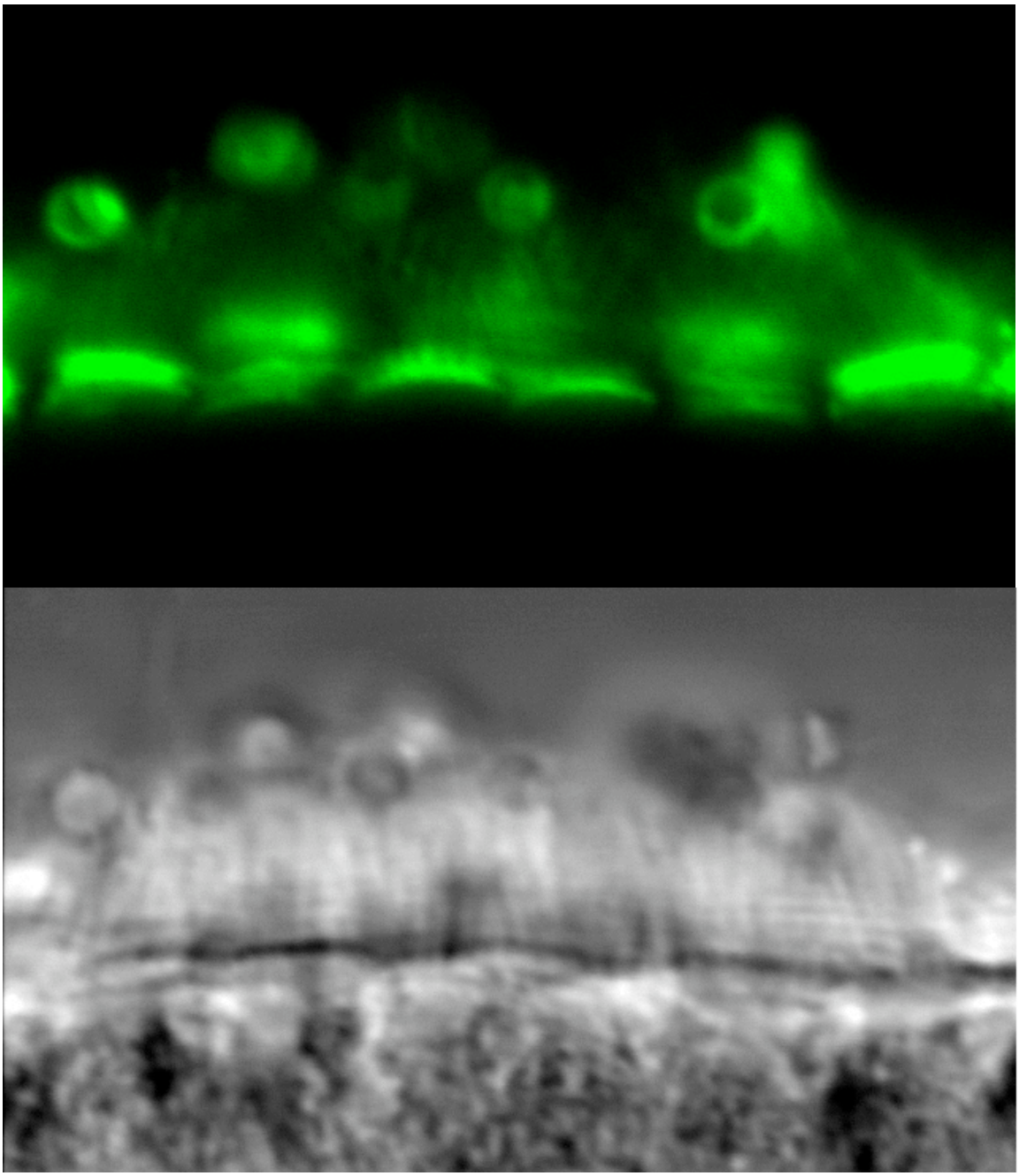

Figure 3.3: *Maackia amurensis* agglutinin labeled hair bundles in the dorsal/basal region of the gecko basilar papilla. Stereociliary shafts are labeled by this lectin with more intense labeling at the taper and kinociliary bulb.

Table 1: Intensity of labeling of different fluorophore-conjugated lectins along the length of stereocilia from the gecko basilar papilla. A rating of 10 corresponds to strong labeling.

Lectin	Taper	Shaft	Tip	Kinocilium	Bulb
Con-A	6	4	5	0	7
DSL	10	5	4	2	8
ECL	2	1	2	2	6
GSL I	0	4	6	0	1
LcH	2	2	2	0	8
LEL	0	0	0	1	1
MAA	10	4	4	2	10
PNA	0	0	0	0	0
SBA	0	0	0	0	2
SJA	0	0	0	0	3
SNA	0	0	1	1	3
STL	2	1	1	3	6
WGA	4	3	4	5	8
GSL II	0	0	0	0	5
CCA	2	1	1	1	0
HMA	0	0	1	5	1
LFA	1	0	1	3	4

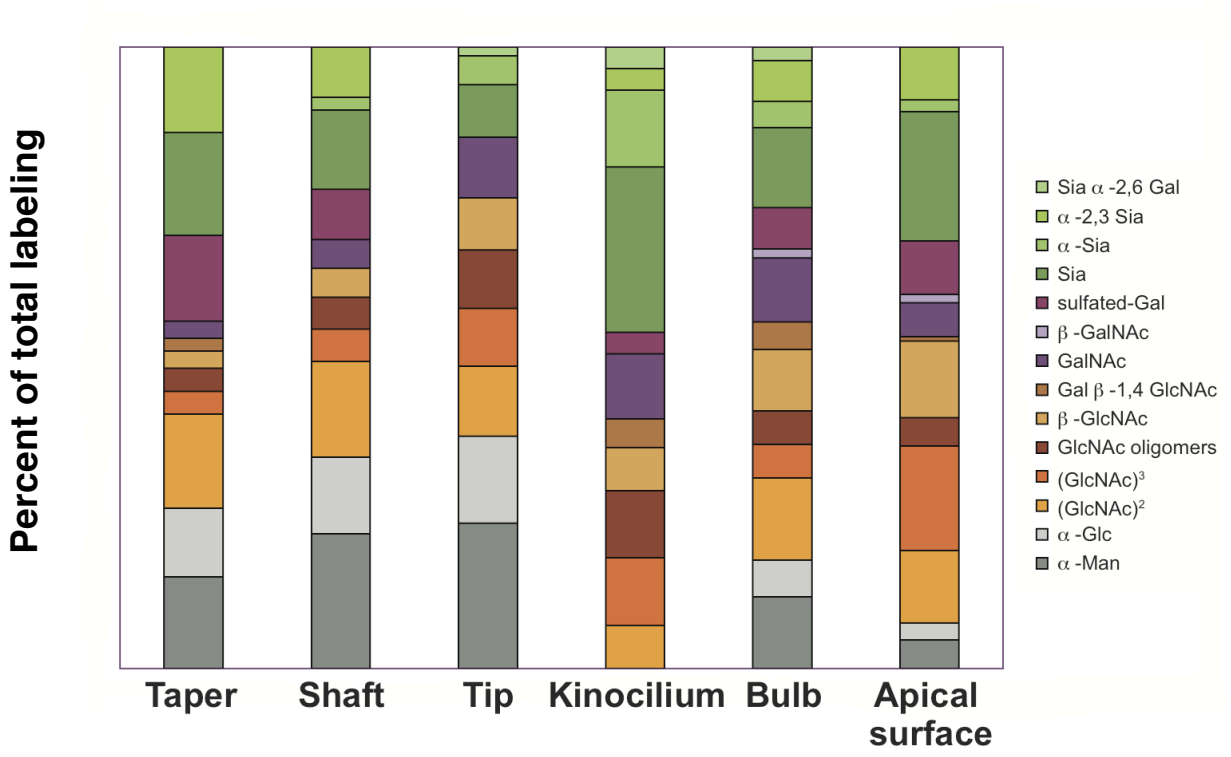

Figure 3.4: Relative intensities of lectin labeling corresponding to different sugar moieties. Sugar types are grouped by color, with uncharged sugars in grey. The kinocilium appears coated with only charged sugars because lectins labeling uncharged sugars labeled stereociliary shafts, making it impossible to distinguish them from the kinocilium.

tonotopic axis. *Erythrina cristagalli* lectin labeled only the kinociliary bulbs of hair bundles at the apical end of the papilla, but labeled all regions of hair bundles, though to differing extents in the basal end of the papilla. The pattern of *Maackia amurensis* agglutinin labeling was similar. Other lectins displayed stranger patterns of labeling: *Homarus americanus* lectin and *Sambucus nigra* lectin labeled the apical surface of what seemed to be a random selection of hair cells (Figure 3.5).

Unfortunately, a number of lectins that are considered to have the same specificity, for example, concanavalin A and *Lens culinaris* lectin or *Solanum tuberosum*, *Datura stramonium,* and *Lycopersicon esculentum* lectins, did not exhibit consistent patterns of labeling. Lectins are highly specific yet the methods of specificity testing do not reflect the biological level of glycan complexity. Regardless, these data indicate that hair bundle glycans vary in their spatial distribution along stereocilia.

Hair bundles from the anole were also labeled with a number of lectins. In some anole hair bundles, the tallest row of stereocilia presented a different set of glycans than their shorter neighbors (Figure 3.6). While anole and gecko stereocilia exhibited similar labeling with lectins such as concanavalin A (Figure 3.6), lectins such as *Maackia amurensis* agglutinin yielded robust staining in gecko and none in anole. Similarly, whereas peanut agglutinin strongly labels avian hair bundles (Goodyear and Richardson, 1994), we saw no labeling in papillae of either lizard. Together, these findings and electrophoretic observations

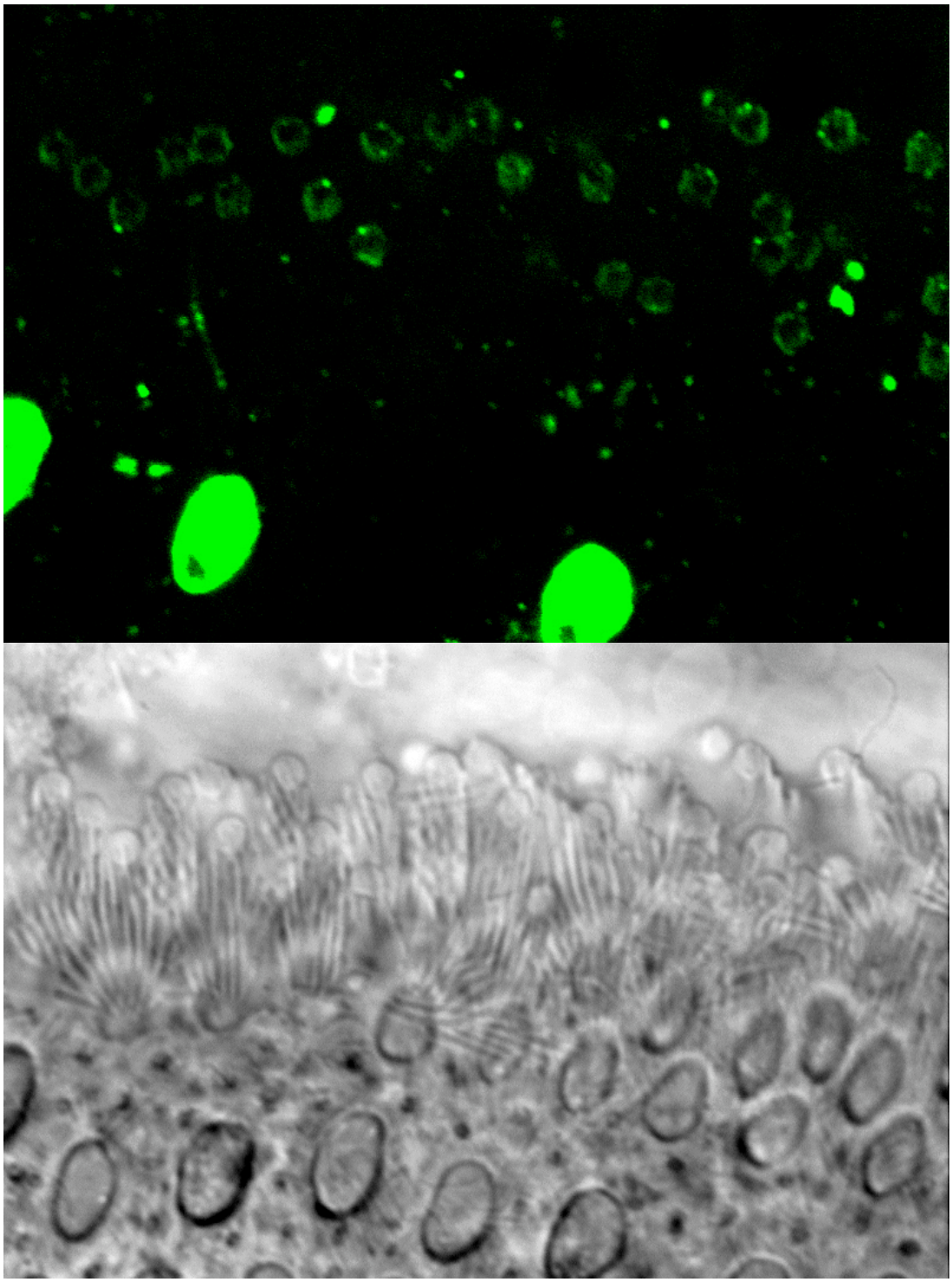

Figure 3.5: *Sambucus nigra* lectin labeled hair bundles in the gecko basilar papilla. Kinociliary bulbs and the apical surfaces of seemingly random cells are labeled by this lectin.

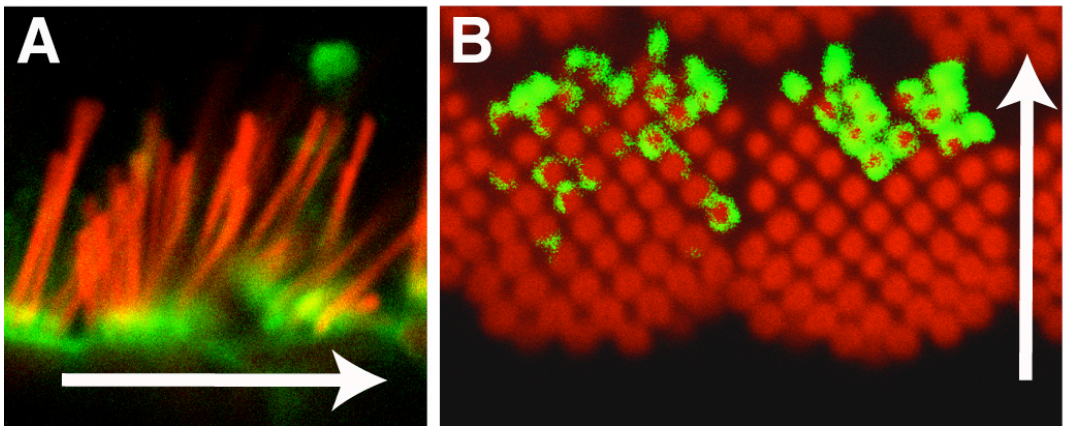

Figure 3.6: A lectin, concanavalin A (green), and actin-indicator, phalloidin (red), labeled hair bundles in the anole basilar papilla. Stereocilia are labeled by concanavalin A in the taper region of most stereocilia, and along the shaft of only the tallest stereocilia. Hair bundles are viewed in profile, A, and B, from above. Arrows indicate axis of mechanosensitivity.

of lizard stereocilia suggest that while the glycocalyx charge density and thickness are similar between species, the sugars making up that glycocalyx differ.

While the majority of the lectins we tested are sensitive to sugar moieties typically present in *N*- and *O*-linked sugars, one lectin tested, cholera-toxin B-subunit, is sensitive to GM1 gangliosides, glycosphingolipids known to interact with one another in both *cis* and *trans* orientations (Boggs et al., 2008; Hakomori, 2002). Unlike the other lectins tested, cholera-toxin B-subunit had highly regular pattern of binding focused at the lateral side of the distal tips of stereocilia, their point of contact (Figure 3.7).

3.3.2 CHEMICAL LABELING OF SIALIC ACID RESIDUES

To avoid the uncertainties of lectin labeling, a more chemical labeling technique was also employed; periodate oxidation and aniline-catalyzed oxime ligation (PAL) can be used to introduce aminooxy-labeled tags onto sialylated glycoproteins on living cells (Zeng et al., 2009). A mild oxidation by periodate generates aldehydes on endogenous sialic acids. Then, an aniline-catalyzed oxime ligation introduces a biotin tag, which can then be labeled with an avidin-conjugated fluorophore. When this technique was applied to the hair bundles of the bullfrog sacculus, hair bundle stereocilia were labeled, especially at their distal tips (Figure 3.8). Unfortunately, this technique was successful with neither gecko nor anole papillar tissues, which blebbed and internalized labeled molecules.

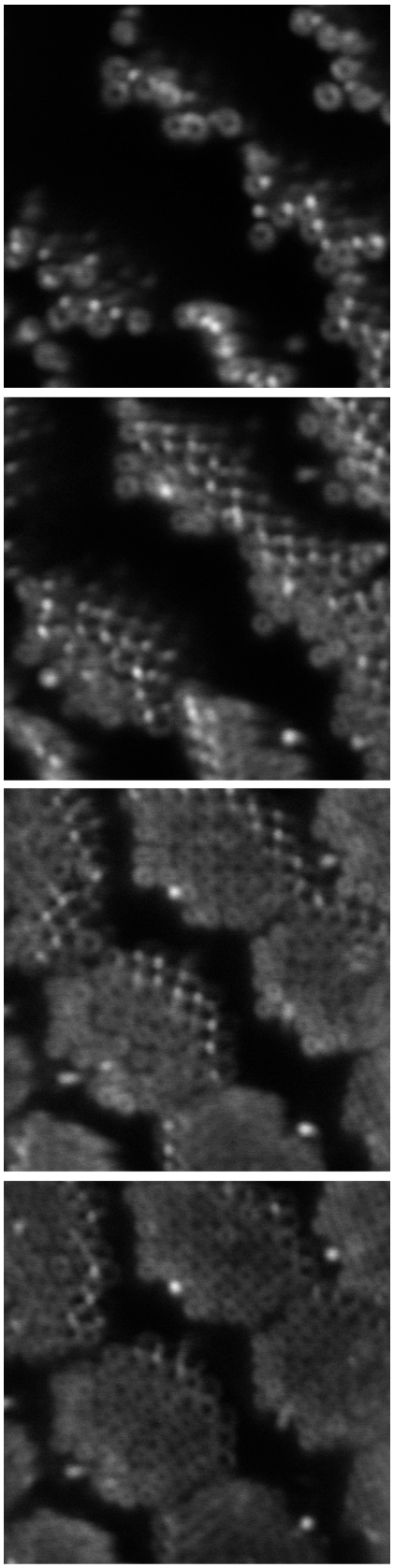

Figure 3.7: GM1 ganglioside distribution in the hair bundle. Anole basilar papilla hair bundles labeled with quantum-dot-conjugated cholera toxin B subunit, a lectin that preferentially labels GM1 gangliosides, imaged with 2-photon microscopy (in collaboration with Samuel Lagier). Uppermost panel shows only the tips of the tallest stereocilia. Note the puncta at the junctions between stereocilia along the axis of mechanosensitivity.

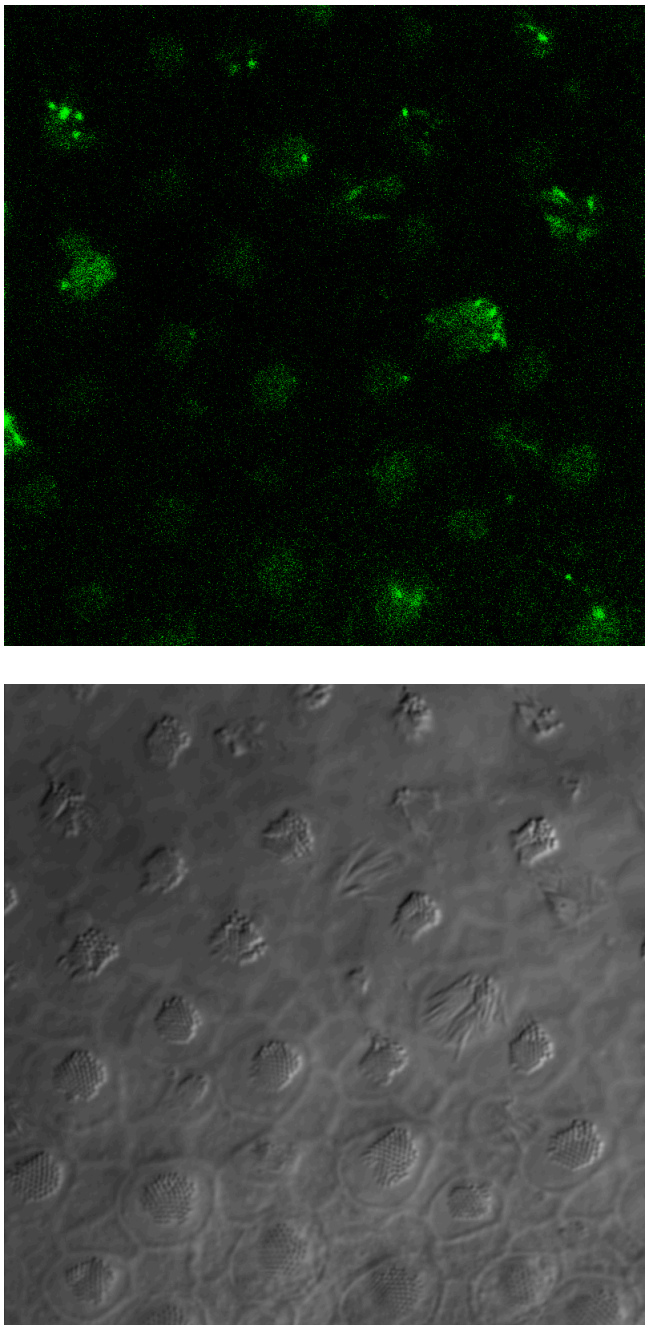

Figure 3.8: Chemical labeling of sialic-acid in the bullfrog's sacculus using the PAL technique. Hair bundles are viewed from above. Note puncta appear toward stereociliary distal tips.

3.4 GLYCOCALYX THICKNESS

3.4.1 ELECTRON MICROSCOPY

In hopes of quantifying thickness or density of the stereociliary glycocalyx, we used high-pressure rapid-freeze and freeze-substitution techniques for electron microscopy sample preparation. These methods, used together, are thought to dramatically reduce typical fixation artifacts associated with electron microscopy through the rapid freezing and then slow dehydration and embedding of the tissue at very low temperature (Dahl and Staehelin, 1989). However, in this technique the rapid-freeze step occurs as the sample is plunged at extreme speed and pressure into a bath of liquid nitrogen. This dramatic movement often significantly damaged the fragile basilar papilla. In the rare cases when damage was less severe and tissue was decently-stained, an extensive glycocalyx was apparent (Figure 3.9).

3.4.2 SIZE EXCLUSION

In another attempt to quantify glycocalyx thickness, a size-exclusion method was employed: membrane-labeled anole stereocilia were imaged by confocal microscopy in the presence of high molecular weight fluorescent dextrans. If the glycocalyx is quite long, a gap would be apparent between the fluorescence profile of the membrane dye, essentially a point source of fluorescence, and the fluorescence well of the excluded fluorescent dextran (Figure 3.10). To make these measurements, the approximate point-spread

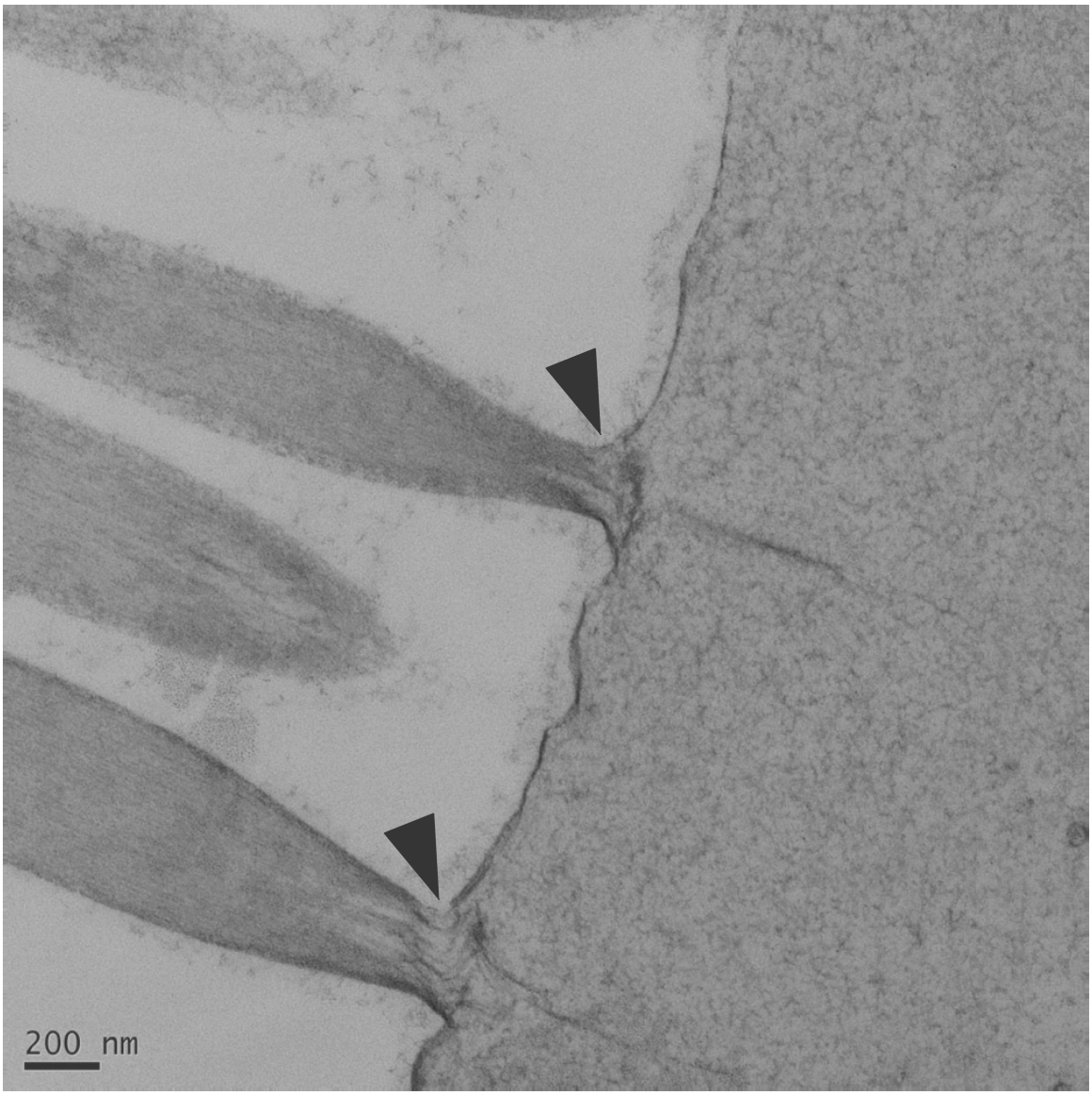

Figure 3.9: Transmission electron micrograph of the taper region of a gecko basilar papillar hair bundle prepared by high-pressure rapid-freeze and freeze-substitution techniques. Note both the extensive glycocalyx and the damage to the stereociliary rootlets from the fixation procedure at the point of insertion of the stereocilia into the cuticular plate (arrows).

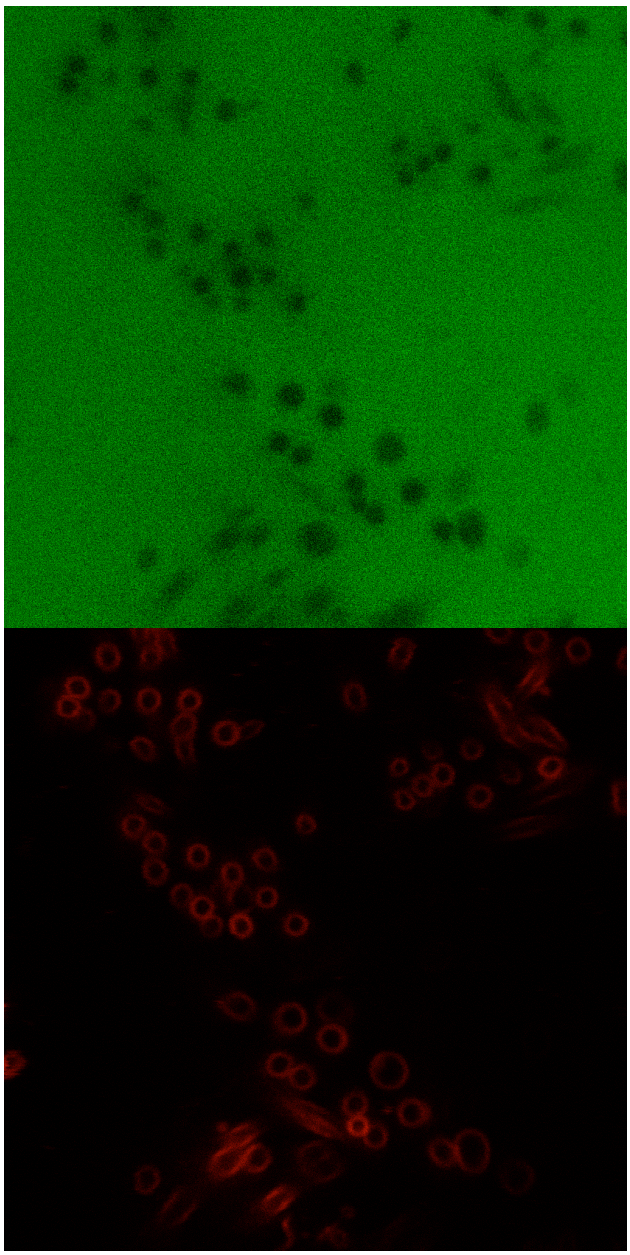

Figure 3.10: Size exclusion assay. Anole stereocilia from above, with membranes labeled with di-8-ANEPPS (red), surrounded by 70,000 MW fluorescein dextran (green).

function was obtained empirically in Matlab using Weiner filtering and Lucy-Richardson deconvolution was performed to reduce noise. Unfortunately, the resolution of the confocal microscope was not sufficient to discriminate the separation, and none of the membrane dyes tractable for use on the hair bundle were amenable to stimulated-emission-depletion microscopy. It is possible that with a different combination of dyes, stimulated-emission-depletion microscopy would make this technique feasible.

3.5 Summary Discussion

Using capillary electrophoresis I have established that stereocilia of organs from multiple species all bear a negatively charged polymer brush glycocalyx, though its density and/or charge varies between species and/or organs. From the lectin-labeling, while we have not determined which sugars make up the glycocalyx, these sugars do have differential representation in different regions of the hair bundle and along the length of the stereocilia.

Why and how might the glycocalyx vary along individual stereocilia? If different regions of stereociliary membrane perform different functional roles, the glycocalyx decorating those membranes is likely to differ as well. The membrane surfaces in the region of contact between the distal tips of stereocilia are likely to have particular functional properties: these glycocalyces should be functionalized for either adhesion or extreme lubrication. The lipids and proteins in the membrane itself also might be specialized to enable the sliding of

mechanotransduction machinery through the lateral membrane of the upper stereocilium, or perhaps for membrane stretching in the distal tip of the lower stereocilium. Functional specialization of the local *N*-linked sugars might be brought about by targeting of appropriately glycosylated membrane proteins to that region. Alternately, specialized extracellular proteoglycans might be secreted and bound at or near the distal tips of stereocilia. Lastly, certain glycolipids and glycosphingolipids might be targeted to specific regions of stereocilia, altering both membrane composition and glycocalyx in that region.

Results presented here suggest that there is an extensive glycocalyx in the taper region of stereocilia, because so many lectins labeled this region. Another possibility is that the sugars in the region were simple more accessible, though this is unlikely given the robust labeling of GM1 at the distal tips of stereocilia. We conclude that significant portion of the stereociliary glycocalyx is likely to be composed of N-linked sugars, because when they are removed through partial deglycosylation, stereocilia show a different electrophoretic profile. In spite of this, cholera toxin B-subunit labeling indicates that there are glycocalyx specializations at the distal ends of stereocilia involving glycosphingolipids like GM1. Gangliosides such as GM1 are important components of neural membranes and have been shown to form adhesions between cell membranes in a variety of systems (Boggs et al., 2008; Hakomori, 2002).

The variation we observed here in charge density between lizards and frogs is more likely to reflect the different adaptations of the basilar papilla and the

sacculus than species differences. The flat, glove-like, sacculus has a large tectorial mass that covers and separates individual hair bundles into somewhat separate compartments, and into which the uppermost stereocilia and kinocilium insert. The sacculus is a vibration-sensing organ, sensitive to rather low frequencies, 10-1 kHz. The lizard basilar papilla is a long tubular organ specialized for audition, for these two species of lizard, ~1-7 kHz. In the gecko, half the hair cells are lightly crowned with a tectorial curtain and the other half are split into groups of four hair bundles that each share a smaller mass called a sallet. In the anole, the majority of hair cells are free-standing, sensing only the motion of the surrounding fluid, with a small fraction of hair bundles far at one end of the papilla covered in a tectorial structure. Generally, lizard stereocilia are larger and thicker than those in the frog sacculus, and when brought together, they form differently shaped hair bundles. All of these properties are likely to impose different constraints on the glycocalyx if it is indeed involved in stereociliary cohesion.

Lastly, it is unfortunate that we were unable to make an accurate estimate of the glycocalyx thickness. Either the electron microscopy or the size exclusion assay might yield results with further effort, time and resources.

4 DIVALENT-MEDIATED STEREOCILIARY COHESION

4.1 FORCE-FIBER PHOTOMICROMETRY

If divalent-mediated adhesion between stereociliary glycocalyces provides a significant force holding the hair bundle together, the distal tips of stereocilia should form adhesive connections upon contact in physiological solution. A force-fiber photomicrometer was built to investigate the adhesive forces between stereocilia. The mechanical properties of hair bundles have been extensively characterized with force-fiber photomicrometry, where bundle motion is measured in response to forces applied by a flexible glass fiber of calibrated stiffness (Benser et al., 1996; Denk et al., 1989; Martin and Hudspeth, 1999). With this technique, force is applied by a piezoelectrical actuator attached to the base of a flexible glass stimulus fiber whose fine tip contacts the sample. The magnified shadow of the fiber's tip is cast onto a dual photodiode. When the forces acting on the glass fiber's tip deflect it, the shadow on the photodiodes shifts, indicating the direction and force of deflection with a resolution of approximately 1 nm and 1 ms (Benser et al., 1996).

While extremely useful, as with any method, force-fiber photomicrometry has a number of limiting factors, most salient of which is the velocity-dependent hydrodynamic drag on the force fiber as it moves through fluid. The forces one can measure with the system are limited by the properties of the fiber used, the optical properties of the tissue, and the linear range of the photodiode pair. When measuring mechanical properties of an intact hair bundle, these limits pose few

significant problems, but for these studies of inter-stereociliary friction and adhesion, they force a number of constraints. For example, in an ideal experiment, one might wish to rub the distal tip of one stereocilium along the full linear length of another. In these experiments this was not possible given the 700 nm linear range of the photodiodes.

4.2 IONIC SOLUTIONS OF THE INNER EAR

Most vertebrate cochleae have two main compartments, each with its own physiological extracellular fluid: the perilymph surrounds hair-cell and supporting-cell basal surfaces, while endolymph surrounds hair bundles and hair-cell apical surfaces (Figure 1.2). The osmolarities of both fluids are comparable to that of the plasma for the species in question (Jahn and Santos-Sacchi, 2001). The major difference between endolymph and perilymph is the predominant cation: Na^+ in perilymph and K^+ in endolymph (Gelfand, 2009; Jahn and Santos-Sacchi, 2001). This differentiates endolymph from every other extracellular fluid in the body.

Ions, especially Ca^{2+} ions, mediate many essential hair cell functions, namely hair bundle movement (Cheung and Corey, 2006; Ricci et al., 1998), adaptation (Cheung and Corey, 2006; Eatock, 2000; Martin and Hudspeth, 1999; Ricci et al., 1998; Tinevez et al., 2007; Wu et al., 1999), and electrical resonance (Armstrong and Roberts, 2001; Art and Fettiplace, 1987; Ricci and Fettiplace, 1998). The physiological importance of the ionic compositions of endolymph and

perilymph has motivated several studies in a wide variety of species ranging from fish to mammals (Bosher and Warren, 1978; Citron et al., 1956; Corey and Hudspeth, 1983b; Couloigner et al., 1999; Crawford et al., 1991; Enger, 1964; Freeman et al., 1994; Freeman et al., 1993; Makimoto and Silverstein, 1974; Rusch and Thurm, 1989; Silverstein and Schuknecht, 1966; Sterkers et al., 1988). In mammals, the endolymph Ca^{2+} concentration is approximately 250 μM and Mg^{2+} approximately 110 μM (Bosher and Warren, 1978). Due to the geometry of the lizard basilar papilla, it is likely that previous attempts to isolate and measure ionic concentrations from endolymph have suffered from cross-contamination with perilymph, indicated by the notable ionic similarities to perilymph (Sterkers et al., 1988). From studies monitoring the health of lizard basilar papilla tissue in varying solutions (Freeman et al., 1993), it is likely that the physiological Ca^{2+} and Mg^{2+} concentrations in endolymph are extremely low, less than 10 μM.

4.3 ADHESION

4.3.1 DISTAL TIPS OF STEREOCILIA ADHERE TO ONE ANOTHER UPON CONTACT

To investigate the possibility of divalent mediated adhesion between stereociliary glycocalyces, we brought the distal tips of stereocilia together and monitored the forces between them in a variety of different ionic conditions. In order to rub one stereocilium against another, a stimulus force fiber coated with a glycocalyx-binding lectin was brought into contact with an isolated and unattached

stereocilium lying parallel with the stimulus fiber's tip. After some tens of seconds of contact between fiber and stereocilium, sometimes attachments were formed. Stereocilia were considered firmly attached if no part of the stereocilium jittered in a manner indicative of brownian motion and if the stereocilium showed no torsion when manipulated against other stereocilia or against the chamber's surface. With this stereocilium firmly attached approximately parallel to the glass fiber, the distal end of the stereocilium could then be rubbed against the distal end of another attached to the bottom of the experimental chamber (Figure 4.1). The two stereocilia were rubbed against one another at 90° in an arrangement similar to that of a surface-force apparatus (Raviv et al., 2003). Although this arrangement differs from the parallel orientation encountered in hair bundles, it provides a well-defined, point-like apposition impossible to obtain experimentally with the more physiological arrangement. Because this experiment required that the experimenter differentiate the blunt distal end from the tapered basal end of each stereocilium, we used anole stereocilia 10-20 μm in length and 1 μm in diameter. The distal tip regions brought into contact were defined as the distal-most 1-2 μm of the stereocilia. In the course of the experiment, if either the upper or lower stereocilium began to show the above-mentioned indications of detachment from the fiber or the chamber's surface, respectively, the pair of stereocilia was discarded.

When two stereocilia were brought into contact, attachments were formed between them. Attachments became stronger with increased normal force on the

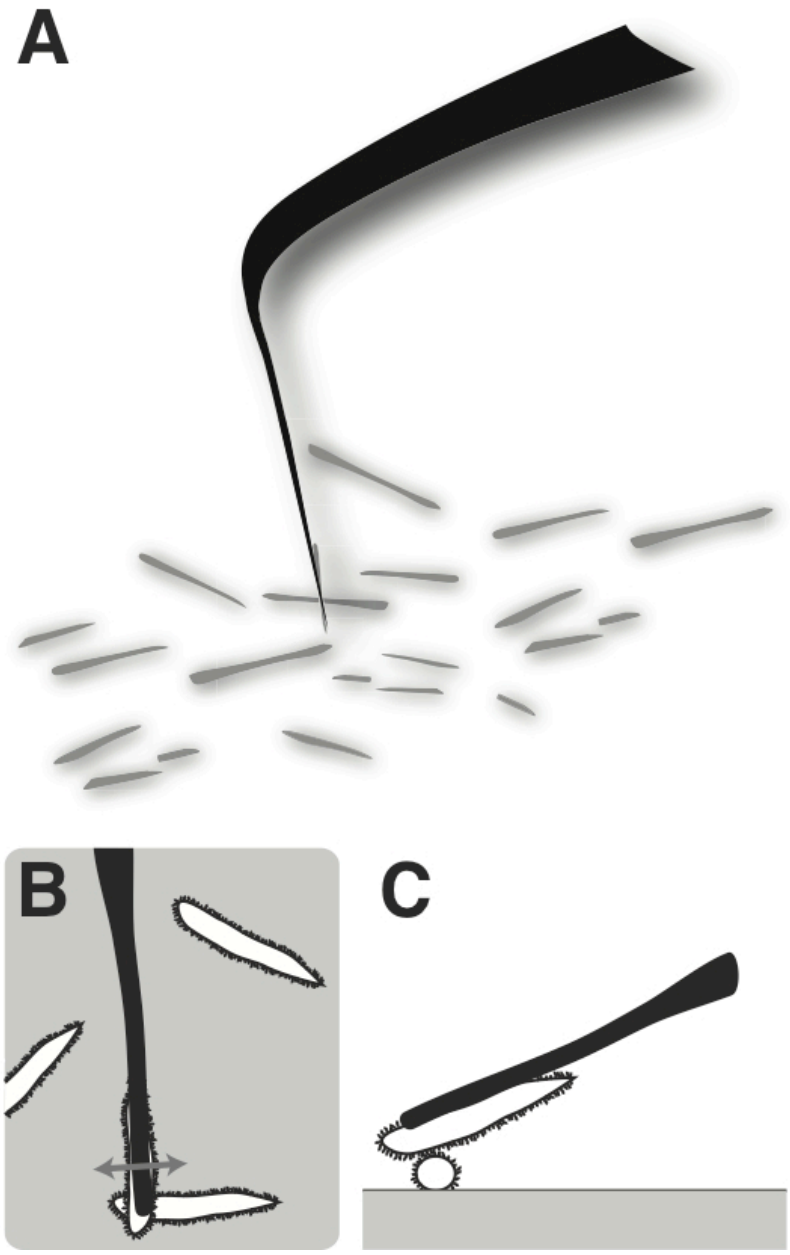

Figure 4.1: Experimental geometry. A, schematic of force fiber and isolated stereocilia. B, In a schematic surface view, a stereocilium immobilized at the tip of a fiber is rubbed back-and-forth (darker grey double arrow) against a second stereocilium affixed to the coverslip bottom of the experimental chamber. C, A schematic lateral view illustrates the contact between the stereocilia. Lowering the base of the fiber produces a downward force normal to the bottom of the chamber pressing the two stereocilia together.

glass fiber in the downward vertical direction. To investigate this adhesion and the associated frictional forces, I moved the base of the stimulus fiber back-and-forth in a 1 Hz triangle wave with a peak-to-peak magnitude of 700 nm (Y). From the extent of the fiber's flexion, as determined from the fibers tip's position X and the fiber's stiffness K_{SF}, we measured the force applied at the tip of the stimulus fiber F_{SF}, which reflected the friction between the stereocilia, $\xi_{FRICTION}$, as well as the hydrodynamic drag on the moving fiber and stereocilium, ξ_{SF}:

$$F_{SF} = K_{SF}(Y - X) = (\xi_{SF} + \xi_{FRICTION})\frac{dX}{dt}$$

The stimulus fiber with attached stereocilium was lowered in 125 nm steps until the two stereocilia came into contact, at which point many cycles of response were measured. The stimulus fiber was then lowered an additional 125 nm and additional responses were recorded. This was repeated for a total of five normal force levels for each pair of stereocilia.

The response during each cycle of movement was visualized in a displacement-force plot (Figure 4.2). Two measurements were obtained: first, the amount of energy dissipated, which is equal to the area of the displacement-force hysteresis loop, and second, the adhesion between the two surfaces, which is given by the slope of the displacement-force relation. We present adhesion in the units newtons-per-meter, though adhesion is typically given in force per unit area, newtons-per-meter-squared. We cannot measure the area of contact between two stereocilia, but because stereocilia are put in contact at a right angle to one another, as in a surface forces apparatus (Raviv et al., 2003), their area of contact

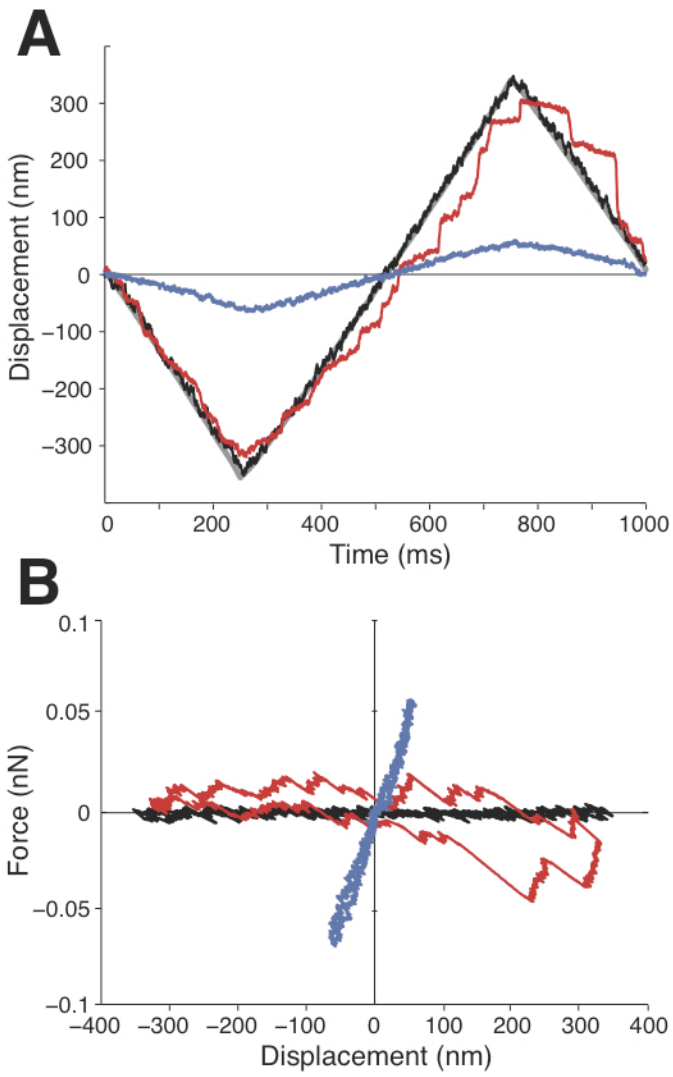

Figure 4.2: The traces show representative single cycles of movement by a fiber's tip. The motion of the free tip (black) is almost indistinguishable from the superimposed record of the fiber's base movement (gray). In endolymph, early contact with a second stereocilium on the chamber's bottom surface produces an irregular trajectory (red) punctuated by stick-slip events. After many cycles, the same pair of stereocilia stick together firmly and the range of motion is diminished (blue). B, The data from panel (A) are presented as displacement-force relations. The free tip traces a horizontal line (black) indicative of minimal viscous dissipation. Although the tip moves nearly as far in the early contact cycle (red), the stick-slip events produce a substantial dissipation quantified by the area within the trajectory. When the tip is tightly bound in the later contact cycle (blue), dissipation is low; the slope of the trajectory represents the adhesion of the interaction.

is as point-like as possible. When the fiber is moving through liquid without contact between the two stereocilia, a small amount of energy is dissipated through hydrodynamic drag; because the fiber is unimpeded, however, the adhesion does not stray from zero. The behavior of a given pair of stereocilia is characterized by plotting energy dissipated against the adhesion.

As stereocilia were rubbed together in endolymph, adhesion and dissipation values from each cycle fell into strongly skewed distributions with long high-value tails. This is likely because in the majority of back and forth cycles, no attachments were made, neither strongly dissipative nor elastic; when attachments were made, they resulted in high-value tails in the stiffness distributions (Figure 4.3).

4.3.2 Sensitivity of stereociliary adhesion ionic strength and ion type

To test the hypothesis that inter-stereociliary adhesion stems from the electrostatic tethering of glycocalyces, we brought stereocilia together under ionic conditions that varied from physiological endolymph in a variety of ways to test different hypotheses. The artificial endolymph used here contained $< 10\,\mu$M of Ca^{2+} or Mg^{2+}, consistent with what has been measured in lizard endolymph (Freeman et al., 1993). Adhesion between stereocilia should be reduced under a number of conditions. When these tethering divalent ions are removed from endolymph with divalent chelators such as EDTA or EGTA adhesion should decline due to the absence of tethering molecules. Adhesion should decline when glycocalyx binding sites are removed through deglycosylation. When the ionic

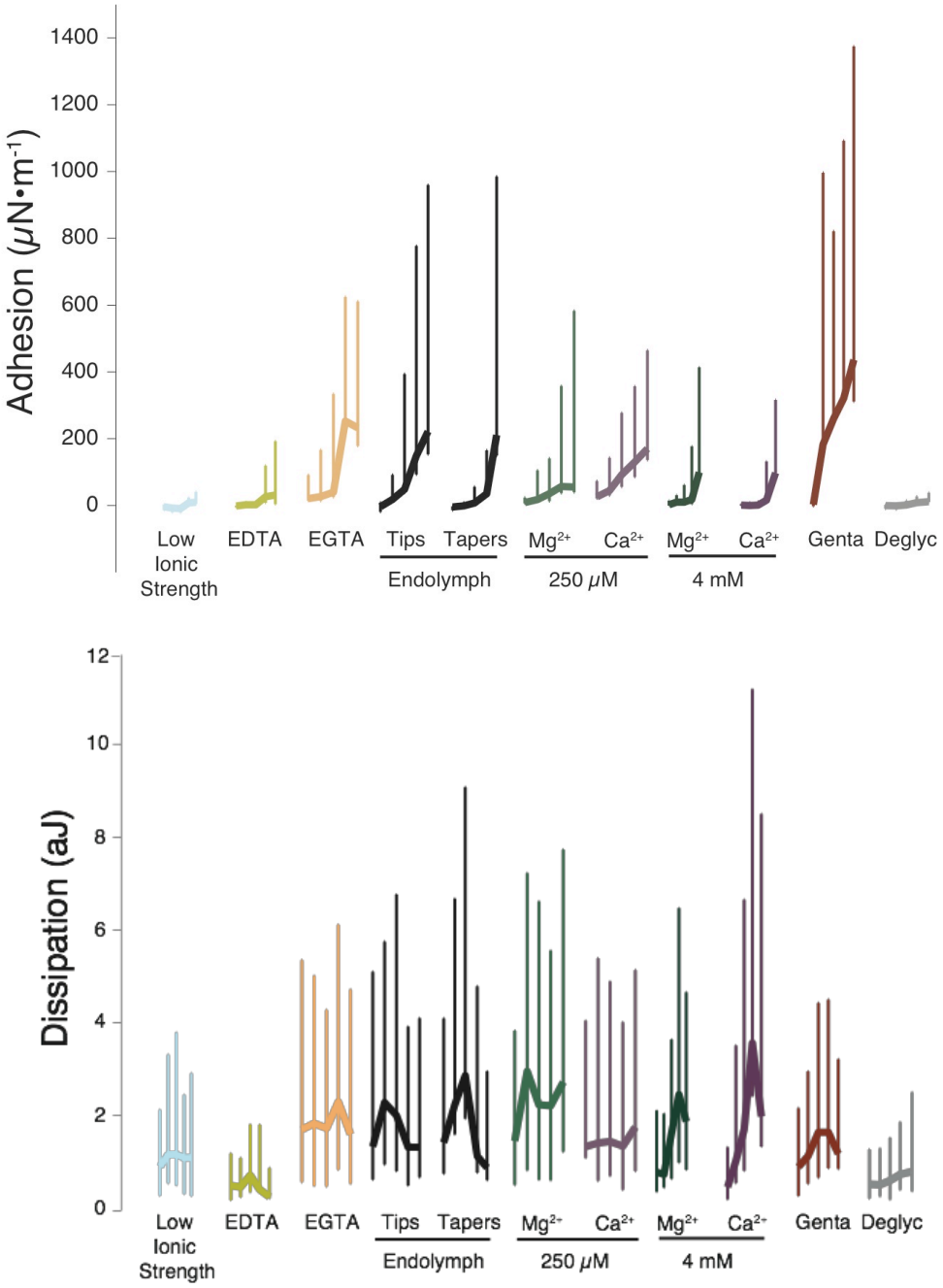

Figure 4.3: Median adhesion and dissipation values ± quartiles for each vertical force of each condition. The leftmost position of each condition corresponds to 0 nm vertical force, the rightmost, 500 nm. Broadly, adhesion is more informative than dissipation. While the adhesion and dissipation observed in endolymph conditions and in endolymph supplemented with EGTA, or small concentrations of Mg^{2+} or Ca^{2+} did not vary much, the deglycosylation, EDTA, and low ionic strength conditions all exhibited reduced adhesion and dissipation values. Gentamicin dramatically increased adhesion. Note the non-monotonic progression of dissipation under most conditions.

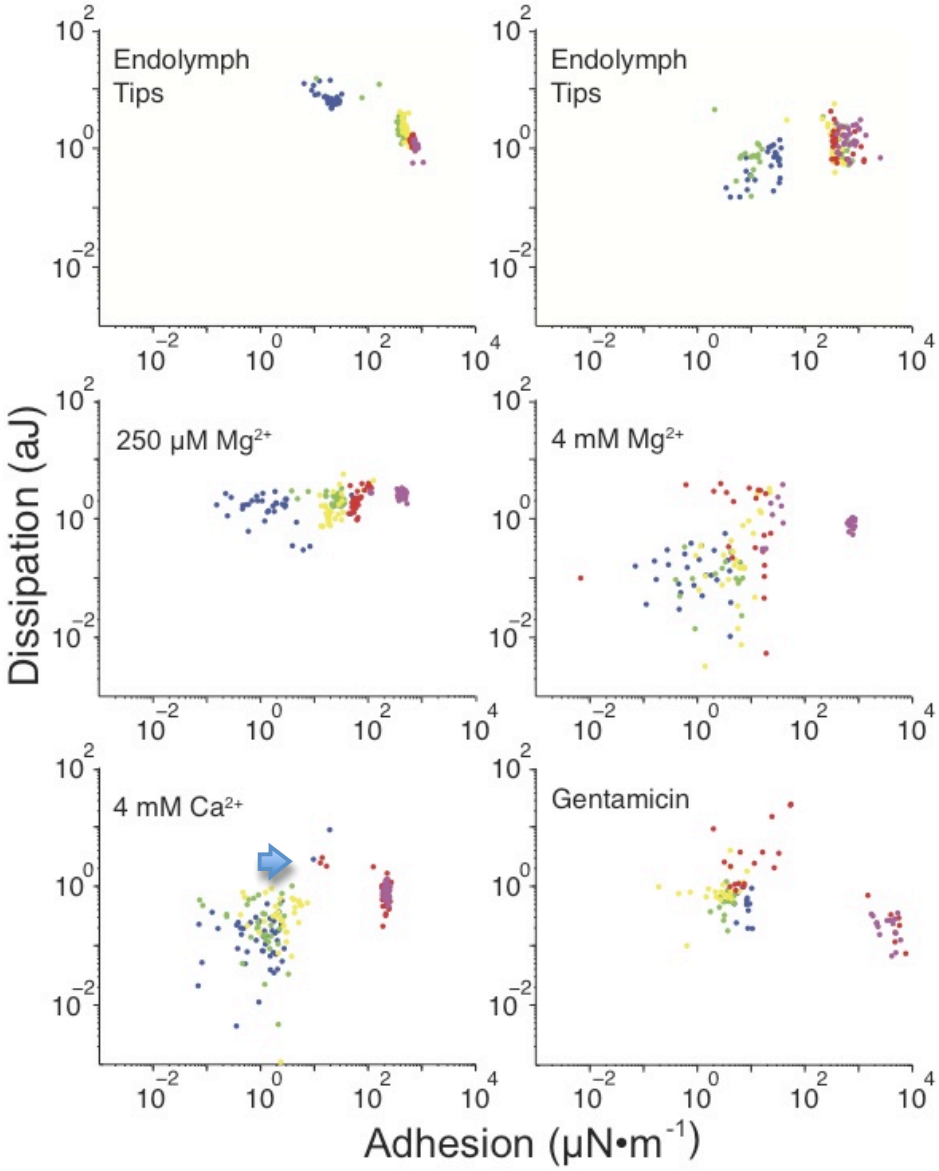

Figure 4.4: Doubly logarithmic plots of energy dissipation as a function of inter-stereociliary adhesion under different conditions. a, Examples of stereociliary pairs measured under different conditions. Individual cycles of rubbing are plotted in points of different colors depending on the normal force: blue, 0 nm or first contact; green, -125 nm; yellow, -250 nm; red, -375 nm; purple, -500 nm. The responses during individual cycles of movement disclose two regimes. In each plot, the points to the left reflect little to no attachment, with fiber motion affected by friction between the stereocilia; the points to the right signal firm attachment between the stereocilia. Some pairs, such as that depicted at the bottom left, displayed a higher-dissipation transition in which elastic energy was stored briefly before attachments were broken (arrow). The uppermost two plots portray the variability between experiments within the same condition.

strength of the surrounding solution is lowered, the Debye length of charges within the glycocalyx should increase, resulting in increased lubrication (Klein et al., 1993) and thus decreased adhesion between stereocilia. When divalent-ion concentrations are increased, two opposite effects are possible. If the glycocalyx binding sites are under-saturated with divalents in physiological endolymph, adhesion should increase with increased divalent concentration. Alternately, if binding sites are ideally saturated with divalents through their tethering of stereocilia in physiological endolymph, then an increase in divalent ion concentration should reduce adhesion between stereocilia through overcharging/charge inversion (Lyklema, 2006). When endolymph is supplemented with high-valence cations such as aminoglycoside antibiotics, such as gentamicin, stereocilia should be tethered more strongly owing to the ability of these molecules to bind multiple monovalent sites. Lastly, if the glycocalyx is indeed adapted for electrostatic glyco-tethering at the distal tips of stereocilia, the glycocalyx at tapered ends of stereocilia are likely to form functionally different adhesions, if any.

Pairs of stereocilia differed in their attachment properties across conditions but showed a consistent force-dependence that also varied by condition. With increasing normal force, many stereociliary pairs often underwent a dramatic transition in adhesion, which rose as much as two decades (Figure 4.4). In the regime below this transition, the stereocilia exhibited a variety of adhesion and

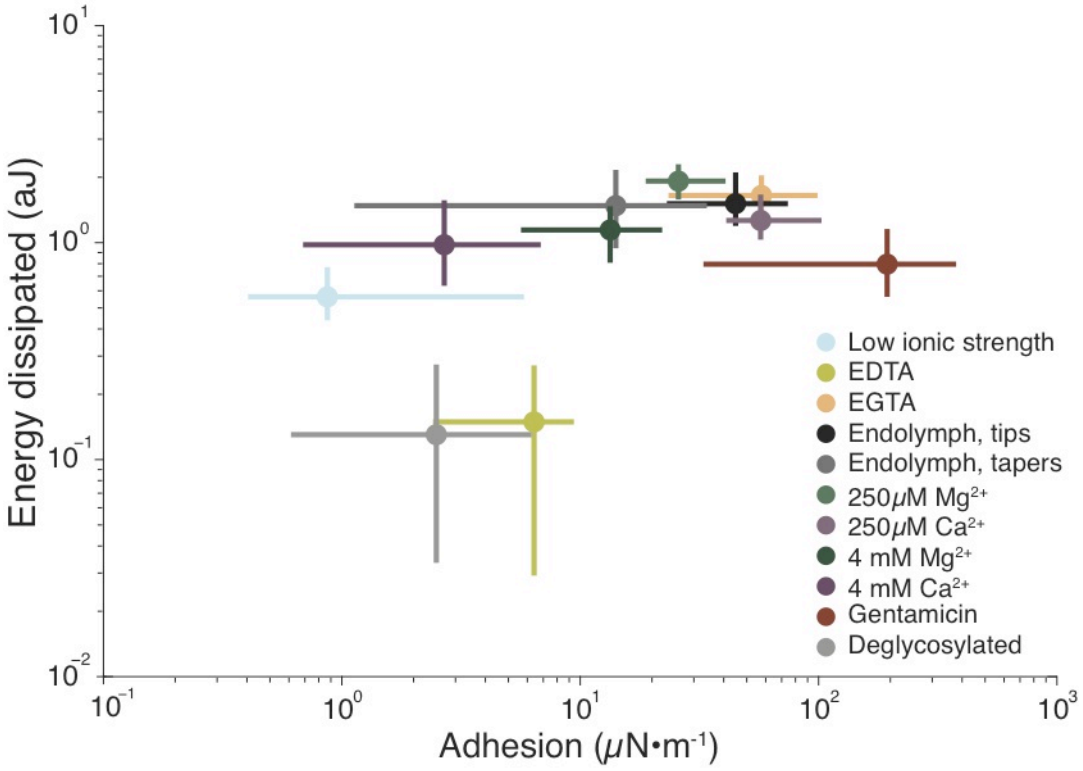

Figure 4.5: The response under each condition is displayed as the median adhesion and dissipation value for all normal forces with error bars encompassing the 40th through the 60th percentiles of the distributions. The median value for distal ends of stereocilia in endolymph falls in the transition region between adhesion regimes. The various perturbation conditions alter the progression of attachment and thus the position of the median adhesion and dissipation values. Deglycosylation and chelation of divalent cations greatly lower dissipation and eliminate tight attachments between stereocilia. Addition of gentamicin promotes rapid attachment. For the successive treatments listed in the key, the numbers of cycles analyzed were respectively 636, 354, 693, 1266, 774, 921, 1050, 927, 1233, 879, and 693. Approximately equal proportions of cycles were recorded for each normal force under all conditions.

dissipation values up to a critical adhesion value. In the high-adhesion regime after the transition, the two stereocilia were firmly attached: dissipation was reduced and adhesion values were consistent and high. A transition region of high dissipation sometimes occurred between the two regimes (Figure 4.4 arrow). The progression across the transition varied in reversibility depending on the normal force and ionic conditions.

This dynamic progression of attachment is reflected in the comparison of all conditions by the median adhesion and energy dissipation values over all normal forces (Figure 4.5). Median values for conditions in which adhesion is predicted to be weak (low ionic strength solution, deglycosylated stereocilia, and endolymph supplemented with EDTA, a Ca^{2+} and Mg^{2+} chelator) fall into the low-adhesion regime associated with poor attachment. Median values for stereocilia bound with gentamicin, a multivalent cation, fall firmly in the high-adhesion regime associated with strong attachment, consistent with gentamicin's ability to fuse stereocilia *in vivo* (Takumida et al., 1989a). Values for the distal tips of stereocilia rubbed together in endolymph and in mildly altered ionic conditions (endolymph supplemented with either the Ca^{2+}-chelating EGTA, 250 μM Ca^{2+}, or 250 μM Mg^{2+}) all clustered in the high-dissipation transition region between the two adhesion regimes. The dramatic difference between the two chelators is notable; chelation of Ca^{2+} yielded little change to inter-stereociliary adhesion while chelation of both Ca^{2+} and Mg^{2+} resulted in a strong inhibition of adhesion. The addition of 4 mM Ca^{2+} or Mg^{2+} to the endolymph surrounding stereocilia reduced

adhesion, tilting these conditions into the low-adhesion regime, indicating overcharging through an over-saturation of binding sites. Adhesion values between tapered ends of stereocilia were highly variable but less adhesive than attachments between the distal tips, indicating functional variation in the adhesive properties of the glycocalyx along stereocilia.

Clear transitions between adhesion regimes were visible in two-thirds of the 72 stereociliary pairs measured over all conditions, though the properties of these transitions varied by condition (Figure 4.6). Attachment was irreversible between 18 pairs of stereocilia, mostly in the 4 mM Mg^{2+} and gentamicin conditions; no irreversible attachments were seen between deglycosylated stereocilia or stereocilia in low ionic strength solution. In all conditions, attachment typically occurred at the -250 nm normal force level with the exception of the deglycosylated condition, where adhesion transitions occurred rarely and only at the greatest normal forces. For most transitioning stereociliary pairs, the average separation between the two adhesion regimes scaled logarithmically with the average transition starting adhesion value (Figure 4.6E). Nearly all out-lying stereociliary pairs were pairs in which stereocilia attached irreversibly, displaying a high adhesion increase in relation to starting adhesion. The separation between the two adhesion regimes likely corresponds to the strength of the attachment made during the transition, with greater increases in adhesion corresponding to stronger attachments. The strength of the attachment is likely a function of both the number of accessible binding sites and their interaction strength.

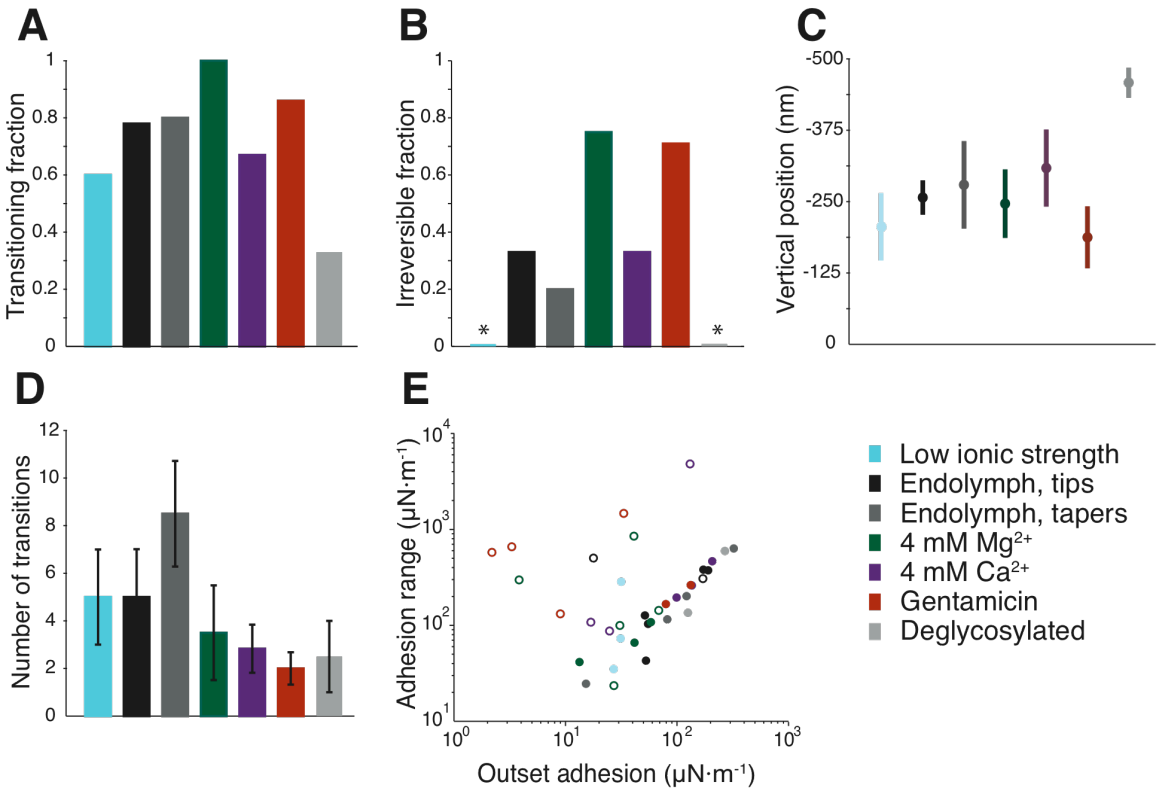

Figure 4.6: Properties of adhesion transitions. A, The fraction of stereociliary pairs exhibiting an adhesion transition varies with the ionic conditions. Note that all stereociliary pairs measured in high Mg^{2+} exhibited transitions as opposed to the deglycosylation condition where only ~1/3 of stereociliary pairs did. B, Fraction of stereociliary pairs in each condition in which the first crossing of the adhesion gap is irreversible. Asterisks indicated conditions in which no irreversible crossings occurred. Note that approximately 75% of crossings were irreversible in the high Mg^{2+} and gentamicin conditions. C, The average vertical position ±SEM at which stiffness transitions occurred, approximation for the vertical force, varies with ionic conditions. Deglycosylated stereocilia only exhibited transitions at the highest vertical forces. D, For each condition, the number of stiffness transitions was found for each pair of stereocilia, then presented as the average (±SEM) across pairs. Stereocilia rubbed at their tapered ends yielded many more transitions than did other conditions. E, For each pair of stereocilia that exhibited stiffness transitions, average stiffness at start of stiffness transition is plotted against the average width of the stiffness transition on a doubly logarithmic plot. If the stiffness transition was irreversible, the point is hollow.

4.4 STICK-SLIP BETWEEN STEREOCILIA

4.4.1 STICK-SLIP FRICTION

The measures of stiffness and dissipation over 1 s cycles ignore much of the detail present in the original recordings. It was apparent from individual records that stick-slip motion occurred as the two stereocilia were rubbed against one another (Figure 4.2). Stick-slip motion occurs when two surfaces slide against one another and become partially attached; as the two surfaces advance farther, the force on the area of connection increases until the connection ruptures, dissipating the energy previously held in the elastic connection between the surfaces.

4.4.2 STEREOCILIARY DISTAL VERSUS TAPERED ENDS

To analyze this behavior, we extracted the stick-slip events with a method for finding variably sized steps in noisy data. Recording in endolymph, we observed 1,775 slip events over 1,266 cycles measured between the distal tips of stereocilia. More than 80% of the slip events occurred at the three smallest vertical loads. When the slip magnitudes were plotted according to cumulative probability, power-law behavior emerged: large slip events were exponentially rarer than small ones (Figure 4.7A). Because of the inability of our system to exert large forces or to measure steps larger than 350 nm, the data could not be extended for more than one decade of slip magnitude.

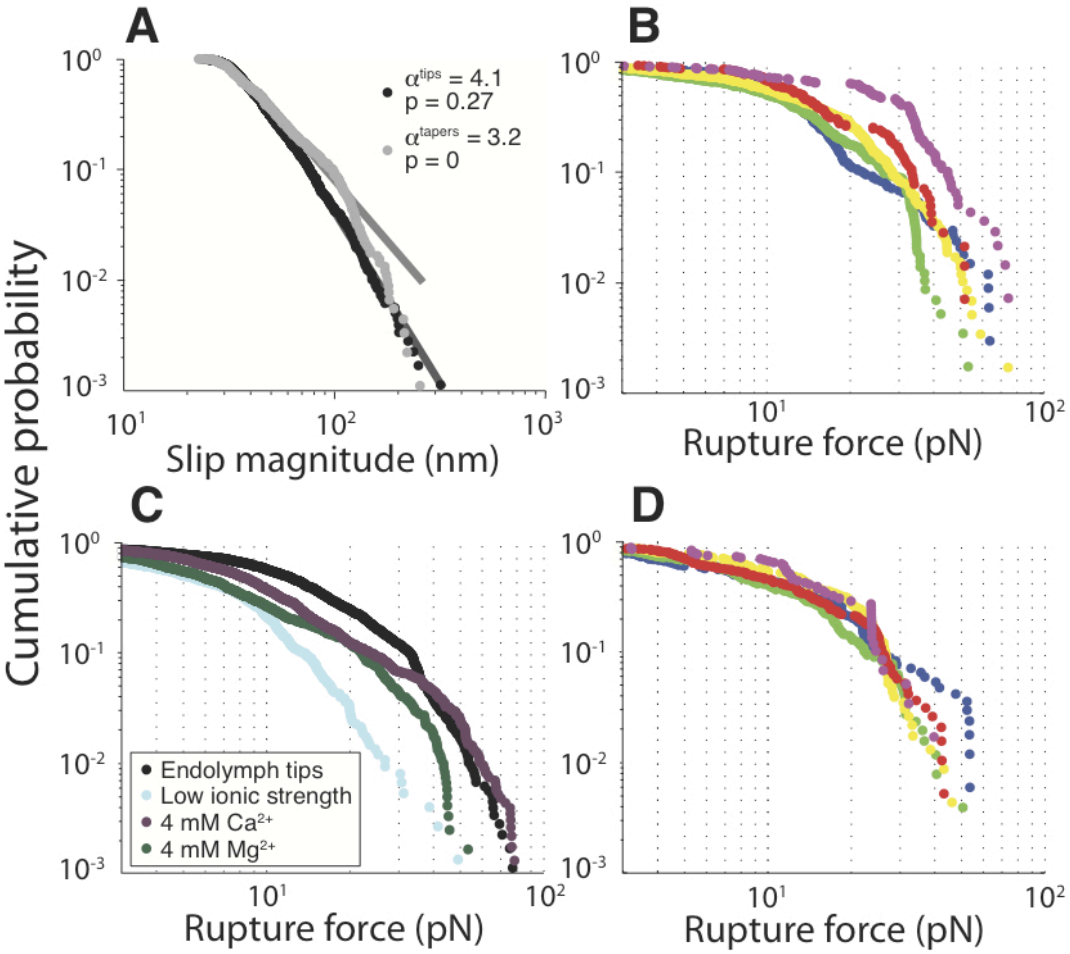

Figure 4.7: Analysis of stick-slip events. A, Inverted power-law relationship between magnitude of slip event and slip frequency is only valid between stereociliary tips (black), not stereociliary tapers (grey). Cumulative probability is plotted against slip magnitude for individual slip events, circles, and the fits are plotted as solid lines. Fitting was done by maximum likelihood and the Kolmogorov-Smirnov test was used to compute *p*-values for goodness of fit; the null hypothesis that the data originated from a power law distribution was accepted at all significance levels less than the *p*-value. Cumulative probability plots of rupture forces for individual slip events between stereociliary tips, B, and tapers, D, according to vertical force load: blue, 0 nm or first contact; green, -125 nm; yellow, –250 nm; red, -375 nm; purple, -500 nm. Rupture forces from different conditions are compared with data from all vertical force loads combined, C.

The rupture force achieved just prior to a slip event between distal tips of stereocilia revealed a clear dependence on the vertical force (Figure 4.7B). The greater the vertical force, the more force the attachment between stereocilia could sustain before reaching the breaking point.

In view of the variation in sugar distribution along the length of stereocilia, we sought differences in the stick-slip properties of distal and tapered ends of stereocilia. The slip sizes for tapered ends deviated significantly from a power-law distribution. Furthermore, tapered ends of stereocilia exhibited no dependence of the rupture force on the vertical force (Figure 4.7D). The inter-stereociliary attachments between tapered ends exhibited lower rupture forces, especially at high vertical loads, than the attachments between the distal tips.

4.4.3 Comparison across Conditions

In comparisons of the cumulative distributions of rupture forces collected for all vertical forces under different conditions (Figure 4.7C), endolymph provided an environment in which stereociliary attachments could hold the greatest forces before rupturing. However, in the 4 mM-Ca^{2+} condition, the highest rupture forces exceeded the highest rupture forces seen in the endolymph condition, indicating that Ca^{2+}-tethered attachments can be quite strong. In the high Mg^{2+} condition the broad reduction in rupture force without such an extreme value tail suggested that the force-bearing capacity of Mg^{2+}-tethered attachments is low. The forces required to rupture inter-stereociliary attachments in low-ionic-strength solution were comparatively quite small.

The comparison of conditions by the number of slips observed over the total number of cycles measured (nS/nC) revealed still more variation, especially when separated into nS/nC at each vertical force (Figure 4.8). The nS/nC between the distal tips of stereocilia rubbed in endolymph peaked at rather low vertical force, between 125 and 250 nm. High Ca^{2+} dramatically increased the average number of slips per cycle, but slip number peaked at greater vertical force, 375 nm. The gentamicin and deglycosylated stereociliary pairs exhibited few slip events at all vertical forces, but each with different causes: stereocilia were strongly attached in the presence of gentamicin and thus displayed few slip events, while few attachments were made at all when stereocilia were deglycosylated, again yielding few slips events. In the presence of 250 μM Ca^{2+}, remarkably few slip events occurred, suggesting that stereocilia may have been well attached, but without particularly high stiffness.

4.5 DO THESE ADHESIONS CORRESPOND TO TOP CONNECTORS?

Given the enzymatic intractability of top connectors and our observations of promiscuous glycan- and divalent-dependent attachments between the distal tips of stereocilia, it is possible that top connectors are more stable version of the attachments observed here. Top connectors have previously been observed in the lizard (Csukas et al., 1987), and the extracellular and potentially glycosylated protein stereocilin has been associated with top connectors in mammals (Verpy et al., 2008). To test whether the attachments observed here might correspond to

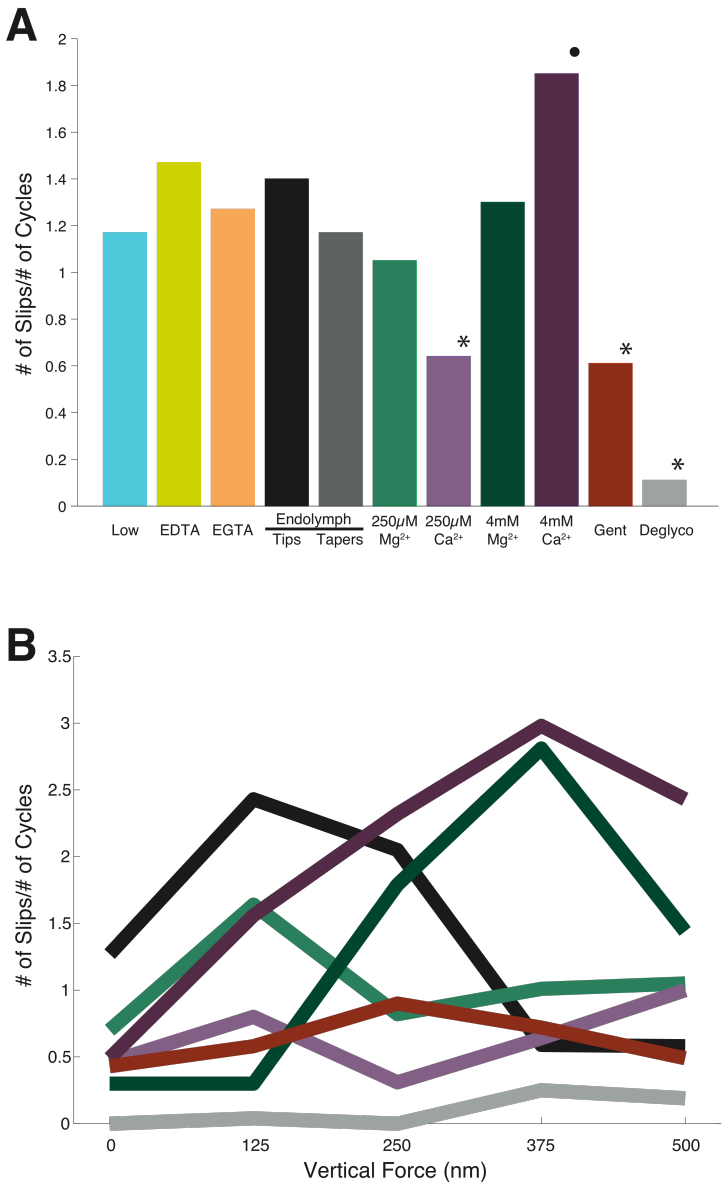

Figure 4.8: Comparison of conditions by number of slips observed over number of cycles measured: A, across all conditions, and B, selected conditions by vertical force. Asterisks signify notably low slip:cycle ratio, which can have different underlying causes: either extremely stable adhesion (gentamicin) or negligible adhesion (deglycosylation). The filled circle identifies the high Ca^{2+} condition in which many slips were observed. In panel B, note the difference in progression of slip frequency over vertical force, the slope, between distal tips in endolymph versus all other conditions.

top connectors, I labeled anole hair bundles with antibodies made against segments of mouse-stereocilin. Stereocilia did indeed label with stereocilin-B antibodies, more strongly at the distal rather than tapered ends, but the point-like adhesions visible in mammals were not clearly present (Figure 4.9). Puncta did sometimes occur at the distal tips of stereocilia, but it was not clear whether the labeling was specific.

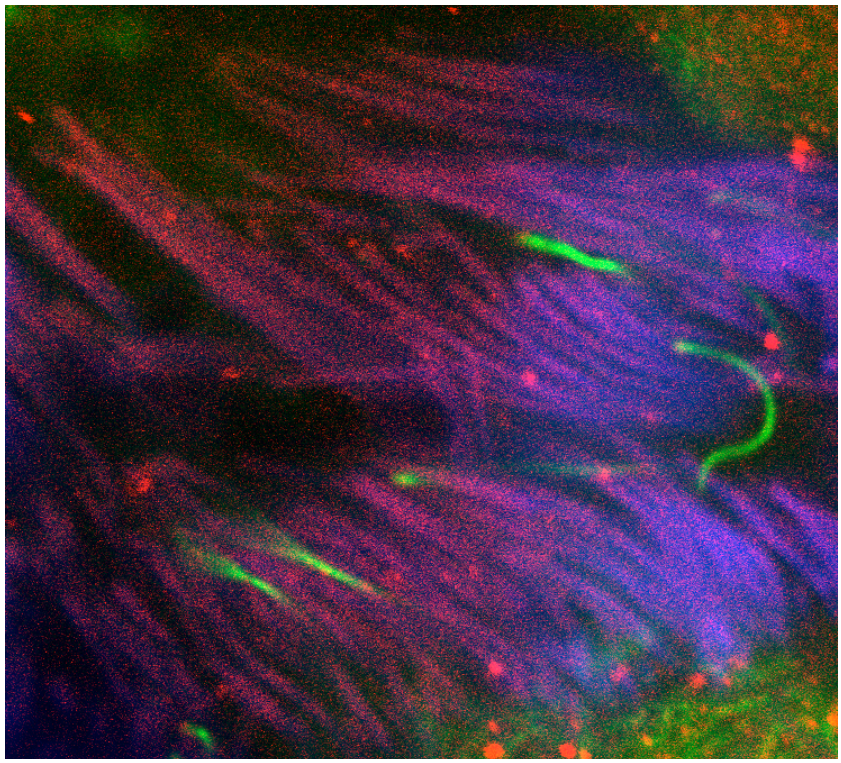

Figure 4.9: Stereocilin in the anole hair bundle. Phalloidin labels the actin of the stereocilia (blue), antibodies against acetylated tubulin (green) mark kinocilia and intracellular structures, and antibodies against stereocilin (red) label the shafts of stereocilia, more intensely toward their distal tips.

5 DISCUSSION

5.1 SUMMARY

These results provide evidence for divalent-mediated adhesion between stereocilia. When the distal tips of two stereocilia were apposed under physiological ionic conditions they formed elastic connections with adhesiveness that varied greatly with the ionic milieu. When *N*-linked sugars were enzymatically removed from stereocilia, these connections did not form. The elastic connections were sensitive to multivalent cations: sometimes strong but scarce connections occurred in the presence of Ca^{2+}, weak but plentiful connections in the presence of Mg^{2+}, and near-fusion in the presence of the polycation gentamicin. Inter-stereociliary connections were greatly reduced and weakened in low-ionic-strength solution. Stick-slip movement was observed between rubbed stereocilia, and surprisingly, the magnitude-frequency relation of stick-slip between distal tips of stereocilia in endolymph mirrored that observed in earthquakes and other natural phenomena (Bak and Tang, 1989).

5.2 ELASTIC CONNECTIONS

An exciting possibility is that the elastic connections observed here might correspond to top connectors joining stereocilia just below tip links. However, the stiffness values we have observed are significantly lower than predicted on the basis of whole-bundle deflections (Baumgart, 2010; Karavitaki and Corey, 2010).

This is unsurprising for a number of reasons: in contrast to the stable top connectors present in intact hair bundles, the connections observed here are formed as they are measured, where they typically grow stronger over time. By electron microscopy, top connectors appear to be composed of many overlapping filaments (Nagel et al., 1991; Nayak et al., 2007). Perhaps only a fraction of such filaments made contact over the course of the present experiments, due either to non-native physical orientation or because some essential secreted glycoproteins were lost during stereociliary isolation. In order to measure stick-slip movements, it was necessary to use fibers of rather low stiffness. I was consequently unable to exert forces greater than 140 pN. Owing to the slight fiber rotation that occurred when two stereocilia were strongly bound, the fibers could not measure stiffness values greater than 4000 μN/m. Taken together with the ability of top connectors to withstand enzymatic treatments, it is possible that top connectors may indeed be formed by specific glycan-glycan interactions. This could be tested by deglycosylating hair bundles and checking for top connectors by electron microscopy, though this approach might be confounded by the stereociliary fusion which often results from deglycosylation of intact hair bundles (unpublished observation).

Why might the hair bundle form elastic connections that could potentially reduce mechanosensitivity? If two apposing surfaces are slid against one another, some amount of energy will be lost to dissipation in the form of heat even with extremely low frictional coefficients. On the contrary, when two such surfaces

are attached to one another with elastic connections, energy can be stored in those elastic connections and then recovered, so long as the attachments are not ruptured. Although ruptures occurred in our experiments, the stereociliary connections between glycocalyces *in vivo* are rarely challenged with displacements as great as those applied here. Interstereociliary connections should therefore withstand the forces associated with physiological shearing without slip events and dissipation. However, it is possible that slip events might occur adaptively at times *in vivo* if the hair bundle is challenged with harmfully extreme displacements.

One hypothesis, potentially testable with a different orientation of stereocilia, is that at low frequency, these attachments might slide within the stereociliary membrane: this would allow for connections between stereocilia to be quite stiff, yet stereocilia would be able to shear. Another possibility that might be mediated by Mg^{2+}-based attachments is that many weak attachments, when sheared, could be formed at the leading edge and disrupted at the lagging edge, in a manner similar to migrating leukocytes and keratinocytes. This might be tested with a different type of force micrometry such as optical tweezers that would allow longer-range movement. The two possibilities, sliding or attachment/re-attachment, would have different force signatures, former smooth and the latter jagged with stick-slip-like jumps.

5.3 IONIC SENSITIVITY OF CONNECTIONS

We found that inter-stereociliary adhesions are sensitive to the valence, type, and concentration of multivalent ion present in surrounding solutions. Mg^{2+}-induced attachments had a relatively low rupture force but were often irreversible, whereas Ca^{2+}-induced attachments exhibited a greater rupture force but were more strongly inhibited by an increase in free Ca^{2+}. The irreversibility of Mg^{2+}-induced attachments highlights the functional differences between divalent ions. Ca^{2+} and Mg^{2+} are similar in many of their physical properties but differ dramatically in their rates of water substitution (Diebler et al., 1969): Mg^{2+} retains oxygen ligands for nearly 10^{-5} s but Ca^{2+} does so for only 10^{-8} s. Prolonged interaction with the oxygen atoms present in sugars of the glycocalyx might account for the irreversibility of interstereociliary attachments in the presence of Mg^{2+}. The effects of Mg^{2+} also bear on the ability of dietary Mg^{2+} to reduce noise-induced hearing loss (Attias et al., 2003; Attias et al., 1994; Haupt and Scheibe, 2002; Joachims et al., 1993; Scheibe et al., 2000; Scheibe et al., 2002). Although the mechanism by which Mg^{2+} protects against hearing loss is unknown, stiffening of the hair bundle through increased cohesion by Mg^{2+} might contribute. If this is indeed true, Mg^{2+} supplements might slightly increase the threshold of hearing, making one less sensitive, but this has not been tested in the literature.

That attachment strength declines in the high-Ca^{2+} condition suggests the possibility of charge reversal or overcharging. This phenomenon, which occurs when a negatively charged surface is so heavily coated with multivalent cations

that it appears positively charged, is a classical feature of surfaces capable of counterion-mediated attraction (Lyubartsev and Nordenskiold, 1995). The study of charge reversal began more than 50 years ago and the phenomenon has been reported in such diverse systems as lipid vesicles, colloids, Langmuir monolayers, nanofiltration membranes, and flexible polyelectrolytes (Butler et al., 2003; Grønbech-Jensen et al., 1997; Ha and Liu, 1997; Kornyshev and Leikin, 1999; Lyubartsev et al., 1998). The mechanism of charge reversal is still debated but is often explained in terms of specific chemical interactions between ions such as hydrogen bonding, hydrophobic bonding, and complex formation (Faraudo and Travesset, 2007; Lyklema, 2006). Alternately, overcharging can be explained on the basis of ion-ion correlations, a more physical rather than chemical type of interpretation (Lyklema, 2009).

It would be desirable to observe the effects of the ions tested here on the glycocalyx in the intact hair bundle. However, Ca^{2+} can affect hair bundle mechanics and electrophysiology in many ways independent of its effects on the glycocalyx. The extracellular concentration of Ca^{2+} affects the rate at which adaptation occurs by altering the driving force for Ca^{2+}, which in turn affects the hair bundle's internal adaptation machinery (Cheung and Corey, 2006; Hudspeth, 2008; Ricci and Fettiplace, 1998; Ricci et al., 1998), with higher Ca^{2+} concentrations increasing the rate of adaptation. Additionally, high concentrations of Ca^{2+} can, to some extent, block the transduction channel through overcrowding at the pore (Cheung and Corey, 2006; Ricci and Fettiplace, 1998). Increased

extracellular Mg^{2+} can also reduce mechanoelectrical transduction currents by blocking the mechanotransduction channel, reducing the rate of adaptation. Because of these collected effects it would be difficult to parse the effects of these divalents on the glycocalyx from their effects on transduction within the hair cell. In addition, intact hair bundles often fuse when subjected to deglycosylation (personal observation), further complicating the study of the hair bundle glycocalyx.

Although ototoxicity of aminoglycoside antibiotics results in part from their entry into hair cells through mechanotransduction channels and consequent disruption of intracellular functions (Hutchin and Cortopassi, 1994), the effect of the drugs on the glycocalyx should not be overlooked. Gentamicin's ability to tightly connect stereocilia in these experiments accords with the finding that intra-aural gentamicin injection causes stereociliary fusion (Takumida et al., 1989a; Takumida et al., 1989b). One of the few molecules found to mitigate gentamicin ototoxicity is the lectin concanavalin A (Zheng and Gao, 1999), which we found to bind well to stereocilia. It is possible that the protective mechanism of concanavalin A is to conceal binding sites of the glycocalyx from gentamicin. When concanavalin A is applied to intact hair bundles, their stiffness increases in a manner similar to hair bundles affected by aminoglycoside antibiotics such as gentamicin (Kossl et al., 1990). Both concanavalin A and aminoglycosides have multiple binding sites and while both likely effect this stiffening by cross-linking glycocalyces, they differ in that the effect of concanavalin A is reversible.

Can effects found here be utilized to combat noise-induced hearing loss? If further experiments can be done to determine whether hair bundle stiffening is protective against noise-induced hearing loss, the findings here could provide a means to implement gentle hair bundle stiffening by altering endolymph ionic concentrations. However, while supplemental Mg^{2+} reduces noise-induced hearing loss, it is not clear whether the Mg^{2+} in the endolymph is increased when one is taking supplemental Mg^{2+}. The protective effects of Mg^{2+} on noise-induced hearing loss may be purely due to intracellular actions.

5.4 IDENTITY OF GLYCANS AND POTENTIAL ADHESION MECHANISMS

The structure of the stereociliary glycocalyx is unknown. Typical glycocalyx components, glycoproteins, glycolipids, and proteoglycans, vary in their sugar composition (Gabius, 2009). *N*-linked sugars emerging from transmembrane and membrane-associated proteins are often made up of approximately 14 sugar rings, typically, mannose, N-acetylglucosamine, N-acetylgalactosamine, fucose and sialic acid residues. While N-linked sugars are mostly found emerging from the cell membrane, O-linked sugars can be secreted, in the cytoplasm, nucleus, or attached to plasma-membrane-bound proteins. The most common O-linked sugar is N-acetylgalactosamine, often linked to secreted and membrane-bound proteins in what are often referred to as 'mucin-type' glycans. This reducing terminal N-acetylgalactosamine residue is sometimes also decorated with galactose, N-acetylglucosamine, and sialic acid residues. Generally O-linked

sugars are found on proteoglycans, secreted molecules with a much higher carbohydrate-to-protein ratio than that of glycoproteins. Glycosphingolipids also contribute to the glycocalyx, particularly in neural tissue. Gangliosides are complex glycosphingolipids with a ceramide backbone typically connected to 3-6 esterified sugars, one of which, a sialic acid.

Depending on the precise composition of the glycocalyx at distal tips of stereocilia, different adhesion mechanisms are possible. The simplest mechanism might involve gangliosides, the labeling of which is seen in Figure 3.7: divalent-tethered adhesions would occur between thin, acidic, ganglioside-glycocalyces at the distal tips of stereocilia. If this is indeed the only mechanism at work though, it does not explain why partial removal of N-linked sugars so cleared reduced adhesion. Alternately, a lectin-like molecule such as stereocilin (Sathyanarayana et al., 2009) known to be present at the distal tips of stereocilia (Verpy et al., 2008) might recognize either sugars of glycosphingolipids, or specific N-linked sugars on opposing stereociliary surfaces. Stereocilin may be GPI-anchored to one surface and bind sugars on the other in a manner modulated by divalent cations; in fact, many lectins require Ca^{2+} as a co-factor (Drickamer and Taylor, 1993). However this mechanism does not explain the irreversibility of predominant Mg^{2+}-mediated attachments. Lastly, if the glycocalyces at the distal tips of stereocilia are more extensive with complex, branched, N-linked sugars, Mg^{2+} and to some extent Ca^{2+} ions might organize neighboring sugars on each apposed membrane, making binding sites for

stereocilin more accessible and thus promoting adhesion in a less direct manner.

Before structural information about the identity of glycocalyx components is revealed, these mechanisms can be tested in a few ways. To test the ganglioside mechanism, isolated stereocilia could be pre-treated with the b-subunit of cholera toxin, coating potential binding sites on apposing surfaces and potentially reducing adhesion when stereocilia are brought together. This addition of the B-subunit of cholera toxin to intact hair bundles could disrupt inter-stereociliary adhesions leading to less coherent hair bundle motion. This might be observed either via dual-beam interferometry as in Kozlov et al. 2007 or an alteration in the appearance of horizontal top connectors by electron microscopy.

Lectin binding can usually be inhibited by the addition of an 'inhibitory sugar,' a sugar that mimics the binding ligand. While no inhibitory sugar is known for stereocilin and its status as a lectin has only been proposed from bioinformatic data, many different sugars could be applied to stereocilia to see if they might inhibit adhesion. If stereocilin is indeed extracellular and secreted, it might be possible to make recombinant stereocilin protein in a vertebrate cell line and apply it to a preparation of isolated stereocilia and monitor stereociliary adhesiveness.

If Ca^{2+} and Mg^{2+} are differentially organizing neighboring *N*-linked sugars, leading to different levels of adhesiveness, other divalent ions could be tested in the same manner to ascertain if there are specific organizational structures that lead to different adhesive behavior. If appropriate techniques were developed to image glycocalyx structure, electron microscopy might show differences in

glycocalyx structure in the presence of the different divalent ions.

Lastly, there are some efforts underway to characterize the protein and lipid composition of the hair bundle through mass spectrometry in the lab of Peter Gillespie. These efforts may shed light on the identities of the membrane proteins and glycolipids present, and thus could provide a greater understanding of the identities of glycocalyx components.

5.5 Stick-slip in the Hair Bundle

Stick-slip is a type of friction that we often encounter in our daily lives, from the squeaking of a door, to the licking of a fingertip to turn a page, to the beautiful strains of the string quartet (Benade, 1990; Persson, 2000; Rabinowicz, 1995). Stick-slip systems are defined by the presence of oscillations in movement between two sliding surfaces caused by shifting magnitudes of dissipative sliding friction and elastic energy storage. Stick-slip typically results when the static friction coefficient exceeds the kinetic friction coefficient. There are three principal mechanisms by which this can occur (Berman et al., 1996). The first is based on roughness, whereby irregularities on apposing surfaces cause a temporary increase in frictional force when they pass each other. The distance-dependent mechanism typically operates in dry systems in which there is adhesion between surfaces that creep for some distance before their adhesion is broken. This is the mechanism by which bowed-stringed instruments such as the violin produce sound (Benade, 1990). The third mechanism is the velocity-dependent

rate-and-state model used to model earthquakes (Ruina, 1983; Tse and Rice, 1986), where stick-slip behavior is chaotic, following a power law relating magnitude and frequency (Scholz, 1998). These mechanisms differ in whether they produce stick-slip events periodically, as in the violin, or non-periodically, as with earthquakes (Gutenberg and Richter, 1936; Persson, 2000; Urbakh et al., 2004). Power laws are a signature of self-organized criticality, a process that typically occurs in slowly driven, highly nonlinear systems including earthquakes, financial markets, epidemics, forest fires, and evolution (Bak and Tang, 1989). The power-law behavior in the friction between stereocilia suggests that this process follows the third mechanism.

Stick-slip friction with power-law magnitude-frequency behavior can be recapitulated with the Burridge-Knopoff model (Burridge and Knopoff, 1967), a string of blocks linked together by springs and tethered to one surface by another set of springs. As these blocks slide against a rough surface their sticking and slipping magnitudes and frequencies follow a power law. Although this arrangement and its multidimensional incarnations are typically used to model earthquakes, their geometries and results can be similarly used to understand the stick-slip friction between stereocilia.

Many biological movements utilize transitions between static and sliding friction (Denny, 1980; Niederegger and Gorb, 2006; Perez Goodwyn and Gorb, 2004; Scherge et al., 2001), though few systems have been experimentally analyzed. Snail locomotion is one of the most elegant examples of stick-slip in the

biological world (Denny, 1980). The mucus of the pedal foot of the snail oscillates in its viscosity as translational waves travel down the foot of a snail: the leading edge of the wave pushes the mucus into its liquid state, resulting in sliding friction, while the mucus behind the leading edge solidifies resulting in high static friction and thus allowing the snail to push against it and move forward. California Spiny lobsters use stick-slip to make an anti-predator rasp by rubbing an extension of their antennae over a file-like patch below the eye (Patek and Baio, 2007). Both of these systems exhibit periodic stick-slip. Rats may use stick-slip as a method of textural analysis when whisking (Wolfe et al., 2008).

Here, we have observed chaotic stick-slip behavior between stereocilia of the inner ear, where our observed slip magnitudes followed a Gutenberg-Richter-like power-law typically associated with large-scale, dry, systems such as earthquakes and granular materials (Bretz et al., 2006; Carlson and Langer, 1989; Carlson et al., 1994; Dalton and Corcoran, 2001). It is remarkable to have found similarity between the stick-slip properties of such disparate systems as the microscopic, biological domain of the inner ear and the macroscopic, geological regime of earthquakes. The power-law stick-slip observed here can likely be attributed to the weakly adhesive molecules of the glycocalyx (Chang and Hammer, 2000; Chang et al., 2000; Goetz et al., 1994). A rich literature in physics and material science is devoted to the understanding and controlling of stick-slip phenomena and their governing properties (Persson, 2000; Urbakh et al., 2004). Hopefully, the commonalities in the physical properties of

these systems differing in size by twelve orders of magnitude can inform the study of stick-slip phenomena more broadly.

To extend the range over which this power law is observed one would need to utilize a different force-sensing mechanism to allow greater range of movement. If the power law between the distal tips of stereocilia persisted at larger length scales but not between stereociliary tapers or under perturbation conditions, this would provide useful information to the physics community studying stick slip. It would be interesting to try to alter adhesiveness of another chaotically stick-slipping system to see if similar perturbations could be created.

5.6 The Glycocalyx, Hearing, and Mechanotransduction

Mechanosensation is utilized by biology in many ways ranging from a bacterium's reaction to osmotic stress to a lover's response to a tender caress. The typical recipient for mechanical stimulation is the plasma membrane of the cell, where in response to physical stress, mechanosensitive ion channels change their open probability. The open probability of mechanosensitive channels can be altered by physical stress in a variety of ways: membrane tension, membrane curvature, selective addition or removal of certain lipids in one or the other leaflet of the membrane, and finally, force directly applied to the mechanosensitive channel by a molecule tethered to another cellular component (Gillespie and Walker, 2001; Xiao and Xu, 2010). The molecules of the glycocalyx are in an excellent position to mediate many of these forces and thus alter the

biomechanical environment of the plasma membrane. The layer of cells lining blood vessels provides an example: the endothelium layer is coated with a many-micron-thick glycocalyx known to relate information about extracellular blood flow rate to the intracellular realm (Weinbaum et al., 2003).

An extensive complement of highly glycosylated proteins decorates the extracellular membrane of hair bundle stereocilia. An extreme example is vlgr1, a protein present in taper region of stereocilia that possesses 90 *N*-glycosylation sites in its ectodomain (McMillan et al., 2002). Nearly every protein known to emerge from the stereociliary plasmalemma—cadherin-23, protocadherin-15, otoanchorin, stereocilin, ptprq, usherin, clarin-1—are all glycoproteins (Bhattacharya et al., 2002; Kazmierczak et al., 2007; Nayak, 2010; Rzadzinska et al., 2005; Senften et al., 2006; Siemens et al., 2004; Tian et al., 2009). Mutations in many of these glycosylated hair bundle proteins cause deafness, indicating that their functions are essential to hearing.

Aside from the glycoproteins of the stereociliary glycocalyx, gangliosides, may also play an important role in mechanotransduction. A mutation in ganglioside GM3 synthase, an enzyme essential in the production of lipid-microdomain-component ganglioside GM3, causes deafness by hair-cell degeneration (Yoshikawa et al., 2009). The plasma membranes at the distal tips of stereocilia are highly likely to be specialized for mechanosensation, especially given recent evidence (Beurg et al., 2009) indicating that mechanotransduction channels reside at the lower tip link insertion points, at the distal tips of stereocilia.

Whether or not gangliosides are involved in hair bundle cohesion, they might play an important role in the regulation of the membranes at the distal tips of stereocilia. One method to ascertain the function of these components would be to conditionally disrupt GM3 synthase or GM1 synthase and observed mechanotransduction in hair cells in a cultured organ. There also may be techniques to sequester these components as they are known to cluster, and then observe mechanotransduction.

For any cell whose function relies on its glycocalyx, that glycocalyx is likely to need maintenance. The little-studied phenomenon of membrane shedding might be a way of 'cleaning' or 'refreshing' the glycocalyx in cell types for whom the glycocalyx is functionally important. Membrane shedding, a process by which small vesicles are shed from the plasma membrane, has been observed in the brush border of enterocytes in the gut, in photoreceptors, and in erythrocytes (Beaudoin and Grondin, 1991; McConnell et al., 2009; Williams, 1982). Each of these tissues requires specific but flexible membrane interactions that likely rely on the glycocalyx. When fixed by electron microscopy, hair bundles often have many small neighboring vesicles floating about in the endolymphatic space (A.J. Hudspeth, unpublished observation). These small vesicles may be remnants of such a membrane-shedding glycocalyx-renewal process. A time-lapse microscopy experiment with labeled membranes would be able to confirm or deny this phenomenon.

As a structure that can transduce extracellular forces to intracellular

components, the stereociliary glycocalyx might even play a role in auditory mechanosensation. Given the results presented here, the stereociliary glycocalyx likely functions in hair cell by forming connections between neighboring stereocilia, and in concert with ions of the endolymph, modulating the cohesion of the hair bundle. When the hair bundle is deflected by sound, force is applied to these glyco-adhesions, where they might alter membrane tension, the shape of the membrane, and/or the conformation of important transmembrane proteins. Owing to their privileged positions beside the tip links, such alterations might help shape the dynamics of auditory mechanotransduction.

5.7 Concluding Remarks

In my thesis work, I have explored the role of the stereociliary glycocalyx in hair bundle cohesion and lubrication. While it is not yet clear how hair bundle links, cuticular plate curvature, hydrodynamics and divalent-mediated glyco-tethering all come together to provide hair bundle cohesion, this work is a step forward in our understanding. Concurrent with my work on the electrostatic aspects of the hair bundle, others have been studying the hydrodynamic aspects (Kozlov et al. submitted, Baumgart, 2010). They have found that while the viscosity of the fluid around the hair bundle might provide significant cohesive force, stiff linkages near the distal tips of stereocilia are necessary for the full experimentally observed cohesion. My experiments provide evidence indicating that the distal tips of stereocilia can adhere to one another through electrostatic

tethering of their glycocalyces, potentially filling this niche.

In addition to advancing our understanding of the hair bundle, this work also sheds light on other diverse fields. While the chaotic stick-slip I have observed between stereocilia may or may not be functionally relevant to hair bundle function, it is a surprising physical system in which to find such behavior. The power-law stick-slip of earthquakes is considered an emergent phenomenon, as are power-laws describing the distribution of wealth in communities, forest fires, and financial markets. Given that a power-law in slip magnitudes between stereocilia occurred only between the distal tips of stereocilia in endolymph and not under any of the perturbation conditions, it is possible that evolution has harnessed this emergent property for some adaptive function. Lastly, I hope that another example of functional glycan-mediated cell adhesion further compels biologists to return to the study of the glycocalyx, especially in light of the emerging fields of biomechanics and lipidomics.

APPENDIX 1: INTRA-STEREOCILIARY SHEAR

In Johannes Baumgart's modeling work on the hair bundle, he noted that there might be shear between individual actin filaments within stereocilia. Fimbrin, espin, and other proteins cross-link actin fibers within stereocilia (Rzadzinska et al., 2004; Volkmann et al., 2001). These cross-linking proteins might pivot at their points of contact with the actin filaments affecting the mechanical properties of the stereocilia (Bathe et al., 2008). If the stereociliary cross-links can pivot, stereocilia should bend with a V-shape when pressed at the mid-point, while if instead the cross-links attach to actin without a flexible pivot, stereocilia would bend in a U-shape similar to a beam of wood. I tested these predictions in two ways. Gecko stereocilia were isolated as previously described and allowed to settle in an experimental chamber. When stereocilia attached to a glass surface, they typically attached at both distal and tapered ends and sometimes in between. A stiff force fiber was then used to apply direct force to the midpoint of a given stereocilium and the bending motion was monitored. Stereocilia produced V-shaped bending patterns (Figure A.1). However, such a conformation could also result if the stereocilium were stretched like a rubber band. In order to rule out this possibility, we sought to bend stereocilia pinned against non-adhesive posts. Drosophila fly wings, which are both optically transparent and coated in stiff hydrophobic hairs spaced at approximately 10-20 μm intervals, provided a near ideal substrate for these experiments. Given the wide spacing of the wing hairs, anole stereocilia were used. Again, when stereocilia were bent at their mid-points,

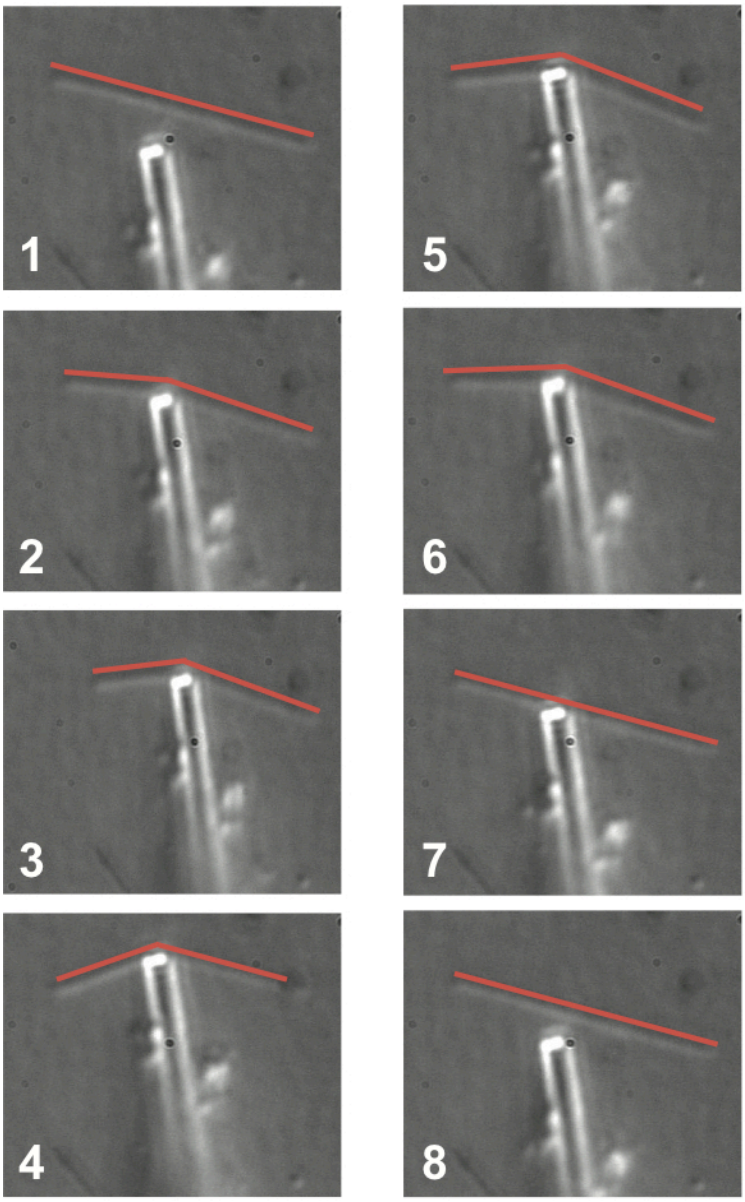

Figure A.1: A glass fiber bending a gecko stereocilium attached to the glass chamber. Note that the stereocilium bends with a V-shape.

they did so in a V-shape indicative of internal pivoting. While qualitatively this seems clear, it would be preferable to have quantitative data indicating the stiffness of the stereocilia bent in this geometry. This is quite possible if a stiff, calibrated, fiber were used to bend stereocilia while simultaneously monitoring by video. Only a steady-state measurement of the fiber's flexion is necessary to obtain the force necessary to bend stereocilia.

APPENDIX 2: A POTENTIALLY USEFUL ARTIFACT

In my attempts to elucidate the mechanism of fast adaptation in the hair bundle, I built a system in which a UV laser beam can shine on a spatial restricted area smaller than a hair bundle, while hair bundle movement is simultaneously monitored by force fiber photomicrometry. Though the original purpose of this system was not accomplished, a potentially useful artifact was discovered in the process. The force fibers absorb photons due to their dark gold-palladium coating. When the force fiber and the UV laser beam were in close proximity, the barrage of photons induced such significant momentum transfer that the force fiber moved in the absence of any other stimuli (Figure A.2). Such momentum transfer did not occur with uncoated force-fibers (Figure A.2). This technique could be utilized to mechanically stimulate objects without the constraints of the hydrodynamically awkward force-fiber or cantilever, if the objects could be 'darkened.' A hair bundle could be made to absorb more photons if coated with lectins conjugated to gold-particles, for example.

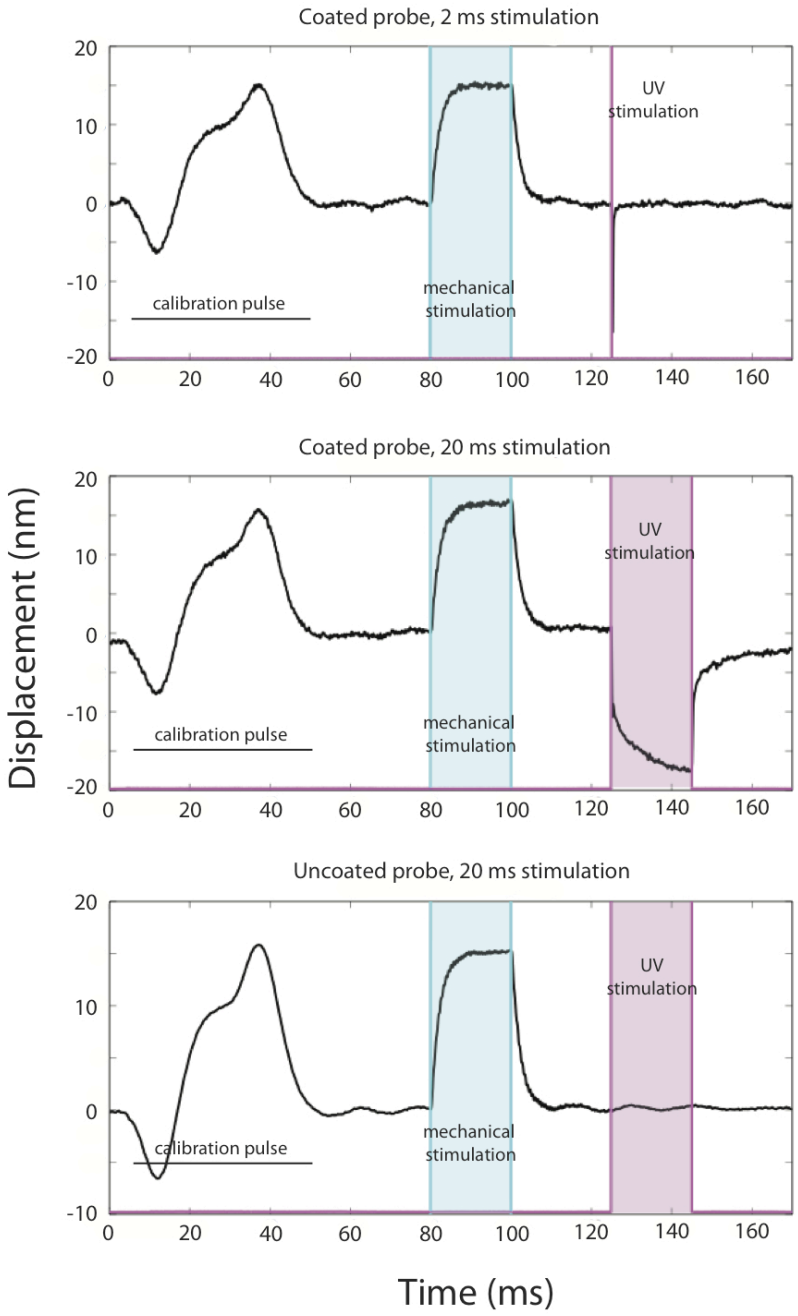

Figure A.2: The UV-fiber effect. A, force-fiber in free-fluid is mechanically moved by a piezoelectrical actuator (blue), then by a 2 ms pulse, upper, or a 20 ms pulse, middle and lower, of focused UV light (magenta). The first two panels show movements of gold-palladium coated fibers, while the last panel displays movements of an uncoated fiber on which the UV has no effect.

REFERENCES

Adato, A., Lefevre, G., Delprat, B., Michel, V., Michalski, N., Chardenoux, S., Weil, D., El-Amraoui, A., and Petit, C. (2005). Usherin, the defective protein in Usher syndrome type IIA, is likely to be a component of interstereocilia ankle links in the inner ear sensory cells. Hum Mol Genet *14*, 3921-3932.

Alberts, B., Johnson, A., Lewis, J., Raff, M., Roberts, K., and Walter, P. (2002). Molecular biology of the cell.

Armstrong, C.E., and Roberts, W.M. (2001). Rapidly inactivating and non-inactivating calcium-activated potassium currents in frog saccular hair cells. J Physiol *536*, 49-65.

Art, J.J., and Fettiplace, R. (1987). Variation of membrane properties in hair cells isolated from the turtle cochlea. J Physiol *385*, 207-242.

Ashwell, G., Hartford (1982). Carbohydrate-specific receptors on the liver Annu Rev Biochem *51*, 531-554.

Assad, J.A., Shepherd, G.M., and Corey, D.P. (1991). Tip-link integrity and mechanical transduction in vertebrate hair cells. Neuron *7*, 985-994.

Attias, J., Bresloff, I., Haupt, H., Scheibe, F., and Ising, H. (2003). Preventing noise induced otoacoustic emission loss by increasing magnesium (Mg2+) intake in guinea-pigs. J Basic Clin Physiol Pharmacol *14*, 119-136.

Attias, J., Weisz, G., Almog, S., Shahar, A., Wiener, M., Joachims, Z., Netzer, A., Ising, H., Rebentisch, E., and Guenther, T. (1994). Oral magnesium intake reduces permanent hearing loss induced by noise exposure. Am J Otolaryngol *15*, 26-32.

Baird, R.A., Schuff, N.R., and Bancroft, J. (1993). Regional differences in lectin binding patterns of vestibular hair cells. Hear Res *65*, 151-163.

Bak, P., and Tang, C. (1989). Earthquakes as a Self-Organized Critical Phenomenon. Journal of Geophysical Research-Solid Earth and Planets *94*, 15635-15637.

Bashtanov, M.E., Goodyear, R.J., Richardson, G.P., and Russell, I.J. (2004). The mechanical properties of chick (Gallus domesticus) sensory hair bundles: relative contributions of structures sensitive to calcium chelation and subtilisin treatment. J Physiol *559*, 287-299.

Bathe, M., Heussinger, C., Claessens, M.M., Bausch, A.R., and Frey, E. (2008). Cytoskeletal bundle mechanics. Biophys J *94*, 2955-2964.

Batters, C., Arthur, C.P., Lin, A., Porter, J., Geeves, M.A., Milligan, R.A., Molloy, J.E., and Coluccio, L.M. (2004). Myo1c is designed for the adaptation response in the inner ear. The EMBO Journal *23*, 1433-1440.

Baumgart, J. (2010). The Hair Bundle: Fluid-Structure Interaction in the Inner Ear. In Von der Fakultat Maschinenwesen (Dresden, Technischen Universitat Dresden).

Bautista, D.M., Movahed, P., Hinman, A., Axelsson, H.E., Sterner, O., Hogestatt, E.D., Julius, D., Jordt, S.E., and Zygmunt, P.M. (2005). Pungent products from garlic activate the sensory ion channel TRPA1. Proc Natl Acad Sci U S A *102*, 12248-12252.

Beaudoin, A.R., and Grondin, G. (1991). Shedding of vesicular material from the cell surface of eukaryotic cells: different cellular phenomena. Biochim Biophys Acta *1071*, 203-219.

Benade, A. (1990). Fundamentals of musical acoustics (Dover Pubns).

Benser, M.E., Marquis, R.E., and Hudspeth, A.J. (1996). Rapid, Active Hair Bundle Movements in Hair Cells from the Bullfrog's Sacculus. Journal of Neuroscience *16*, 5629-5643.

Berman, A.D., Ducker, W.A., and Israelachvili, J.N. (1996). Origin and characterization of different stick-slip friction mechanisms. Langmuir *12*, 4559-4563.

Beurg, M., Fettiplace, R., Nam, J.H., and Ricci, A.J. (2009). Localization of inner hair cell mechanotransducer channels using high-speed calcium imaging. Nat Neurosci *12*, 553-558.

Bhattacharya, G., Miller, C., Kimberling, W.J., Jablonski, M.M., and Cosgrove, D. (2002). Localization and expression of usherin: a novel basement membrane protein defective in people with Usher's syndrome type IIa. Hear Res *163*, 1-11.

Blount, P., and Moe, P.C. (1999). Bacterial mechanosensitive channels: integrating physiology, structure and function. Trends Microbiol *7*, 420-424.

Boggs, J.M., Gao, W., and Hirahara, Y. (2008). Myelin glycosphingolipids, galactosylceramide and sulfatide, participate in carbohydrate-carbohydrate interactions between apposed membranes and may form glycosynapses between oligodendrocyte and/or myelin membranes. Biochim Biophys Acta *1780*, 445-455.

Bosher, S.K., and Warren, R.L. (1978). Very low calcium content of cochlear endolymph, an extracellular fluid. Nature *273*, 377-378.

Boubelik, M., Floryk, D., Bohata, J., Draberova, L., Macak, J., Smid, F., and Draber, P. (1998). Lex glycosphingolipids-mediated cell aggregation.

Glycobiology *8*, 139-146.

Bozovic, D., and Hudspeth, A.J. (2003). Hair-bundle movements elicited by transepithelial electrical stimulation of hair cells in the sacculus of the bullfrog. Proceedings of the National Academy of Sciences *100*, 958-963.

Bretz, M., Zaretzki, R., Field, S.B., Mitarai, N., and Nori, F. (2006). Broad distribution of stick-slip events in slowly sheared granular media: Table-top production of a Gutenberg-Richter-like distribution. Europhys Lett *74*, 1116-1122.

Brittan-Powell, E.F., Christensen-Dalsgaard, J., Tang, Y., Carr, C., and Dooling, R.J. (2010). The auditory brainstem response in two lizard species. J Acoust Soc Am *128*, 787-794.

Bucior, I., and Burger, M.M. (2004). Carbohydrate-carbohydrate interactions in cell recognition. Curr Opin Struct Biol *14*, 631-637.

Bucior, I., Scheuring, S., Engel, A., and Burger, M.M. (2004). Carbohydrate-carbohydrate interaction provides adhesion force and specificity for cellular recognition. J Cell Biol *165*, 529-537.

Burridge, R., and Knopoff, L. (1967). Model and Theoretical Seismicity. B Seismol Soc Am *57*, 341-&.

Butler, J.C., Angelini, T., Tang, J.X., and Wong, G.C.L. (2003). Ion Multivalence and Like-Charge Polyelectrolyte Attraction. Physical Review Letters *91*, 28301.

Carlson, J.M., and Langer, J.S. (1989). Properties of earthquakes generated by fault dynamics. Phys Rev Lett *62*, 2632-2635.

Carlson, J.M., Langer, J.S., and Shaw, B.E. (1994). Dynamics of Earthquake Faults. Rev Mod Phys *66*, 657-670.

Chang, K.C., and Hammer, D.A. (2000). Adhesive dynamics simulations of sialyl-Lewis(x)/E-selectin-mediated rolling in a cell-free system. Biophys J *79*, 1891-1902.

Chang, K.C., Tees, D.F., and Hammer, D.A. (2000). The state diagram for cell adhesion under flow: leukocyte rolling and firm adhesion. Proc Natl Acad Sci U S A *97*, 11262-11267.

Cheung, E.L., and Corey, D.P. (2006). Ca2+ changes the force sensitivity of the hair-cell transduction channel. Biophys J *90*, 124-139.

Choe, Y., Magnasco, M.O., and Hudspeth, A.J. (1998). A model for amplification of hair-bundle motion by cyclical binding of Ca2+ to mechanoelectrical-transduction channels (National Acad Sciences).

Christensen, A.P., and Corey, D.P. (2007). TRP channels in mechanosensation: direct or indirect activation? Nat Rev Neurosci *8*, 510-521.

Citron, L., Exley, D., and Hallpike, C.S. (1956). Formation, circulation and chemical properties of the labyrinthine fluids. Br Med Bull *12*, 101-104.

Clauset, A., Shalizi, C., and Newman, M. (2009). Power-law distributions in empirical data. Siam Review *51*, 661-703.

Corey, D.P. (2009). Cell biology of mechanotransduction in inner-ear hair cells. F1000 Biol Rep *1*.

Corey, D.P., Garcia-Anoveros, J., Holt, J.R., Kwan, K.Y., Lin, S.Y., Vollrath, M.A., Amalfitano, A., Cheung, E.L., Derfler, B.H., Duggan, A.*, et al.* (2004). TRPA1 is a candidate for the mechanosensitive transduction channel of vertebrate hair cells. Nature *432*, 723-730.

Corey, D.P., and Hudspeth, A.J. (1983a). Analysis of the microphonic potential of the bullfrog's sacculus. J Neurosci *3*, 942-961.

Corey, D.P., and Hudspeth, A.J. (1983b). Kinetics of the receptor current in bullfrog saccular hair cells. J Neurosci *3*, 962-976.

Coste, B., Mathur, J., Schmidt, M., Earley, T.J., Ranade, S., Petrus, M.J., Dubin, A.E., and Patapoutian, A. (2010). Piezo1 and Piezo2 are essential components of distinct mechanically activated cation channels. Science *330*, 55-60.

Couloigner, V., Teixeira, M., Sterkers, O., and Ferrary, E. (1999). In vivo study of the electrochemical composition of luminal fluid in the guinea pig endolymphatic sac. Acta Otolaryngol *119*, 200-202.

Crawford, A.C., Evans, M.G., and Fettiplace, R. (1991). The actions of calcium on the mechano-electrical transducer current of turtle hair cells. J Physiol *434*, 369-398.

Csukas, S.R., Rosenquist, T.H., and Mulroy, M.J. (1987). Connections between stereocilia in auditory hair cells of the alligator lizard. Hear Res *30*, 147-155.

Dahl, R., and Staehelin, L.A. (1989). High-pressure freezing for the preservation of biological structure: Theory and practice. Journal of Electron Microscopy Technique *13*, 165-174.

Dalton, F., and Corcoran, D. (2001). Self-organized criticality in a sheared granular stick-slip system. Phys Rev E *63*, -.

Dammer, U., Popescu, O., Wagner, P., Anselmetti, D., Guntherodt, H.J., and

Misevic, G.N. (1995). Binding strength between cell adhesion proteoglycans measured by atomic force microscopy. Science *267*, 1173-1175.

Denk, W., Webb, W.W., and Hudspeth, A.J. (1989). Mechanical Properties of Sensory Hair Bundles are Reflected in their Brownian Motion Measured with a Laser Differential Interferometer. Proceedings of the National Academy of Sciences *86*, 5371-5375.

Denny, M. (1980). Locomotion: the cost of gastropod crawling. Science *208*, 1288-1290.

Diebler, H., Eigen, M., Ilgenfritz, G., Maass, G., and Winkler, R. (1969). Kinetics and mechanism of reactions of main group metal ions with biological carriers. Pure Appl Chem *20*, 93.

Dolgobrodov, S.G., Lukashkin, A.N., and Russell, I.J. (2000). Electrostatic interaction between stereocilia: I. Its role in supporting the structure of the hair bundle. Hear Res *150*, 83-93.

Drickamer, K., and Taylor, M.E. (1993). Biology of animal lectins. Annu Rev Cell Biol *9*, 237-264.

Eatock, R.A. (2000). Adaptation in Hair Cells. Annual Review of Neuroscience *23*, 285-314.

Eatock, R.A., Corey, D.P., and Hudspeth, A.J. (1987). Adaptation of mechanoelectrical transduction in hair cells of the bullfrog's sacculus. Journal of Neuroscience *7*, 2821-2836.

Eggens, I., Fenderson, B., Toyokuni, T., Dean, B., Stroud, M., and Hakomori, S. (1989). Specific interaction between Lex and Lex determinants. A possible basis for cell recognition in preimplantation embryos and in embryonal carcinoma cells. J Biol Chem *264*, 9476-9484.

Endo, Y., Mitsui, K., Motizuki, M., and Tsurugi, K. (1987). The mechanism of action of ricin and related toxic lectins on eukaryotic ribosomes. The site and the characteristics of the modification in 28 S ribosomal RNA caused by the toxins. J Biol Chem *262*, 5908-5912.

Enger, P.S. (1964). Ionic Composition of the Cranial and Labyrinthine Fluids and Saccular D.C. Potentials in Fish. Comp Biochem Physiol *11*, 131-137.

Evans, E.A., and Calderwood, D.A. (2007). Forces and bond dynamics in cell adhesion. Science *316*, 1148-1153.

Faraudo, J., and Travesset, A. (2007). Phosphatidic acid domains in membranes: effect of divalent counterions. Biophys J *92*, 2806-2818.

Fernandez-Busquets, X., Kornig, A., Bucior, I., Burger, M.M., and Anselmetti, D. (2009). Self-recognition and Ca2+-dependent carbohydrate-carbohydrate cell adhesion provide clues to the cambrian explosion. Mol Biol Evol *26*, 2551-2561.

Freeman, D.M., Cotanche, D.A., Ehsani, F., and Weiss, T.F. (1994). The osmotic response of the isolated tectorial membrane of the chick to isosmotic solutions: effect of Na+, K+, and Ca2+ concentration. Hear Res *79*, 197-215.

Freeman, D.M., Hendrix, D.K., Shah, D., Fan, L.F., and Weiss, T.F. (1993). Effect of lymph composition on an in vitro preparation of the alligator lizard cochlea. Hear Res *65*, 83-98.

Furness, D.N., and Hackney, C.M. (1985). Cross-links between stereocilia in the guinea pig cochlea. Hear Res *18*, 177-188.

Furness, D.N., and Hackney, C.M. (1986). Morphological changes to the stereociliary bundles in the guinea pig cochlea after kanamycin treatment. Br J Audiol *20*, 253-259.

Gabius, H. (2009). The sugar code: fundamentals of glycosciences (Wiley-VCH).

Gabius, H.J., Andre, S., Kaltner, H., and Siebert, H.C. (2002). The sugar code: functional lectinomics. Biochim Biophys Acta *1572*, 165-177.

Garcia-Anoveros, J., and Corey, D.P. (1997). The molecules of mechanosensation. Annu Rev Neurosci *20*, 567-594.

Gebauer, M., Watzke, D., and Machemer, H. (1999). The gravikinetic response of Paramecium is based on orientation-dependent mechanotransduction. Naturwissenschaften *86*, 352-356.

Gelfand, S.A. (2009). Essentials of Audiology, Auditory System and Related Disorders (Thieme).

Geyer, A., Gege, C., and Schmidt, R.R. (2000). Calcium-Dependent Carbohydrate-Carbohydrate Recognition between Lewis(X) Blood Group Antigens This research was supported by the Deutsche Forschungsgemeinschaft and the Fonds der Chemischen Industrie. Angew Chem Int Ed Engl *39*, 3245-3249.

Gil-Loyzaga, P., and Brownell, W.E. (1988). Wheat germ agglutinin and Helix pomatia agglutinin lectin binding on cochlear hair cells. Hear Res *34*, 149-155.

Gillespie, P.G., and Cyr, J.L. (2004). Myosin-1 c, the Hair Cell's Adaptation Motor. Annual Review of Physiology *66*, 521-545.

Gillespie, P.G., Wagner, M.C., and Hudspeth, A.J. (1993). Identification of a

120 kd hair-bundle myosin located near stereociliary tips. Neuron *11*, 581-594.

Gillespie, P.G., and Walker, R.G. (2001). Molecular basis of mechanosensory transduction. Nature *413*, 194-202.

Goetz, D.J., el-Sabban, M.E., Pauli, B.U., and Hammer, D.A. (1994). Dynamics of neutrophil rolling over stimulated endothelium in vitro. Biophys J *66*, 2202-2209.

Goodyear, R., and Richardson, G. (1992). Distribution of the 275 kD hair cell antigen and cell surface specialisations on auditory and vestibular hair bundles in the chicken inner ear. J Comp Neurol *325*, 243-256.

Goodyear, R., and Richardson, G. (1994). Differential glycosylation of auditory and vestibular hair bundle proteins revealed by peanut agglutinin. J Comp Neurol *345*, 267-278.

Goodyear, R.J., Legan, P.K., Wright, M.B., Marcotti, W., Oganesian, A., Coats, S.A., Booth, C.J., Kros, C.J., Seifert, R.A., Bowen-Pope, D.F.*, et al.* (2003). A receptor-like inositol lipid phosphatase is required for the maturation of developing cochlear hair bundles. J Neurosci *23*, 9208-9219.

Goodyear, R.J., and Richardson, G.P. (2003). A novel antigen sensitive to calcium chelation that is associated with the tip links and kinocilial links of sensory hair bundles. J Neurosci *23*, 4878-4887.

Grønbech-Jensen, N., Mashl, R.J., Bruinsma, R.F., and Gelbart, W.M. (1997). Counterion-Induced Attraction between Rigid Polyelectrolytes. Physical Review Letters *78*, 2477-2480.

Gutenberg, B., and Richter, C.F. (1936). Magnitude and Energy of Earthquakes. Science *83*, 183-185.

Ha, B.Y., and Liu, A.J. (1997). Counterion-Mediated Attraction between Two Like-Charged Rods. Physical Review Letters *79*, 1289-1292.

Hakomori, S.I. (2002). The glycosynapse. Proc Natl Acad Sci U S A *99*, 225-232.

Haseley, S.R., Vermeer, H.J., Kamerling, J.P., and Vliegenthart, J.F. (2001). Carbohydrate self-recognition mediates marine sponge cellular adhesion. Proc Natl Acad Sci U S A *98*, 9419-9424.

Hasson, T., Gillespie, P.G., Garcia, J.A., MacDonald, R.B., Zhao, Y., Yee, A.G., Mooseker, M.S., and Corey, D.P. (1997). Unconventional Myosins in Inner-Ear Sensory Epithelia. The Journal of Cell Biology *137*, 1287-1307.

Haupt, H., and Scheibe, F. (2002). Preventive magnesium supplement

protects the inner ear against noise-induced impairment of blood flow and oxygenation in the guinea pig. Magnes Res *15*, 17-25.

Holt, J.R., Gillespie, S.K.H., Provance, D.W., Shah, K., Shokat, K.M., Corey, D.P., Mercer, J.A., and Gillespie, P.G. (2002). A Chemical-Genetic Strategy Implicates Myosin-1c in Adaptation by Hair Cells. Cell *108*, 371-381.

Howard, J., and Hudspeth, A.J. (1987). Mechanical Relaxation of the Hair Bundle Mediates Adaptation in Mechanoelectrical Transduction by the Bullfrog's Saccular Hair Cell. Proceedings of the National Academy of Sciences *84*, 3064-3068.

Howard, J., and Hudspeth, A.J. (1988). Compliance of the hair bundle associated with gating of mechanoelectrical transduction channels in the bullfrog's saccular hair cell. Neuron *1*, 189-199.

Hozawa, K., Wataya, H., Takasaka, T., Fenderson, B.A., and Hakomori, S. (1993). Hearing and glycoconjugates: localization of Le(y), Le(x) and sialosyl-Le(x) in guinea pig cochlea, particularly at the tectorial membrane and sensory epithelia of the organ of Corti. Glycobiology *3*, 47-55.

Hu, J., Chiang, L.Y., Koch, M., and Lewin, G.R. (2010). Evidence for a protein tether involved in somatic touch. EMBO J *29*, 855-867.

Hudspeth, A.J. (2008). Making an effort to listen: mechanical amplification in the ear. Neuron *59*, 530-545.

Hutchin, T., and Cortopassi, G. (1994). Proposed Molecular and Cellular Mechanism for Aminoglycoside Ototoxicity. Antimicrobial Agents and Chemotherapy *38*, 2517-2520.

Hynes, R.O. (2002). Integrins: bidirectional, allosteric signaling machines. Cell *110*, 673-687.

Ingber, D.E. (1997). Tensegrity: the architectural basis of cellular mechanotransduction. Annu Rev Physiol *59*, 575-599.

Jacobs, R.A., and Hudspeth, A.J. (1990). Ultrastructural correlates of mechanoelectrical transduction in hair cells of the bullfrog's internal ear. Cold Spring Harb Symp Quant Biol *55*, 547-561.

Jahn, A., and Santos-Sacchi, J. (2001). Physiology of the Ear (Singular Pub Group).

Joachims, Z., Netzer, A., Ising, H., Rebentisch, E., Attias, J., Weisz, G., and Gunther, T. (1993). Oral magnesium supplementation as prophylaxis for noise-induced hearing loss: results of a double blind field study. Schriftenr Ver Wasser Boden Lufthyg *88*, 503-516.

Kamkin, A., and Kiseleva, I. (2007). Mechanosensitive ion channels (Springer).

Kang, L., Gao, J., Schafer, W.R., Xie, Z., and Xu, X.Z. (2010). C. elegans TRP family protein TRP-4 is a pore-forming subunit of a native mechanotransduction channel. Neuron *67*, 381-391.

Karavitaki, K.D., and Corey, D.P. (2010). Sliding adhesion confers coherent motion to hair cell stereocilia and parallel gating to transduction channels. J Neurosci *30*, 9051-9063.

Katori, Y., Hackney, C., and Furness, D. (1996a). Immunoreactivity of sensory hair bundles of the guinea-pig cochlea to antibodies against elastin and keratan sulphate. Cell and Tissue Research *284*, 473-479.

Katori, Y., Tonosaki, A., and Takasaka, T. (1996b). WGA lectin binding sites of the apical surface of corti epithelium: enhancement by back-scattered electron imaging in guinea-pig inner ear. J Electron Microsc (Tokyo) *45*, 207-212.

Kazmierczak, P., Sakaguchi, H., Tokita, J., Wilson-Kubalek, E.M., Milligan, R.A., Muller, U., and Kachar, B. (2007). Cadherin 23 and protocadherin 15 interact to form tip-link filaments in sensory hair cells. Nature *449*, 87-91.

Kellenberger, S., and Schild, L. (2002). Epithelial sodium channel/degenerin family of ion channels: a variety of functions for a shared structure. Physiol Rev *82*, 735-767.

Kemler, R. (1993). From cadherins to catenins: cytoplasmic protein interactions and regulation of cell adhesion. Trends Genet *9*, 317-321.

Ketten, D. (1997). Structure and function in whale ears. Bioacoustics *8*, 103-136.

Killick, R., and Richardson, G.P. (1997). Antibodies to the sulphated, high molecular mass mouse tectorin stain hair bundles and the olfactory mucus layer. Hear Res *103*, 131-141.

Klein, J., Kamiyama, Y., Yoshizawa, H., Israelachvili, J.N., Fredrickson, G.H., Pincus, P., and Fetters, L.J. (1993). Lubrication forces between surfaces bearing polymer brushes. Macromolecules *26*, 5552-5560.

Kloda, A., and Martinac, B. (2001). Molecular identification of a mechanosensitive channel in archaea. Biophys J *80*, 229-240.

Ko, K.S., and McCulloch, C.A. (2001). Intercellular mechanotransduction: cellular circuits that coordinate tissue responses to mechanical loading. Biochem Biophys Res Commun *285*, 1077-1083.

Koch, A.L. (1994). Development and diversification of the Last Universal Ancestor. J Theor Biol *168*, 269-280.

Kojima, N., Fenderson, B.A., Stroud, M.R., Goldberg, R.I., Habermann, R., Toyokuni, T., and Hakomori, S. (1994). Further studies on cell adhesion based on Le(x)-Le(x) interaction, with new approaches: embryoglycan aggregation of F9 teratocarcinoma cells, and adhesion of various tumour cells based on Le(x) expression. Glycoconj J *11*, 238-248.

Koprowski, P., and Kubalski, A. (2001). Bacterial ion channels and their eukaryotic homologues. Bioessays *23*, 1148-1158.

Kornyshev, A.A., and Leikin, S. (1999). Electrostatic Zipper Motif for DNA Aggregation. Physical Review Letters *82*, 4138-4141.

Kossl, M., Richardson, G.P., and Russell, I.J. (1990). Stereocilia bundle stiffness: effects of neomycin sulphate, A23187 and concanavalin A. Hear Res *44*, 217-229.

Kozlov, A.S., Risler, T., and Hudspeth, A.J. (2007). Coherent motion of stereocilia assures the concerted gating of hair-cell transduction channels. Nat Neurosci *10*, 87-92.

Kwan, K.Y., Allchorne, A.J., Vollrath, M.A., Christensen, A.P., Zhang, D.S., Woolf, C.J., and Corey, D.P. (2006). TRPA1 contributes to cold, mechanical, and chemical nociception but is not essential for hair-cell transduction. Neuron *50*, 277-289.

Kwan, K.Y., Glazer, J.M., Corey, D.P., Rice, F.L., and Stucky, C.L. (2009). TRPA1 modulates mechanotransduction in cutaneous sensory neurons. J Neurosci *29*, 4808-4819.

Le Goff, L., Bozovic, D., and Hudspeth, A.J. (2005). Adaptive shift in the domain of negative stiffness during spontaneous oscillation by hair bundles from the internal ear. Proceedings of the National Academy of Sciences *102*, 16996-17001.

Lee, R.T., and Huang, H. (2000). Mechanotransduction and arterial smooth muscle cells: new insight into hypertension and atherosclerosis. Ann Med *32*, 233-235.

Levine, S., Levine, M., Sharp, K.A., and Brooks, D.E. (1983). Theory of the electrokinetic behavior of human erythrocytes. Biophysical Journal *42*, 127-135.

Littlewood Evans, A., and Muller, U. (2000). Stereocilia defects in the sensory hair cells of the inner ear in mice deficient in integrin alpha8beta1. Nat Genet *24*, 424-428.

Lyklema, J. (2006). Overcharging, charge reversal: Chemistry or physics? Colloids and Surfaces A: Physicochemical and Engineering Aspects *291*, 3-12.

Lyklema, J. (2009). Quest for ion-ion correlations in electric double layers and overcharging phenomena. Adv Colloid Interface Sci *147-148*, 205-213.

Lynch, T.M., Lintilhac, P.M., and Domozych, D. (1998). Mechanotransduction molecules in the plant gravisensory response: amyloplast/statolith membranes contain a beta 1 integrin-like protein. Protoplasma *201*, 92-100.

Lyubartsev, A.P., and Nordenskiold, L. (1995). Monte-Carlo Simulation Study of Ion Distribution and Osmotic-Pressure in Hexagonally Oriented DNA. Journal of Physical Chemistry *99*, 10373-10382.

Lyubartsev, A.P., Tang, J.X., Janmey, P.A., and Nordenskiöld, L. (1998). Electrostatically Induced Polyelectrolyte Association of Rodlike Virus Particles. Physical Review Letters *81*, 5465-5468.

Makimoto, K., and Silverstein, H. (1974). Sodium and potassium concentrations in the endolymph and perilymph of the cat. Ann Otol Rhinol Laryngol *83*, 174-179.

Manley, G.A. (1972). Frequency-Response of Ear of Tokay Gecko. Journal of Experimental Zoology *181*, 159-&.

Manley, G.A. (2000). Cochlear mechanisms from a phylogenetic viewpoint. Proc Natl Acad Sci U S A *97*, 11736-11743.

Martin, P., Bozovic, D., Choe, Y., and Hudspeth, A.J. (2003). Spontaneous Oscillation by Hair Bundles of the Bullfrog's Sacculus. Journal of Neuroscience *23*, 4533-4548.

Martin, P., and Hudspeth, A.J. (1999). Active hair-bundle movements can amplify a hair cell's response to oscillatory mechanical stimuli (National Acad Sciences).

Martin, P., and Hudspeth, A.J. (2001). Compressive nonlinearity in the hair bundle's active response to mechanical stimulation. Proceedings of the National Academy of Sciences *98*, 14386.

Martin, P., Hudspeth, A.J., and Julicher, F. (2001). Comparison of a hair bundle's spontaneous oscillations with its response to mechanical stimulation reveals the underlying active process. Proceedings of the National Academy of Sciences *98*, 14380.

Martin, P., Mehta, A.D., and Hudspeth, A.J. (2000). Negative hair-bundle stiffness betrays a mechanism for mechanical amplification by the hair cell. Proceedings of the National Academy of Sciences *97*, 12026.

McConnell, R.E., Higginbotham, J.N., Shifrin, D.A., Jr., Tabb, D.L., Coffey, R.J., and Tyska, M.J. (2009). The enterocyte microvillus is a vesicle-generating organelle. J Cell Biol *185*, 1285-1298.

McMillan, D.R., Kayes-Wandover, K.M., Richardson, J.A., and White, P.C. (2002). Very large G protein-coupled receptor-1, the largest known cell surface protein, is highly expressed in the developing central nervous system. J Biol Chem *277*, 785-792.

Nadrowski, B., Martin, P., and Julicher, F. (2004). Active hair-bundle motility harnesses noise to operate near an optimum of mechanosensitivity. Proc Natl Acad Sci U S A *101*, 12195-12200.

Nagel, G., Neugebauer, D., Schmidt, B., and Thurm, U. (1991). Structures transmitting stimulatory force to the sensory hairs of vestibular ampullae of fishes and frog. Cell and Tissue Research *265*, 567-578.

Nam, J.H., Cotton, J.R., Peterson, E.H., and Grant, W. (2006). Mechanical properties and consequences of stereocilia and extracellular links in vestibular hair bundles. Biophys J *90*, 2786-2795.

Nayak, G.D. (2010). The hair cell antigen/Ptprq: Lipid phosphatase activity, intracellular domain interactors, Apical targeting and Evidence that it is a Proteoglycan. In School of Life Sciences (Sussex, The University of Sussex).

Nayak, G.D., Ratnayaka, H.S., Goodyear, R.J., and Richardson, G.P. (2007). Development of the hair bundle and mechanotransduction. Int J Dev Biol *51*, 597-608.

Neugebauer, D., and Thurm, U. (1987). Surface charges of the membrane and cell adhesion substances determine the structural integrity of hair bundles from the inner ear of fish. Cell and Tissue Research *249*, 199-207.

Neugebauer, D.C., and Thurm, U. (1986). Surface charges influence the distances between vestibular stereovilli. Naturwissenschaften *73*, 508-509.

NIDCD http://www.nidcd.nih.gov/health/hearing/noise.asp.

Niederegger, S., and Gorb, S.N. (2006). Friction and adhesion in the tarsal and metatarsal scopulae of spiders. J Comp Physiol A Neuroethol Sens Neural Behav Physiol *192*, 1223-1232.

Parsons, J.T., Horwitz, A.R., and Schwartz, M.A. (2010). Cell adhesion: integrating cytoskeletal dynamics and cellular tension. Nat Rev Mol Cell Biol *11*, 633-643.

Patek, S.N., and Baio, J.E. (2007). The acoustic mechanics of stick slip friction in the California spiny lobster (Panulirus interruptus). J Exp Biol *210*, 3538-3546.

Perez Goodwyn, P.J., and Gorb, S.N. (2004). Frictional properties of contacting surfaces in the hemelytra-hindwing locking mechanism in the bug Coreus marginatus (Heteroptera, Coreidae). J Comp Physiol A Neuroethol Sens Neural Behav Physiol *190*, 575-580.

Persson, B. (2000). Sliding friction: physical principles and applications (Springer Verlag).

Pickard, B.G., and Ding, J.P. (1993). The mechanosensory calcium-selective ion channel: key component of a plasmalemmal control centre? Aust J Plant Physiol *20*, 439-459.

Pickles, J.O., Brix, J., Comis, S.D., Gleich, O., Koppl, C., Manley, G.A., and Osborne, M.P. (1989). The organization of tip links and stereocilia on hair cells of bird and lizard basilar papillae. Hear Res *41*, 31-41.

Pickles, J.O., Comis, S.D., and Osborne, M.P. (1984). Cross-links between stereocilia in the guinea pig organ of Corti, and their possible relation to sensory transduction. Hear Res *15*, 103-112.

Pickles, J.O., Osborne, M.P., and Comis, S.D. (1987). Vulnerability of tip links between stereocilia to acoustic trauma in the guinea pig. Hear Res *25*, 173-183.

Pincet, F., Le Bouar, T., Zhang, Y., Esnault, J., Mallet, J.M., Perez, E., and Sinay, P. (2001). Ultraweak sugar-sugar interactions for transient cell adhesion. Biophys J *80*, 1354-1358.

Pries, A.R., Secomb, T.W., and Gaehtgens, P. (2000). The endothelial surface layer. Pflugers Arch *440*, 653-666.

Rabinowicz, E. (1995). Friction and wear of materials.

Raviv, U., Giasson, S., Kampf, N., Gohy, J.F., Jerome, R., and Klein, J. (2003). Lubrication by charged polymers. Nature *425*, 163-165.

Ricci, A.J., and Fettiplace, R. (1998). Calcium permeation of the turtle hair cell mechanotransducer channel and its relation to the composition of endolymph. J Physiol *506 (Pt 1)*, 159-173.

Ricci, A.J., Wu, Y.C., and Fettiplace, R. (1998). The Endogenous Calcium Buffer and the Time Course of Transducer Adaptation in Auditory Hair Cells. Journal of Neuroscience *18*, 8261-8277.

Ruina, A. (1983). Slip Instability and State Variable Friction Laws. Journal of Geophysical Research *88*, 359-370.

Rusch, A., and Thurm, U. (1989). Cupula displacement, hair bundle deflection, and physiological responses in the transparent semicircular canal of young eel.

Pflugers Arch *413*, 533-545.

Rzadzinska, A.K., Derr, A., Kachar, B., and Noben-Trauth, K. (2005). Sustained cadherin 23 expression in young and adult cochlea of normal and hearing-impaired mice. Hear Res *208*, 114-121.

Rzadzinska, A.K., Schneider, M.E., Davies, C., Riordan, G.P., and Kachar, B. (2004). An actin molecular treadmill and myosins maintain stereocilia functional architecture and self-renewal. J Cell Biol *164*, 887-897.

Sackmann, E., and Bruinsma, R.F. (2002). Cell adhesion as wetting transition? Chemphyschem *3*, 262-269.

Santacroce, P.V., and Basu, A. (2004). Studies of the carbohydrate-carbohydrate interaction between lactose and GM(3) using Langmuir monolayers and glycolipid micelles. Glycoconj J *21*, 89-95.

Santi, P.A., and Anderson, C.B. (1986). Alcian blue staining of cochlear hair cell stereocilia and other cochlear tissues. Hear Res *23*, 153-160.

Santi, P.A., and Anderson, C.B. (1987). A newly identified surface coat on cochlear hair cells. Hear Res *27*, 47-65.

Sathyanarayana, B.K., Hahn, Y., Patankar, M.S., Pastan, I., and Lee, B. (2009). Mesothelin, Stereocilin, and Otoancorin are predicted to have superhelical structures with ARM-type repeats. BMC Struct Biol *9*, 1.

Scheibe, F., Haupt, H., and Ising, H. (2000). Preventive effect of magnesium supplement on noise-induced hearing loss in the guinea pig. Eur Arch Otorhinolaryngol *257*, 10-16.

Scheibe, F., Haupt, H., Ising, H., and Cherny, L. (2002). Therapeutic effect of parenteral magnesium on noise-induced hearing loss in the guinea pig. Magnes Res *15*, 27-36.

Scherge, M., Gorb, S., and Gorb, S. (2001). Biological micro-and nanotribology: nature's solutions (Springer Verlag).

Scholz, C.H. (1998). Earthquakes and friction laws. Nature *391*, 37-42.

Senften, M., Schwander, M., Kazmierczak, P., Lillo, C., Shin, J.B., Hasson, T., Geleoc, G.S., Gillespie, P.G., Williams, D., Holt, J.R.*, et al.* (2006). Physical and functional interaction between protocadherin 15 and myosin VIIa in mechanosensory hair cells. J Neurosci *26*, 2060-2071.

Siemens, J., Lillo, C., Dumont, R.A., Reynolds, A., Williams, D.S., and Gillespie, P.G. (2004). Cadherin 23 is a component of the tip link in hair-cell stereocilia. Nature *428*, 950-955.

Silber, J., Cotton, J., Nam, J.H., Peterson, E.H., and Grant, W. (2004). Computational models of hair cell bundle mechanics: III. 3-D utricular bundles. Hear Res *197*, 112-130.

Silverstein, H., and Schuknecht, H.F. (1966). Biochemical studies of inner ear fluid in man. Changes in otosclerosis, Meniere's disease, and acoustic neuroma. Arch Otolaryngol *84*, 395-402.

Sterkers, O., Ferrary, E., and Amiel, C. (1988). Production of inner ear fluids. Physiol Rev *68*, 1083-1128.

Sugiyama, S., Spicer, S.S., Munyer, P.D., and Schulte, B.A. (1991). Histochemical analysis of glycoconjugates in gelatinous membranes of the gerbil's inner ear. Hear Res *55*, 263-272.

Sukharev, S.I., Blount, P., Martinac, B., Blattner, F.R., and Kung, C. (1994). A large-conductance mechanosensitive channel in E. coli encoded by mscL alone. Nature *368*, 265-268.

Tadmor, R., Janik, J., Klein, J., and Fetters, L.J. (2003). Sliding Friction with Polymer Brushes. Physical Review Letters *91*, 115503.

Takumida, M., Baggersjoback, D., Harada, Y., Lim, D., and Wersall, J. (1989a). Sensory Hair Fusion and Glycocalyx Changes Following Gentamicin Exposure in the Guinea-Pig Vestibular Organs. Acta Oto-Laryngologica *107*, 39-47.

Takumida, M., Baggersjoback, D., Wersall, J., and Harada, Y. (1989b). The Effect of Gentamicin on the Glycocalyx and the Ciliary Interconnections in Vestibular Sensory Cells - a High-Resolution Scanning Electron-Microscopic Investigation. Hearing Research *37*, 163-170.

Tavi, P., Laine, M., Weckstrom, M., and Ruskoaho, H. (2001). Cardiac mechanotransduction: from sensing to disease and treatment. Trends Pharmacol Sci *22*, 254-260.

Tian, G., Zhou, Y., Hajkova, D., Miyagi, M., Dinculescu, A., Hauswirth, W.W., Palczewski, K., Geng, R., Alagramam, K.N., Isosomppi, J.*, et al.* (2009). Clarin-1, encoded by the Usher Syndrome III causative gene, forms a membranous microdomain: possible role of clarin-1 in organizing the actin cytoskeleton. J Biol Chem *284*, 18980-18993.

Tinevez, J.Y., Julicher, F., and Martin, P. (2007). Unifying the various incarnations of active hair-bundle motility by the vertebrate hair cell. Biophys J *93*, 4053-4067.

Todeschini, R.A., and Hakomori, S.I. (2008). Functional role of glycosphingolipids and gangliosides in control of cell adhesion, motility, and

growth, through glycosynaptic microdomains. Biochim Biophys Acta *1780*, 421-433.

Tse, S.T., and Rice, J.R. (1986). Crustal Earthquake Instability in Relation to the Depth Variation of Frictional Slip Properties. Journal of Geophysical Research-Solid Earth and Planets *91*, 9452-9472.

Tsuprun, V., and Santi, P. (2002). Structure of outer hair cell stereocilia side and attachment links in the chinchilla cochlea. J Histochem Cytochem *50*, 493-502.

Urbakh, M., Klafter, J., Gourdon, D., and Israelachvili, J. (2004). The nonlinear nature of friction. Nature *430*, 525-528.

Varki, A. (1999). Essentials of glycobiology (Cold Spring Harbor Laboratory Pr).

Varki, A. (2007). Glycan-based interactions involving vertebrate sialic-acid-recognizing proteins. Nature *446*, 1023-1029.

Verpy, E., Weil, D., Leibovici, M., Goodyear, R.J., Hamard, G., Houdon, C., Lefevre, G.M., Hardelin, J.P., Richardson, G.P., Avan, P.*, et al.* (2008). Stereocilin-deficient mice reveal the origin of cochlear waveform distortions. Nature *456*, 255-258.

Volkmann, N., DeRosier, D., Matsudaira, P., and Hanein, D. (2001). An atomic model of actin filaments cross-linked by fimbrin and its implications for bundle assembly and function. J Cell Biol *153*, 947-956.

Warchol, M.E. (2001). Lectin from Griffonia simplicifolia identifies an immature-appearing subpopulation of sensory hair cells in the avian utricle. J Neurocytol *30*, 253-264.

Weinbaum, S., Zhang, X.B., Han, Y.F., Vink, H., and Cowin, S.C. (2003). Mechanotransduction and flow across the endothelial glycocalyx. Proceedings of the National Academy of Sciences of the United States of America *100*, 7988-7995.

Welsh, M.J., Price, M.P., and Xie, J. (2002). Biochemical basis of touch perception: mechanosensory function of degenerin/epithelial Na+ channels. J Biol Chem *277*, 2369-2372.

Williams, A.F., and Barclay, A.N. (1988). The immunoglobulin superfamily--domains for cell surface recognition. Annu Rev Immunol *6*, 381-405.

Williams, D.S. (1982). Photoreceptor membrane shedding and assembly can be initiated locally within an insect retina. Science *218*, 898-900.

Wolfe, J., Hill, D.N., Pahlavan, S., Drew, P.J., Kleinfeld, D., and Feldman, D.E. (2008). Texture coding in the rat whisker system: slip-stick versus differential resonance. PLoS Biol *6*, e215.

Wu, Y.C., Ricci, A.J., and Fettiplace, R. (1999). Two Components of Transducer Adaptation in Auditory Hair Cells. Journal of Neurophysiology *82*, 2171-2181.

Wunderlich, R.W. (1982). The effects of surface structure on the electrophoretic mobilities of large particles. J Colloid Interface Sci *88*, 385-397.

Xiao, R., and Xu, X.Z. (2010). Mechanosensitive channels: in touch with Piezo. Curr Biol *20*, R936-938.

Yoshikawa, M., Go, S., Takasaki, K., Kakazu, Y., Ohashi, M., Nagafuku, M., Kabayama, K., Sekimoto, J., Suzuki, S., Takaiwa, K.*, et al.* (2009). Mice lacking ganglioside GM3 synthase exhibit complete hearing loss due to selective degeneration of the organ of Corti. Proc Natl Acad Sci U S A *106*, 9483-9488.

Zeng, Y., Ramya, T.N., Dirksen, A., Dawson, P.E., and Paulson, J.C. (2009). High-efficiency labeling of sialylated glycoproteins on living cells. Nat Methods *6*, 207-209.

Zheng, J.L., and Gao, W.Q. (1999). Concanavalin A protects hair cells against gentamicin ototoxicity in rat cochlear explant cultures. J Neurobiol *39*, 29-40.